PHOTOLUMINESCENCE STUDIES OF THE ELECTRON-HOLE DROPLET AND THE IMPURITY BAND IN Si(P)

by

JUAN ADALBERTO ROSTWOROWSKI

B.Sc., Universidad Nacional de Ingeniería, Perú, 1969
M.Sc., The University of British Columbia, 1972

A THESIS SUBMITTED IN PARTIAL FULFILLMENT OF

THE REQUIREMENTS FOR THE DEGREE OF

DOCTOR OF PHILOSOPHY

in

THE FACULTY OF GRADUATE STUDIES

(Department of Physics)

We accept this thesis as conforming
to the required standard

THE UNIVERSITY OF BRITISH COLUMBIA

March, 1977

In presenting this thesis in partial fulfilment of the requirements for an advanced degree at the University of British Columbia, I agree that the Library shall make it freely available for reference and study. I further agree that permission for extensive copying of this thesis for scholarly purposes may be granted by the Head of my Department or by his representatives. It is understood that copying or publication of this thesis for financial gain shall not be allowed without my written permission.

Department of Physics

The University of British Columbia
2075 Wesbrook Place
Vancouver, Canada
V6T 1W5

Date April 29, 77

ABSTRACT

The photoluminescence spectrum of phosphorus-doped silicon at dopant concentrations ranging from 1.2×10^{17} cm^{-3} to 4.0×10^{19} cm^{-3} is studied as a function of excitation intensity. The spectra are interpreted in terms of two types of recombination events, one attributed to the recombination of oppositely charged carriers inside an electron-hole droplet and the other outside due to the recombination of free holes with electrons in the impurity band.

The latter type of event gives rise to a new photoluminescence peak observed for the first time. The line shape of this peak compares very well with a first principle calculation of the impurity band density of states within the Hubbard model.

Existing theories for the ground state energy of an electron-hole droplet in n-type heavily doped silicon are reviewed and new numerical results are presented. However, within the present model droplets are not theoretically understood at this time in heavily-doped silicon.

TABLE OF CONTENTS

LIST OF TABLES

LIST OF FIGURES

Figure | Page

ACKNOWLEDGEMENTS

I wish to thank my supervisor Dr. R. R. Parsons for his friendship, encouragement and helpful guidance throughout this investigation.

In the course of this work I have benefited from daily stimulating discussions for which special thanks are due to Dr. R. Barrie, Dr. B. Bergersen, Dr. M. Eswaran, Dr. P. Jena, Dr. G. Kirczenow and Mr. M. L. W. Thewalt. I am also grateful to Dr. H. Gush for the loan of a Ge detector.

A heartfelt thanks to Tere and Juan Enrique for their sacrifices, patience and understanding.

The research of this thesis was supported by National Research Council of Canada grants to R. R. Parsons and B. Bergersen.

CHAPTER 1

INTRODUCTION

1.1 General Introduction

A silicon crystal is an indirect band gap semiconductor. The ground state of the crystal corresponds to all states in the valence bands being full and all in the conduction band being empty. If an electron is excited across the energy gap, a hole is left in the valence band and an electron-hole pair is created. In this investigation only photo-excitation is used to create these pairs. The oppositely charged carriers attract each other and at low temperatures can bind to form an exciton.[1]

Due to the indirect band gap of silicon the radiative annihilation of an exciton requires the creation or annihilation of a crystal momentum-conserving phonon.[2] At low temperatures the creation of a phonon is strongly favoured as a momentum conserving process. Because the probability of simultaneous annihilation of an exciton and the creation of a phonon is low, excitons have a long lifetime, typically 60 μ sec, and therefore a large range of exciton densities is experimentally attainable.

Keldysh[3] in 1968 predicted that excitons under increasing concentration will behave just as a gas behaves under increasing pressure; at some critical concentration there will be a condensation into a "liquid." A vast amount of experimental work[4] (photoluminescence, photoconductivity, light-scattering, etc.) has verified the existence of this condensed phase which has become known as the "electron-hole-droplet" (EHD). For intrinsic silicon, as well as germanium, the ground state properties of the EHD have been extensively studied and good agreement between experiment[5, 6] and theory[7-10] has been found.

Controversy has arisen concerning the existence of the condensate in heavily-doped silicon. In recent photoluminescence studies Halliwell and Parsons[11] were able to infer from photoluminescence studies that high densities of non-equilibrium carriers condense into droplets even at impurity concentrations where screening effects prohibit exciton formation. Furthermore, they hypothesize that the EHD exists in samples with donor concentrations above the critical concentration, $n_{crit} \simeq 3 \times 10^{18}$ phosphorus cm^{-3}, for the semiconductor-metal transition[12, 13].

Martin and Sauer[14], on the other hand, argue that there is no EHD in samples with phosphorus concentrations close to and above n_{crit}.

1.2 Purpose and Outline of this Thesis

The initial main purpose of this thesis was to find out whether the condensate exists in metallic silicon. This could best be done by repeating the photoluminescence experiments of Halliwell and Parsons[11] in heavily-doped silicon with extensive improvement in instrumentation. With better signal-to-noise ratio a detailed comparison could be made between the experimental and theoretical line shapes[5,15] for the EHD. Two orders of magnitude improvement in detectivity allowed the study of the photoluminescence spectrum of Si(P) as a function of excitation intensity and the spectra are found to contain two components, the first of these is interpreted in terms of the recombination of an electron-hole pair inside the drop; the second in terms of the recombination outside the drop, in the gas phase. At low excitation intensity the droplets are few and far apart and most recombination events occur in the gas phase. As the excitation intensity is increased the EHD line grows. An important aspect of this thesis is to show that by studying the spectra at various excitation intensities the recombination emission of electron-hole

pairs in the two coexisting phases can be disentangled.

It will be shown that the EHD line shape is very well described in terms of the recombination emission in a degenerate electron-hole plasma with fixed carrier density. The gas phase line shape arises from the recombination of a free hole with electrons in the "Impurity Band"[16] (IB), and it will be argued that this line shape describes very closely the impurity band density of states.

Despite the wide variety of experimental techniques used in the past (electrical conductivity, Hall mobility, magneto-resistance, magnetic susceptibility, NMR and ESR properties)[12] the impurity band was not well understood for donor concentrations near n_{crit}. The photoluminescence detection of the impurity band density of states in samples containing impurity concentrations above and below n_{crit} is of capital importance to test our understanding of the semiconductor-metal transition.

In Chapter 2 a description of the experimental apparatus is presented. The experimental results and the analysis of the data are presented in Chapter 3 and in Appendix A the experimental results in heat-treated samples are described.

In Chapter 4 the description of the Hubbard model[17] of the impurity band applicable for donor densities below n_{crit} will be presented. The results of less successful approaches appearing in the literature are also shown. The theoretical background to these approaches is given in Appendix B.

In Chapter 5 the theoretical model of Bergersen et al[18, 19] for the EHD in heavily doped material is reviewed and corrected numerical results

are presented. It will be shown that within this model, contrary to previous results[18, 19] the EHD is not theoretically predicted. A general discussion and conclusion will be presented in Chapter 6.

Appendices C and D are concerned with the numerical work done by the author for the different aspects of this thesis.

The main results of this investigation have already been published.[19-21]

CHAPTER 2

EXPERIMENTAL DETAILS

2.1 Sample Preparation

Single crystals of vacuum float zone phosphorus-doped silicon purchased from General Diode Corp. and Ventron Electronic Corp. were used. The impurity concentration was determined by room temperature resistivity measurements using a four-point probe on the face of the ingot before and after cutting the slice. The crystal face was polished and etched for 30 seconds in a mixture of HNO_3 and HF (5:1) before measurements were made. The resistivity was determined by averaging at least ten measurements made at various positions on the crystal face. The standard deviations of the mean were found to be less than two percent. If the difference in the mean resistivity before and after cutting the slice was more than two percent the sample was rejected.

The concentration of phosphorus impurities was determined from the measured resistivities using the Irvin chart.[22] The accuracy of the donor concentration is estimated to be within ±8 percent for all samples used in this investigation and mostly reflects the author's confidence limit in the Irvin chart.[22]

The slices of silicon crystal were cut typically to 3 x 5 x 20 mm^3 and etched as described above to remove surface damage. No change in the photoluminescence signal was found if the sample was polished; therefore, sample polishing was discontinued at an early stage of this investigation.

The heat treatment studies were done on samples cut from the same slices mentioned above. The samples were then heated to 1150° C in a

helium atmosphere for 30 minutes and immediately quenched to room temperature in acetone. The samples were then etched as previously described. Halliwell[23] has pointed out that the effects of the heat treatment will disappear if the samples are left at room temperature for several days. Therefore, when measurments were not performed immediately after heat treatment, the samples were stored in liquid nitrogen.

All photoluminescence experiments were done with the sample immersed in liquid helium. The optical cryostat held three litres of liquid helium and provided an average running time of about 15 hours. The temperature could be varied by changing the vapor pressure of the helium liquid. To check whether the sample was in thermal equilibrium with the bath the photoluminescence spectrum of intrinsic silicon was obtained under the same experimental conditions used in the measurement of the doped crystals. The line shape of the recombination emission* due to free excitons[25], which is highly temperature dependent, did not change for all optical excitation levels reported here.

2.2 Photoluminescence Spectrometer

A Spectra Physics Model 120 continuous He-Ne laser with 5mW power output at 6328 Å wavelength was used for low excitation intensities; a Spectra Physics Model 165 continuous argon-ion laser with a maximum power output of 2W at 5145 Å wavelength was used as a source for high excitation intensities. The irradiated area was a spot of 1 to 3 mm in diameter.

---

*The photoluminescence line shape of free excitons was not observed to agree with previously reported work[24, 25] and triggered the interest of Thewalt and Parsons in our laboratory, who subsequently did very interesting work[26] in this area.

A modification of the optical tail piece of the inner helium can of the cryostat was necessary. The tail piece was originally made of good quality pyrex tubing. and this arrangement worked well when the photoluminescence signals were large as in the case of those reported in this investigation for samples containing less than 10^{18} phosphorus cm^{-3}. For more heavily-doped samples, however, the photoluminescence signal is very weak and background radiation originating in the pyrex tubing dominates the observed spectrum. Therefore, the lower part of the pyrex tubing was replaced with a fluorescence cell made of spectrosil, a synthetic silica, manufactured by Thermal Syndicate Ltd. Although the manufacturer does not mention any low temperature properties, the low temperature fusion technique used in the production of this cell withstands the thermal shock when cooled to liquid helium temperatures.

The recombination radiation was collected from the excited surface in order to minimize the effects of free carrier absorption in the heavily-doped samples. The photoluminescence spectra did not need correction for absorption in the sample because the absorption coefficient is known to be slowly varing in the energy region of interest.[27] The optimization of the collection of recombination radiation is not a trivial problem because of silicon's high refractive index $n \sim 4$. The radiation leaving the sample is concentrated in a small solid angle. An optimum arrangement was found in matching the f/number of the collection optics to that of the spectrometer with an off-axis elliptical mirror with approximately three fold magnification.

The recombination radiation was analyzed with a homemade 56 cm f/3.5 monochromator of Czerny-Turner design fitted with a Bausch & Lomb Inc.

grating blazed at 1.6 μ with 600 groves/mm. The grating was used in the second order. The optical configuration is shown in Fig. 2.1. To eliminate infrared emission from the laser a Corning filter CS 4-96 was placed at the output of the argon-ion laser; a Corning filter CS 1-57 was used for the He-Ne laser. A Corning filter CS 7-57 was placed at the exit slits of the spectrometer to prevent any laser light from reaching the detector. For signal detection a R.C.A. (67-07-B) germanium photodiode detector-preamplifier system operated at liquid nitrogen temperature with detectivity $D^*(1.268\mu, 91\ Hz, 1\ Hz) = 4.234 \times 10^{13}$ cm-$Hz^{\frac{1}{2}}$/RMS Watt and noise-equivalent-power NEP $(1.268\mu, 91\ Hz, 1\ Hz) = 1.056 \times 10^{-14}$ RMS Watt/$Hz^{\frac{1}{2}}$ was used. This value should be compared to 4×10^{-13} RMS Watt/$Hz^{\frac{1}{2}}$ for the dry ice cooled PbS detector used by Halliwell.[22]

Further signal amplification was obtained with a low noise pre-amplifier (PAR-113, Princeton Applied Research Corp.). The excitation light was chopped at approximately 90 Hz and the detector signal was phase-sensitive detected (PAR-121 Lock-in, Princeton Appried Research Corp.) and finally integrated over times of typically three seconds. The resulting analog signal was electronically converted to a digital one and stored in the memory of a mini-computer (Nova 2, Data General Corp.).

The signal-to-noise of the weaker spectra obtained in this investigation were further improved by signal averaging. To achieve automatic signal averaging the mini-computer was interfaced[28] with the monochromator. The data were finally punched on paper tape at the end of the experiment for future analysis.

It should be pointed out that the improved detectivity used in this

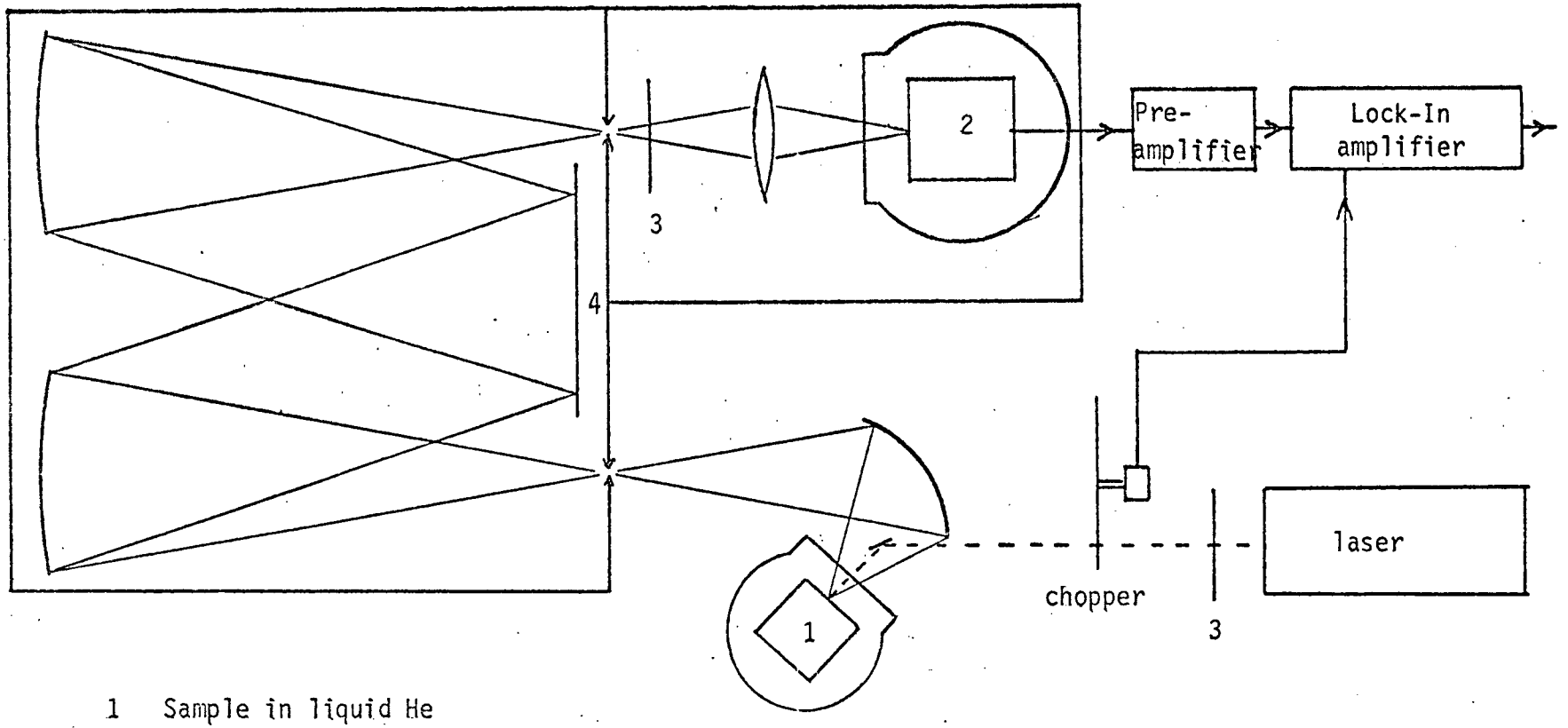

1 Sample in liquid He

2 Ge detector and preamplifier system in liquid N_2

3 Filters

4 Grating

Figure 2.1: Experimental optical configuration.

investigation and the automatic averaging facility of the present set-up allowed spectral line shape analysis on signals over 200 times weaker than those reported by Halliwell and Parsons.[11]

2.3 Signal Averaging

A block diagram of the digital equipment and peripherial devices used for signal averaging and data analysis (described in Chapter 3 and Appendix C) is shown in Fig. 2.2. The interface was designed and built by M.L.W. Thewalt and a full description of it is found in his thesis.[28] In this section a general overview only will be given.

An important part of this interface is the device called the "spectrometer controller".[28] In simple terms, this device translates a binary coded number from the computer into a train of pulses. Each pulse increments the monochromator's stepping motor and the rotational direction is determined by the sign of the binary number (two's complement used for negative numbers). In addition to the spectrometer controller it is convenient to use a programmable interval timer (PIT) which allows one to set an integration time for each wavelength positions. The interaction of the mini-computer with the above mentioned devices occurs only in giving the devices the parameters of the task to be performed and in receiving confirmation that the task has been completed. The computer is consequently free for many other tasks.

In the signal averaging mode the computer is programmed to reset the integrator by means of a digital output device immediately after the PIT is started. The integrator will continue in operation until it is reset. While the integration of the detected signal is being performed the computer is used to display on the scope data stored in its memory. The vertical

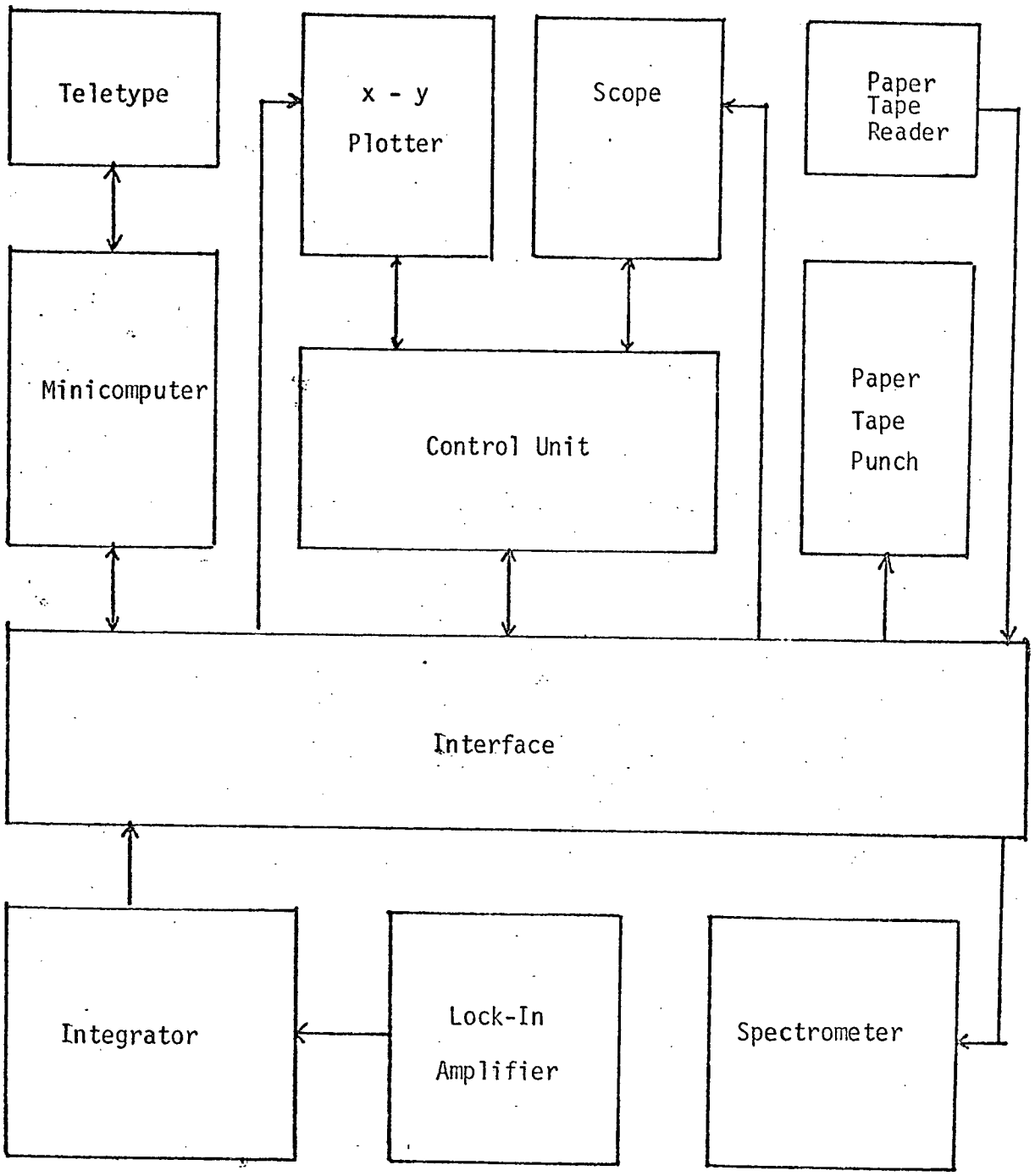

Figure 2.2: Block diagram of the digital equipment and peripherial devices used for signal averaging and data analysis.

analog voltages displayed on the scope are obtained by electronically converting the digital information in a memory location and the horizontal voltages are obtained with a digital to analog conversion of a number proportional to the memory location. The scope display allows the experimentalist to observe the spectrum as it is measured. At the end of each memory sweep the computer is programmed to test the status of the PIT. If the integration time has expired, the computer terminates the integration of the signal by transferring control to the analog-to-digital converter (ADC) while conversion of the analog signal is performed the computer starts the spectrometer controller with a new set of parameters. During the time that the spectrometer controller is performing its task the computer will test whether or not the analog-to-digital conversion has been completed and then compute a new average and standard deviation for the signal for the last spectrometer position.

The cycle described above continues until the last point of the spectrum has been measured and if signal average is to be used the spectrometer is returned to the first wavedrive position. The experimentalist may decide after inspecting the spectrum displayed on the scope that the signal-to-noise ratio is adequate and interrupt the signal averaging. The data stored in memory can then be plotted on an x-y recorder. The analog voltages required are obtained using digital to analog converters (DAC) as in the case of the scope display. The horizontal axis may be calibrated in units of wavelength or energy. For future use the binary coded spectrum stored in memory is transferred to paper tape using the high speed paper tape punch (HSPTP).

CHAPTER 3

EXPERIMENTAL RESULTS AND ANALYSIS

3.1 Introduction

As pointed out in Chapter 1 radiative recombination of an electron-hole pair in intrinsic silicon is accompanied with the simultaneous emission of a momentum conserving phonon. In doped material the interaction of the pair with an impurity relaxes the momentum conservation and an extrinsic component is observed in both the absorption[27] and photoluminescence.[11, 25] This component is commonly referred to as the "no-phonon (NP)" process.[11, 25] The NP process does not change the energy of the transition, unlike the phonon assisted recombination which results in photoluminescence peaks shifted down by the energy expended in the creation of the phonon.

Table 3.1 lists the energies of the phonons assisting the recombination as measured in photoluminescence studies by other investigators.[25, 29] The identification of the phonon is done by comparison to the energies measured by inelastic neutron scattering.[30] Since the strongest recombination emission in phosphorus-doped silicon is assisted by creating a transverse optical (TO) phonon[11, 14, 25, 29] all the line shape analysis has been performed on the TO phonon assisted portions of the spectrum*.

3.2 The Photoluminescence of Si (P)

Figure 3.1a. shows the spectrum of a sample containing 1.2×10^{17}

*In reality, the TO phonon assisted recombination overlaps with the longitudinal optical (LO) phonon assisted portion of the spectrum but cannot be resolved. We will justify later on in this Chapter the neglect of the LO phonon replica in the analysis of the spectra.

TABLE 3.1

PHONON ENERGIES

TRANSVERSE ACOUSTICAL (TA)	18.7 meV
LONGITUDINAL ACOUSTICAL (LA)	undetected
TRANSVERSE OPTICAL (TO)	58.0 meV
LONGITUDINAL OPTICAL (LO)	56.1 meV

TABLE 3.2

EFFECTIVE MASSES

m_l	.9163 m_o
m_t	.1905 m_o
$m_e^* = (m_l\, m_t^2)^{1/3}$	.3216 m_o
m_{lh}	.154 m_o
m_{hh}	.523 m_o
$m_h^* = (m_{lh}^{3/2} + m_{hh}^{3/2})^{2/3}$	.5773 m_o

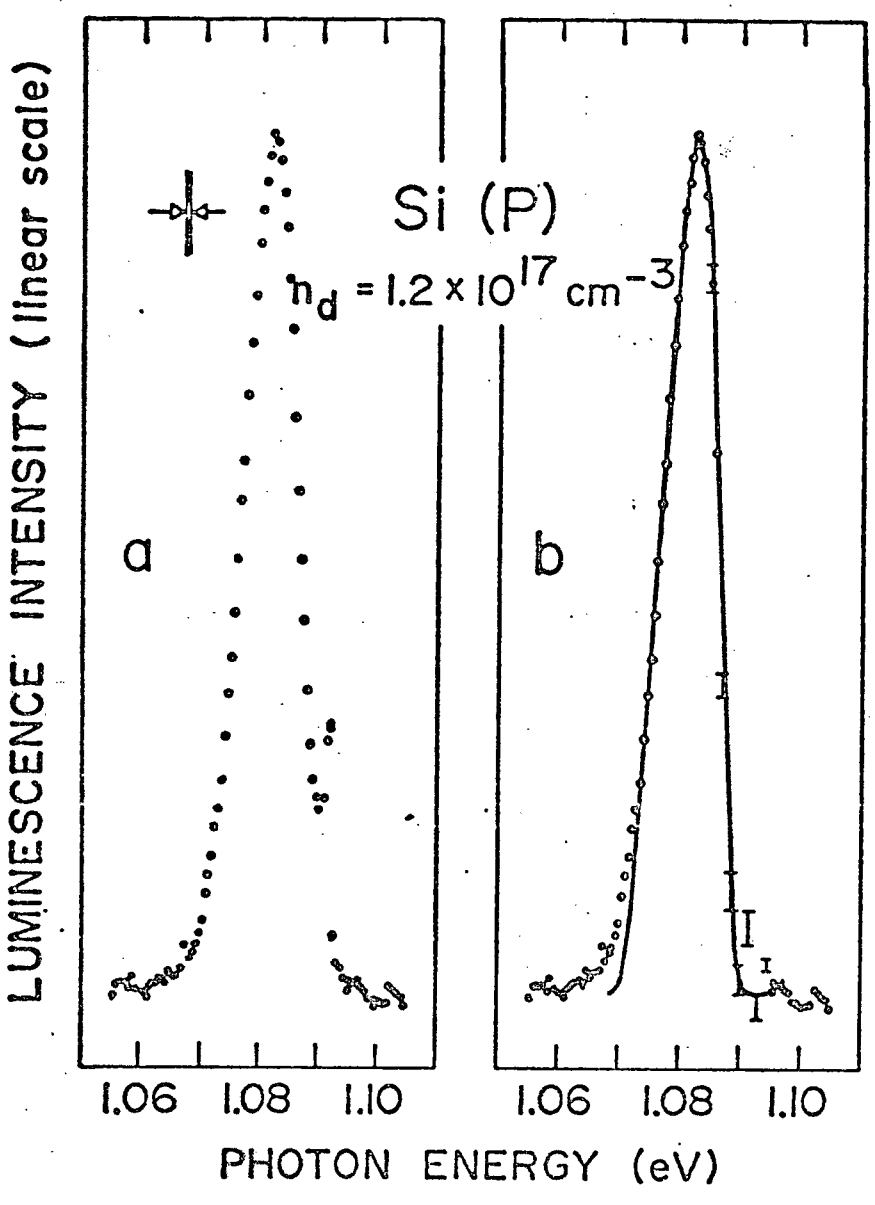

Figure 3.1: a) Photoluminescence spectrum of silicon containing 1.2×10^{17} phosphorus cm^{-3} at T = 4.2 K and 120 Wcm^{-2} excitation level. The strong broad peak is attributed to the electron-hole drop (EHD), the weaker to the bound exciton (BE).

b) Solid circles show the experimental EHD line shape obtained by subtracting the BE line shape from the spectrum shown in (a). The errors in subtraction are shown. The solid curve is the theoretical fit to the EHD line shape.

phosphorus cm^{-3}. The excitation intensity is approximately 120 Wcm^{-2}. The spectrum shows two overlapping peaks: a broad one at low energies attributed[11, 14] to the EHD and a sharper one associated with an exciton bound to a neutral phosphorus impurity[11, 14, 25, 29]. Since the relative intensity of these peaks depends on the excitation level the two overlapping peaks can be separated. The bound exciton (BE) peak strongly dominates the spectrum at very low excitation level (.1 Wcm^{-2}) and is used, properly scaled, to subtract the BE peak from the spectra obtained at excitation intensities in the range of 10 to 200 Wcm^{-2}. In this manner the EHD line shape shown in Figure 3.1b. is obtained.

To reinforce the identification of this peak[11, 14] with the EHD it will be shown that, as in the case of intrinsic material[5, 15], the line shape of the EHD peak is well understood in terms of the recombination radiation of an electron-hole pair in a degenerate electron-hole plasma of fixed density. The solid line in Figure 3.1b. shows an EHD theoretical line shape obtained by a convolution integral of densities of state[5, 15].

$$I_{TO}(h\nu) \propto \int_0^\infty \int_0^\infty N(E_e)N(E_h)f(E_e)f(E_h)\delta(h\nu - E_{pair} + E_h^F + E_e^F - E_e - E_h + h\nu_{TO})\,dE_e\,dE_h \quad , \tag{3.1}$$

where E_e and E_h are respectively the electron and hole energies in the conduction and valence bands; $N(E_e)$ and $N(E_h)$ are the respective densities of state; $f(E_e)$ and $f(E_h)$ are the Fermi-Dirac distribution functions taken at the helium bath temperature; E_e^F and E_h^F the Fermi energies for the electrons and holes; E_{pair} is the energy required to add one more electron-hole pair to the EHD and is determined, at very low temperatures, by the high energy threshold of the luminescence peak[31]. A theoretical fit has been performed

by assuming the EHD to be charge neutral, that is, the total electron density (n_c) is equal to the density of positively charged donor ions (n_d) plus the density of photocreated holes (n_h). It will be assumed that the carriers effectively screen any bound impurity states, thus, n_d is determined by the impurity concentration. The bands are assumed to be parabolic and the effective masses which describe them were assumed to be independent of doping. The band parameters used in this calculation are listed in Table 3.2. The TO phonon energy is given in Table 3.1 and as discussed in the previous Chapter the sample temperature is that of the helium bath. The fit is performed by varying two parameters: E_{pair} which fixes the energy position and n_h which changes the line shape and width for a given impurity density (n_d). The parameters giving the best fit* are listed in Table 3.3 as a function of impurity concentration and the uncertainties quoted reflect the amount by which they have to be varied so that a clearly bad fit is obtained.

The spectrum shown in Figure 3.2 was obtained from a sample containing 5.7×10^{17} phosphorus cm^{-3}. The excitation intensity is approximately 160 Wcm^{-2}. The line shape of the EHD peak centered at 1.0835 eV is independent of excitation intensity in the range 1 Wcm^{-2} to 200 Wcm^{-2} used in this experiment. The solid curve in Figure 3.2 shows the theoretical fit. The BE peak (1.09 eV) is not observed. The peak appearing at low energy (1.061 eV) is attributed to the recombination of an electron in the impurity states with a free hole. Study of this peak at low excitation level is obscured by the

---

*The theoretical EHD line shape calculated by assuming that the recombination is assisted by the creation of TO, as well as, LO phonons (10 to 1 ratio and 1.8 meV apart[32]) is the same as the one calculated assuming no LO phonon assistance except far in the wings. The systematic error introduced in the fitting parameters by neglecting the LO phonon replica are judged to be well below the uncertainties quoted in Table 3.3.

TABLE 3.3

BEST FIT PARAMETERS*

$n_d(\times 10^{18}\ cm^{-3})$	$E_{pair}(eV)$	$n_h(\times 10^{18}\ cm^{-3})$
.12	1.1471(5)	3.0(1)
.57	1.1469(5)	1.9(1)
1.8	1.1394(5)	1.3(1)
2.45	1.1374(5)	1.3(1)
3.0	1.1352(5)	1.3(1)
3.9	1.132 (1)	1.2(1)
5.0	1.131 (1)	1.15(10)
11.0	1.130 (1)	1.6(2)

*The parameters obtained for $n_d = .12 \times 10^{18}\ cm^{-3}$ are in agreement with theoretical calculations of Bergersen et al[19]. As will be shown in Chapter 5, there is to date no reliable theoretical calculation of this parameters for higher impurity concentrations.

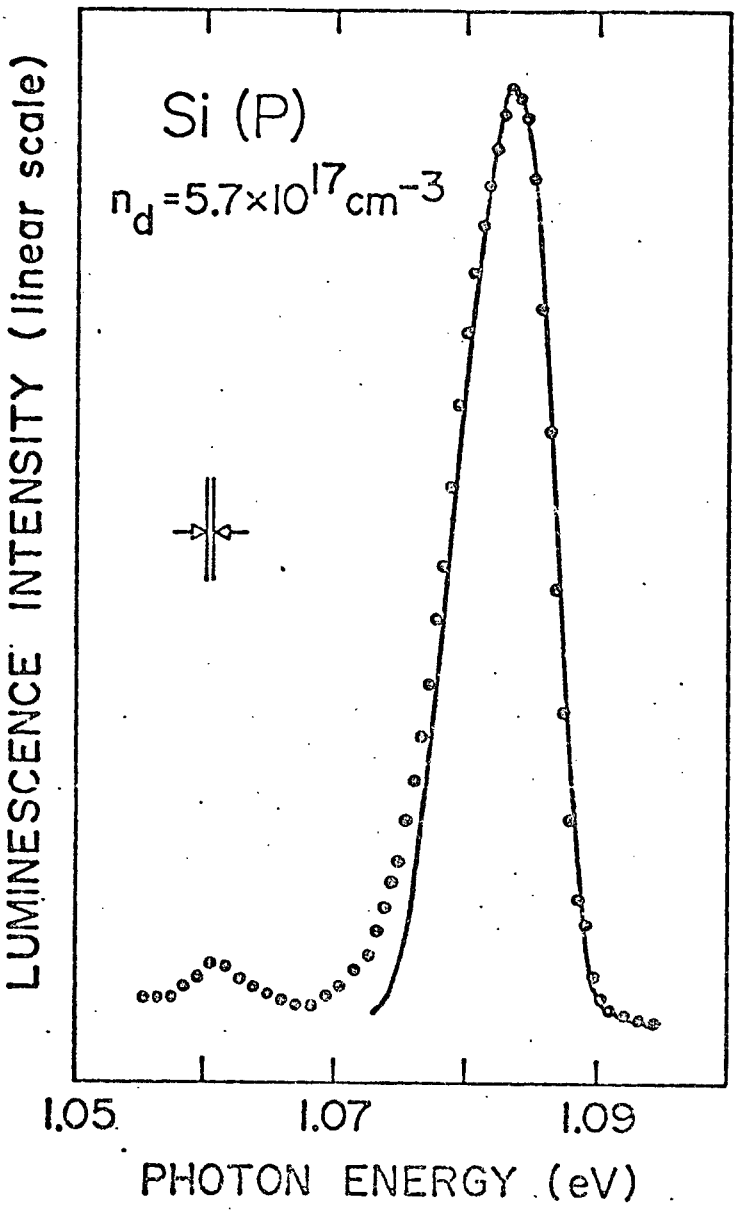

Figure 3.2: The photoluminescence spectrum of silicon containing 5.7×10^{17} phosphorus cm^{-3} at T = 4.2 K and 160 Wcm^{-2} excitation level is given by solid circles. The solid curve shows the theoretical fit to the EHD line shape.

appearance of a broad peak at 1.045 eV which dominates the spectrum. The spectrum represented by solid circles in Figure 3.3 is obtained from the same sample using an excitation intensity of approximately 20 Wcm^{-2}. The spectrum represented by flags was obtained from a sample containing both phosphorus and boron with concentrations in the order of 10^{17} and 10^{16} atoms cm^{-3} respectively. The excitation intensity was approximately 8 Wcm^{-2}. Because of the general agreement of these two spectra and the expectation of observing a broader peak at lower energy for the recombination of an electron in the impurity band with a hole bound to an acceptor-ion[33], it is reasonable to attribute the broad peak at 1.045 eV to donor-acceptor[33] recombination.

Samples with 3.1×10^{17} and 3.7×10^{17} phosphorus cm^{-3}, intermediate to the impurity concentrations of samples discussed above, have also been studied. The photoluminescence study of these samples as a function of excitation level is observed to be in close agreement with that of Martin and Sauer[14] for a sample containing 1.8×10^{17} phosphorus cm^{-3}. A single recombination band is observed at high excitation intensity. With decreasing excitation level this band changes line shape and exhibits evidence of structure at low excitation intensity. Martin and Sauer[14] argued that these changes in line shape were indicative of a profound change in the electronic states. An alternative explanation is that the BE peak is very broad and overlaps the EHD peak to form a single broad band. The changes in this band with excitation level can be attributed to the change in the relative intensities of the EHD and BE emissions with excitation level.

As pointed out in Chapter 1, a great emphasis in this work has been

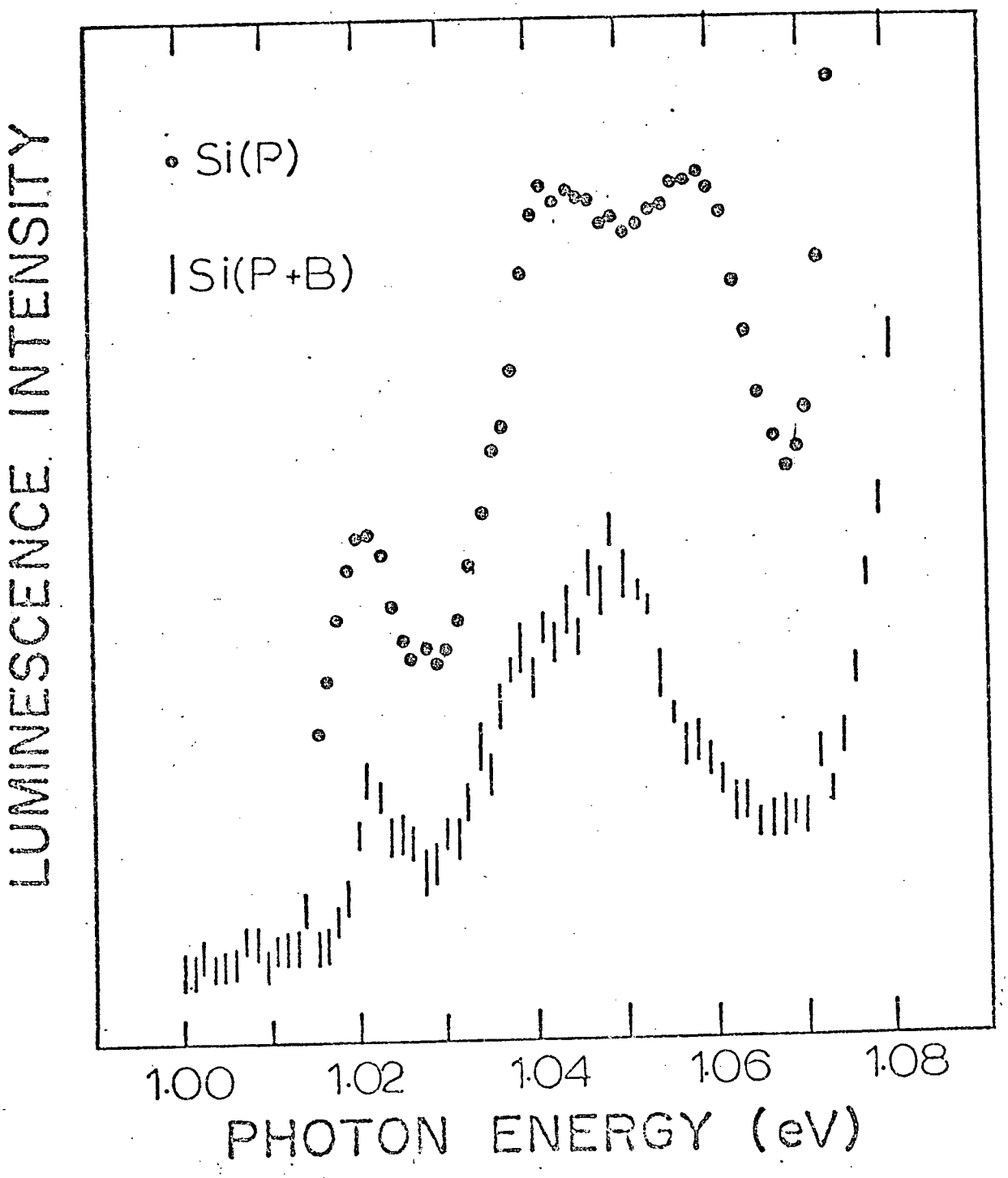

Figure 3.3: The photoluminescence spectrum of silicon containing 5.7×10^{17} phosphorus cm^{-3} at 4.2K and 20 Wcm^{-2} excitation level represented by solid circles is compared to that of a compensated sample containing, both, phosphorus (10^{17} cm^{-3}) and boron (10^{16} cm^{-3}) at 4.2K and 8 Wcm^{-2} excitation level represented by flags (two standard deviations from 15 scans). The peak at 1.045 eV is attributed to donor-acceptor recombination.

given to the data and analysis of samples containing 1.8×10^{18} cm^{-3} to 3.9×10^{18} cm^{-3} because the donor concentration range covered by these samples goes from slightly below to slightly above n_{crit} for the metal-semiconductor transition.

Figure 3.4 shows the spectra of a sample containing 1.8×10^{18} phosphorus cm^{-3}. Figure 3.4a. shows the spectrum at high excitation level (200 Wcm^{-2}) and the observed peak is attributed to the recombination within the EHD. This hypothesis is supported by the good theoretical fit of the EHD line shape showed by the solid curve. Figure 3.4b. shows the spectra at intermediate (20 Wcm^{-2}) and low (.1 Wcm^{-2}) excitation level. The spectra show clearly two peaks and the peak at high energy is again attributed to the EHD. The other peak is observed for the first time and is attributed to the recombination of an electron in the impurity band (IB) with a free hole. The IB peak is observed at approximately 25 meV below the position predicted[34] for an isolated impurity given by:

$$h\nu = E_{gap} - E_{imp} - h\nu_{TO} \quad , \qquad (3.2)$$

where the band gap energy is 1.1698 eV at 4.2K and the ionization energy of phosphorus in silicon is 45.3 meV[35]. This shift to lower energies at $n_d = 1.8 \times 10^{18}$ cm^{-3} may be explained by the conduction and valence band developing tails[36, 37] into the forbidden gap or by a lowering of the ground state energy of the bound electrons because of the overlap of the donor electron wave functions[38].

The spectra in Figure 3.4b. have been scaled so that the low energy tails of the IB peaks are superimposed. The line shape of the EHD peak obtained by subtracting these two spectra is the same as the one obtained at high excitation intensities shown in Figure 3.4a. The line shape of the IB peak is obtained by subtracting the experimental EHD line shape (Figure

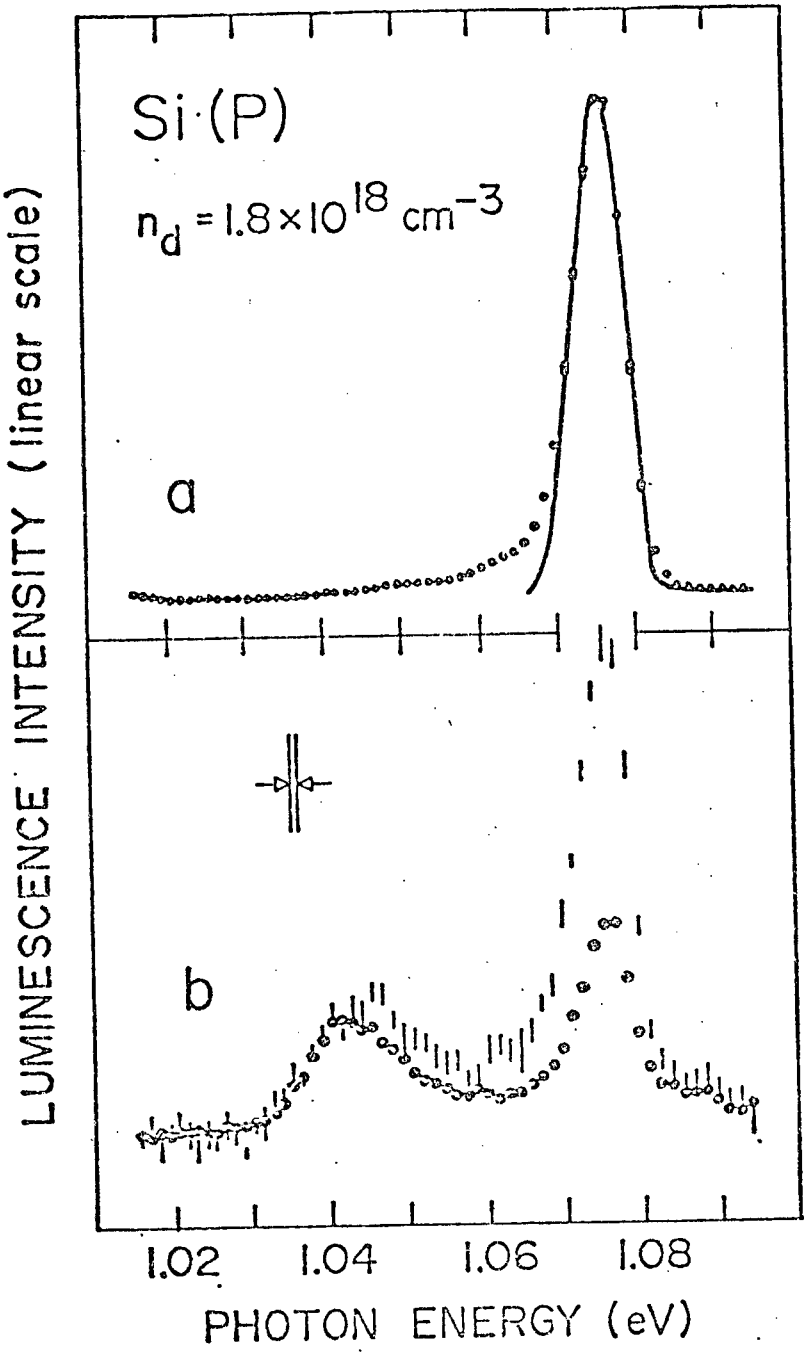

Figure 3.4: Photoluminescence spectra of silicon containing 1.8×10^{18} phosphorus cm^{-3} at 4.2 K.

a) Solid circles show the spectrum at high excitation level (200 Wcm^{-2}). The peak is attributed to the EHD. The solid curve shows the theoretical fit to the EHD line shape.

b) The flags (two standard deviations from 6 scans) show the spectrum at intermediate excitation level (20 Wcm^{-2}) and the solid dots (50 scans) the spectrum at low level (.1 Wcm^{-2}). The peak at high energies is attributed to the EHD, the other to the impurity band. The spectra have been scaled for comparison.

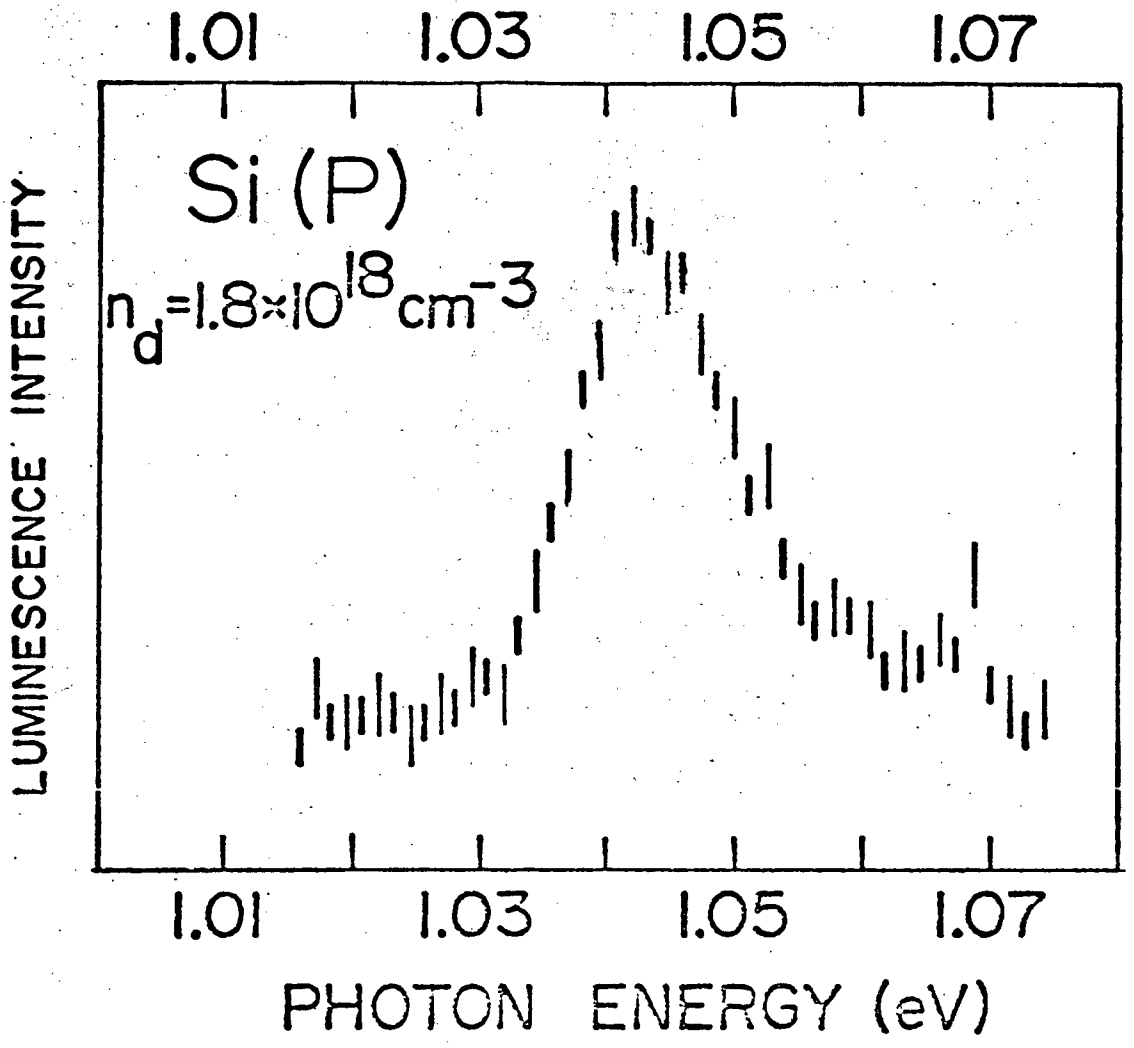

Figure 3.5: Experimental photoluminescence line shapes for an electron in the impurity band and a free hole of phosphorus-doped silicon containing 1.8×10^{18} cm^{-3}. Impurity band line shapes at excitation levels of 5 Wcm^{-2} (long flags) and .1 Wcm^{-2} (short flags) are shown. The flags represent two standard deviations due to signal averaging and to the subtraction process referred to in the text.

3.4a.) from the low excitation level (.1 Wcm^{-2}) spectrum. As shown in Figure 3.5 the same IB line shape arises from an intermediate excitation (5 Wcm^{-2}) spectrum. The recombination emission of electrons in the impurity band and free holes in the valence band is proportional to the convolution of the densities of state of the two bands. Since only those states of the valence band within approximately kT of the band maximum are unoccupied and at 4.2 K this energy is negligible compared to the width of the observed IB peak the experimental IB line shape gives directly the density of states in the impurity band. In Chapter 4 the calculated impurity band density of states within several models are compared with this experimental line shape.

Figure 3.6 shows the spectra of a sample containing $2.45x10^{18}$ phosphorus cm^{-3}. The solid dots in Figure 3.6a. show the spectrum at high excitation intensity (200 Wcm^{-2}). The solid curve is a theoretical fit to the EHD line shape. The flags in Figure 3.6b. show the spectrum at intermediate intensity (20 Wcm^{-2}) while the solid circles indicate the spectrum at low intensity (.1 Wcm^{-2}). A second peak is clearly visible at low excitation level which, as in the previously discussed sample, is attributed to IB recombination. There is no discernible difference between the EHD line shape observed by subtracting the two spectra shown in Figure 3.6b. from the EHD spectrum shown in Figure 3.6a. Figure 3.7 shows the IB experimental line shape obtained by subtracting the EHD line shape given by the spectrum shown in Figure 3.6a. from the low excitation level spectrum (.1 Wcm^{-2}) shown in Figure 3.6b.

The spectra for a sample containing $3.0x10^{18}$ phosphorus cm^{-3} are shown later in this Chapter. The spectral analysis of these data follows very closely the one described above and is not included here. The results are listed together with those of other samples in Table 3.3.

Figure 3.8a. shows two spectra of a sample containing $3.9x10^{18}$

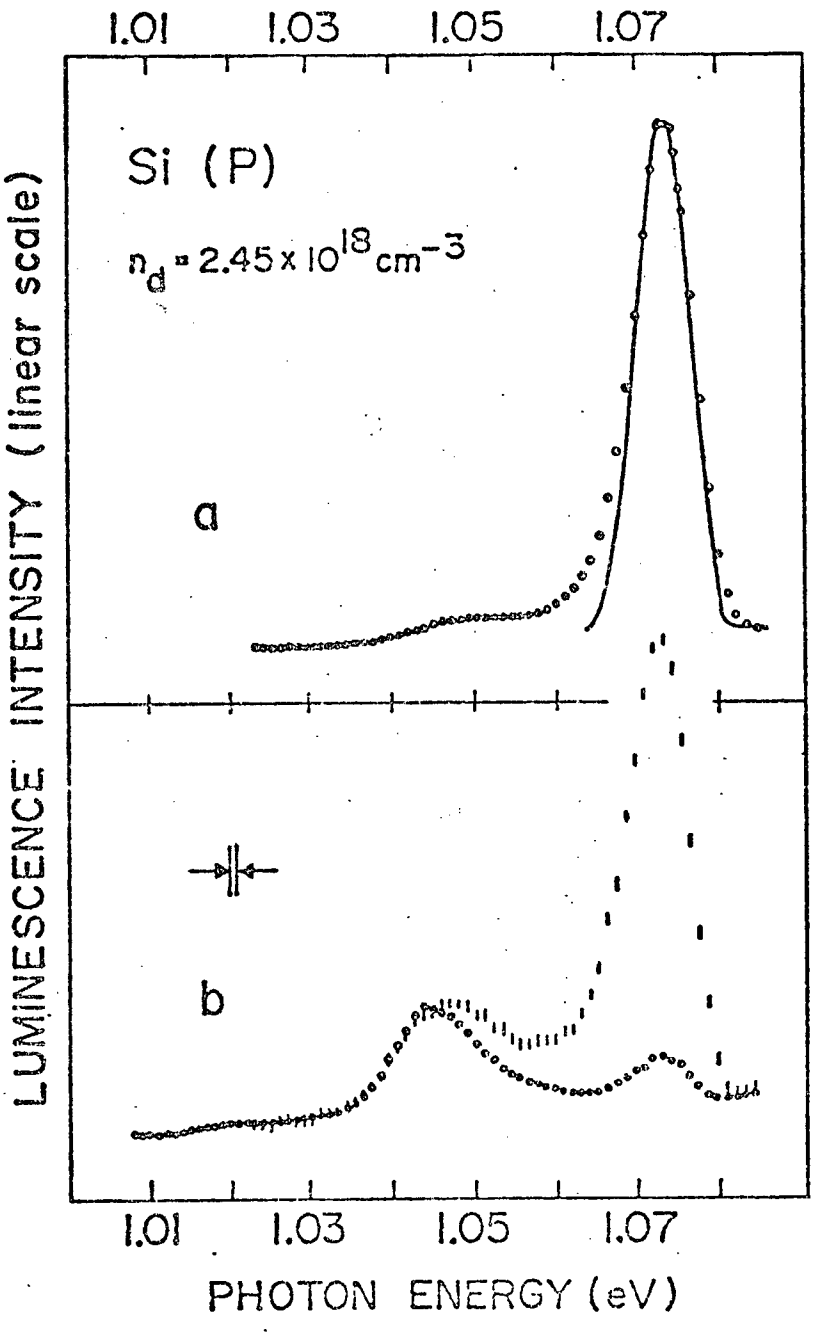

Figure 3.6: Phololuminescence spectra of silicon containing 2.45×10^{18} phosphorus cm^{-3} at 4.2 K

a) Solid circles show the spectrum at high excitation level (200 Wcm^{-2}). The peak is attributed to the EHD. The solid curve shows the theoretical fit to the EHD line shape.

b) The flags (two standard deviations from 6 scans) show the spectrum at intermediate level (20 Wcm^{-2}) and the solid dots (40 scans) the spectrum at low level (.1 Wcm^{-2}). The peak at high energies is attributed to the EHD, the other to the IB. The spectra have been scaled for comparison.

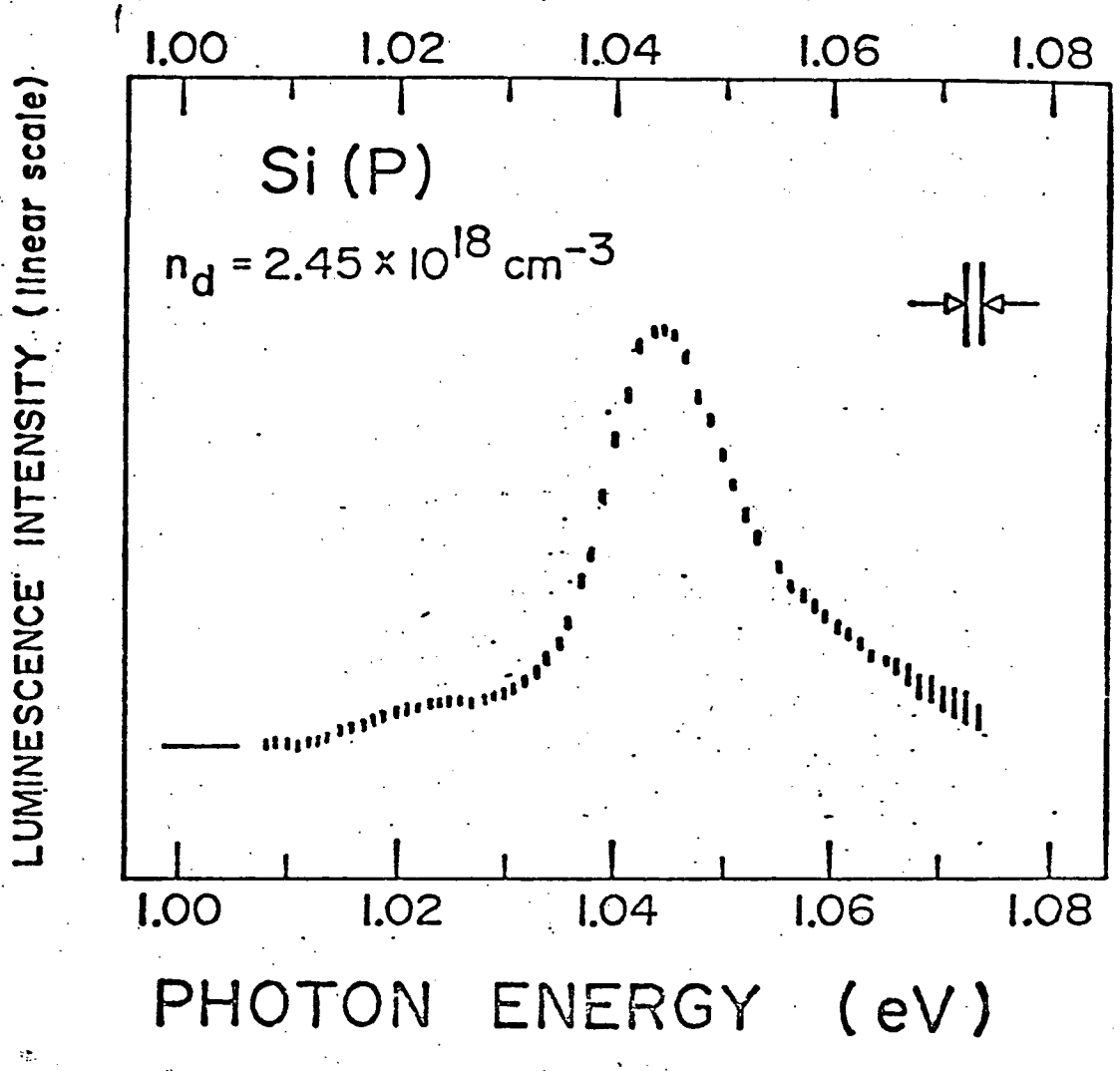

Figure 3.7: IB experimental photoluminescence line shape of phosphorus-doped silicon containing 2.45 x 10^{18} cm^{-3}. The excitation intensity is approximately .1 Wcm^{-2}. The flags represent two standard deviations due to signal averaging and to the subtracting process referred to in the text.

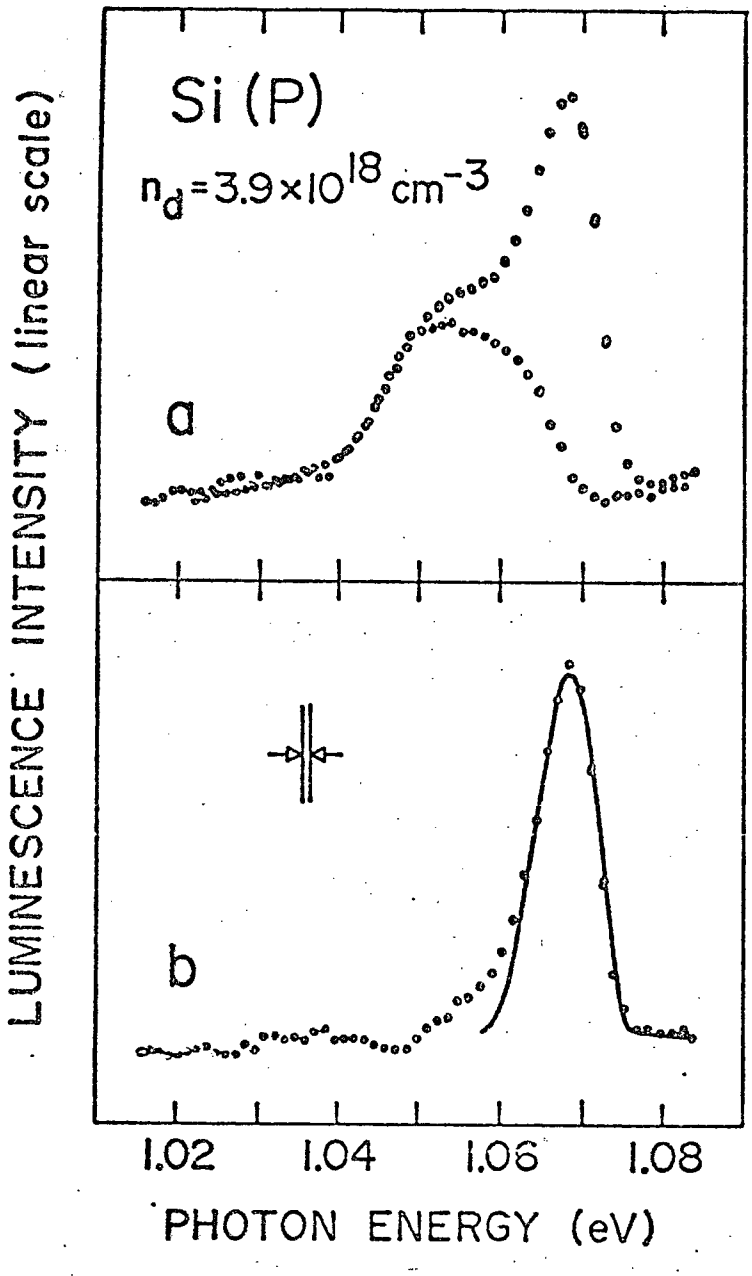

Figure 3.8: a) Photoluminescence spectra of silicon 3.9×10^{18} phosphorus cm^{-3} at T = 4.2 K are shown at two excitation levels. At high excitation level 200 Wcm^{-2}, 1 scan) both the impurity band (IB) and the EHD peaks are observed and at low level (.2 Wcm^{-2}, 60 scans) the IB peak strongly dominates.

b) The solid circles give the EHD line shape obtained by subtracting the two spectra in figure (a). The solid curve shows the theoretical fit to the EHD line shape.

phosphorus cm^{-3}. The high excitation level spectrum (200 Wcm^{-2}) shows both the EHD and the IB peaks. In the low level spectrum (.2 Wcm^{-2}) the IB peak strongly dominates the spectrum. The line shape of the EHD peak obtained by subtracting these two spectra is shown in Figure 3.8b. In similar fashion the EHD line shape has been obtained as a function of excitation levels in the range of 10 to 200 Wcm^{-2} and this line shape is not observed to change. The solid curve in Figure 3.8b. shows the theoretical fit to the EHD peak. The two superimposed IB peaks shown in Figure 3.9 were obtained by subtracting the EHD line shape (Figure 3.8b.) from intermediate (20 Wcm^{-2}) and high excitation level (200 Wcm^{-2}) spectra. The line shape is not observed to change in this range of excitation intensities and is very nearly that observed in the low level excitation spectrum.

The spectra of a sample containing 5×10^{18} cm^{-3} will be shown later in this chapter. The spectral analysis is not given here since it may be inferred from those of the previously discussed samples containing 3.9×10^{18} cm^{-3} and those of the 1.1×10^{19} cm^{-3} to be discussed below. The numerical values resulting from the analysis are listed in Table 3.3.

Figure 3.10 shows the spectra of a sample containing 1.1×10^{19} cm^{-3}. The excitation intensities are: a) high (150 Wcm^{-2}), b) intermediate (20 Wcm^{-2}) and c) low (2 Wcm^{-2}). The EHD peak very strongly dominates the high excitation level spectrum. The IB peak very strongly dominates the low level one. The photoluminescence intensity for samples with impurity concentrations above n_{crit} decreases strongly with increasing concentration and in addition the relative intensity of the EHD and IB peaks becomes more strongly dependent on excitation level. As shown in Figure 3.10c., only the IB peak is observed at low excitation level. The solid curve in Figure 3.10a.

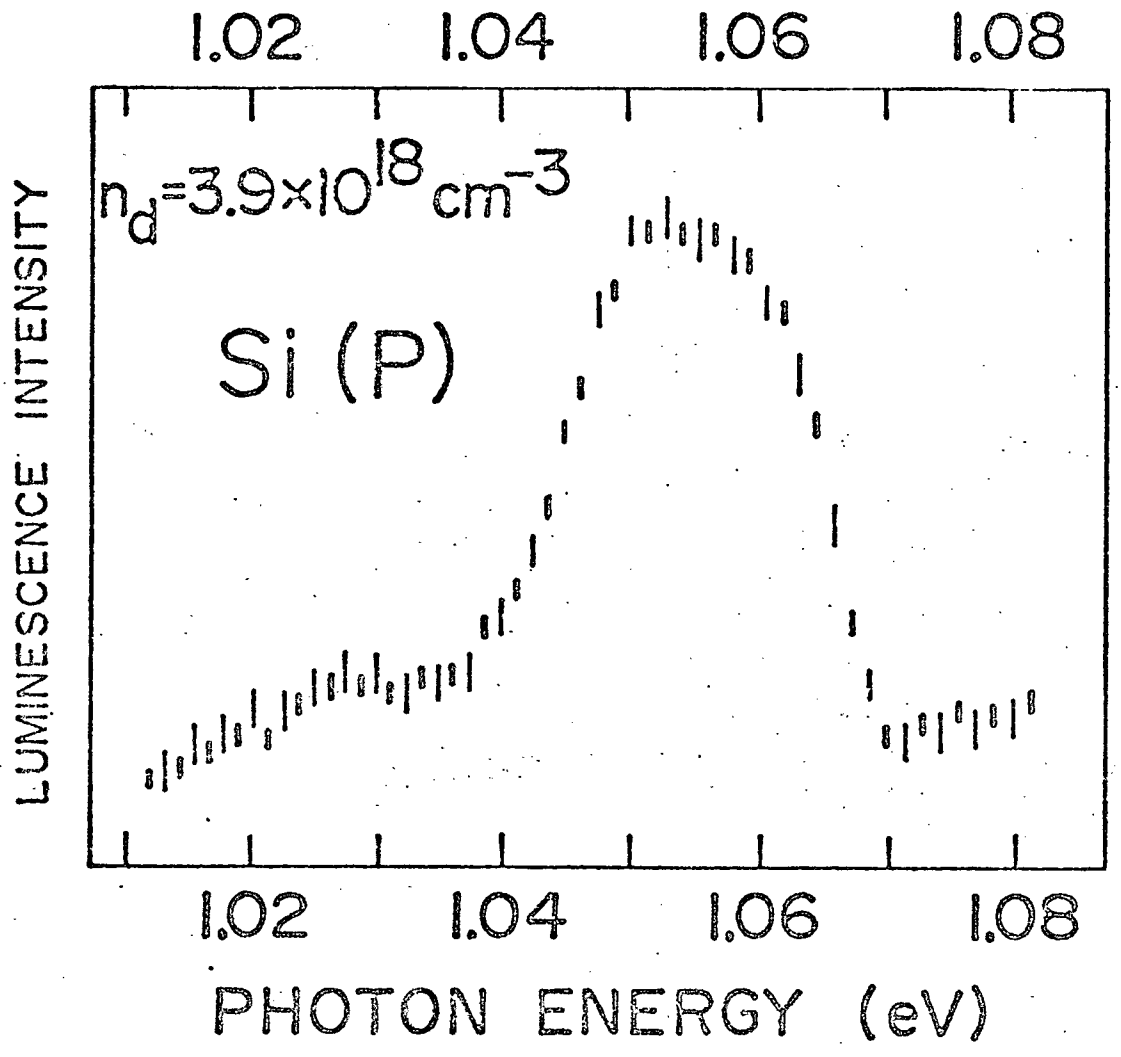

Figure 3.9: IB experimental photoluminescence line shapes of phosphorus-doped silicon containing 3.9 x 10^{18} cm^{-3}. Impurity band line shapes at excitation levels of 20 Wcm^{-2} (short flags) and 200 Wcm^{-2} (long flags) are shown. The flags represent two standard deviations due to signal averaging and to the subtracting process referred to in the text.

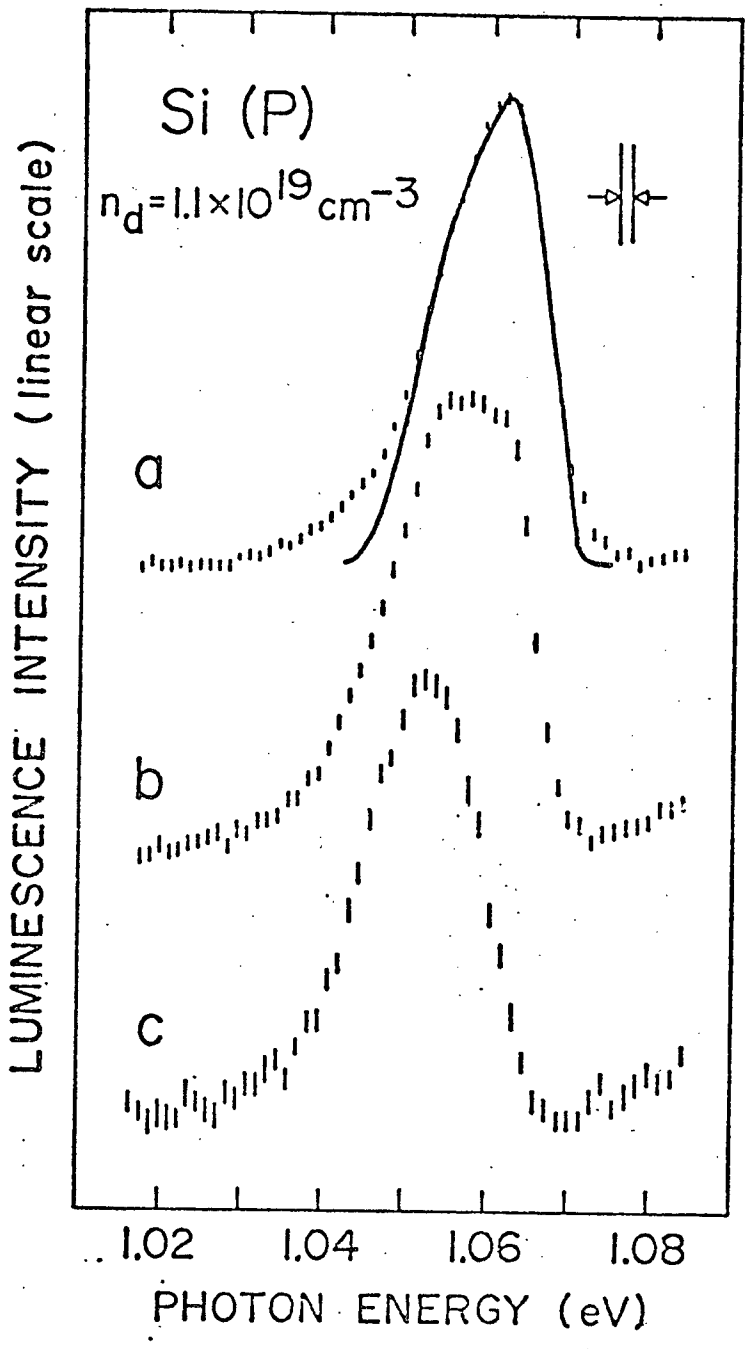

Figure 3.10: Photoluminescence spectra of silicon containing 1.1×10^{19} phosphorus cm^{-3} at T = 4.2 K are shown at three excitation levels.

a) At high excitation level (150 Wcm^{-2}, 5 scans) the EHD peak dominates the spectrum. The solid curve shows the theoretical fit to the EHD line shape.

b) At intermediate level (20 Wcm^{-2}, 15 scans) both the IB and EHD peaks are observed.

c) At low level (2 Wcm^{-2}, 35 scans) the IB peak dominates the spectrum.

shows the theoretical fit to the EHD peak. The EHD line shape is independent of excitation level in the range 80 to 200 Wcm^{-2}. The spectrum at intermediate excitation intensity (Figure 3.10b.) can be reproduced by adding the high excitation level spectrum (Figure 3.10a.) to the low level one (Figure 3.10c.), properly scaled.

For phosphorus-doped silicon a second characteristic concentration,[12] $n_{cb} \simeq 2 \times 10^{19}$ cm^{-3}, is evidenced in the measurement of the Knight shift of the NMR absorpiton peak for ^{29}Si as a function of impurity concentration. Alexander and Holcomb[12] argue that the Fermi level is above the conduction band edge for impurity concentrations greater than n_{cb}.

Figure 3.11 shows two spectra of a sample containing 4.0×10^{19} cm^{-3}. High (150 Wcm^{-2}) and low (5 Wcm^{-2}) excitation intensities have been used. The line shape of the observed peak depends on the excitation intensity within the range 5 Wcm^{-2} to 200 Wcm^{-2}. The line shape of the peak shows a decrease in the slope of the low and high energy side with increasing excitation level. These changes in line shape with excitation level could be interpreted in terms of unresolved broad EHD and IB peaks; however, one cannot make firm conclusions because of the absence of structure in the photoluminescence spectrum for 4.0×10^{19} cm^{-3}.

A summary of the photoluminescence studies in heavily phosphorus-doped silicon as a function of donor concentration at high excitation levels is shown in Figure 3.12. At this excitation level, the IB peak is only clearly observable at impurity concentrations close to the metal-semiconductor transition. Since Halliwell and Parsons[11] used higher excitations than those reported here it is not surprising that they were unable to detect the IB peak. The monotonic shift of the high energy threshold of the EHD peak to

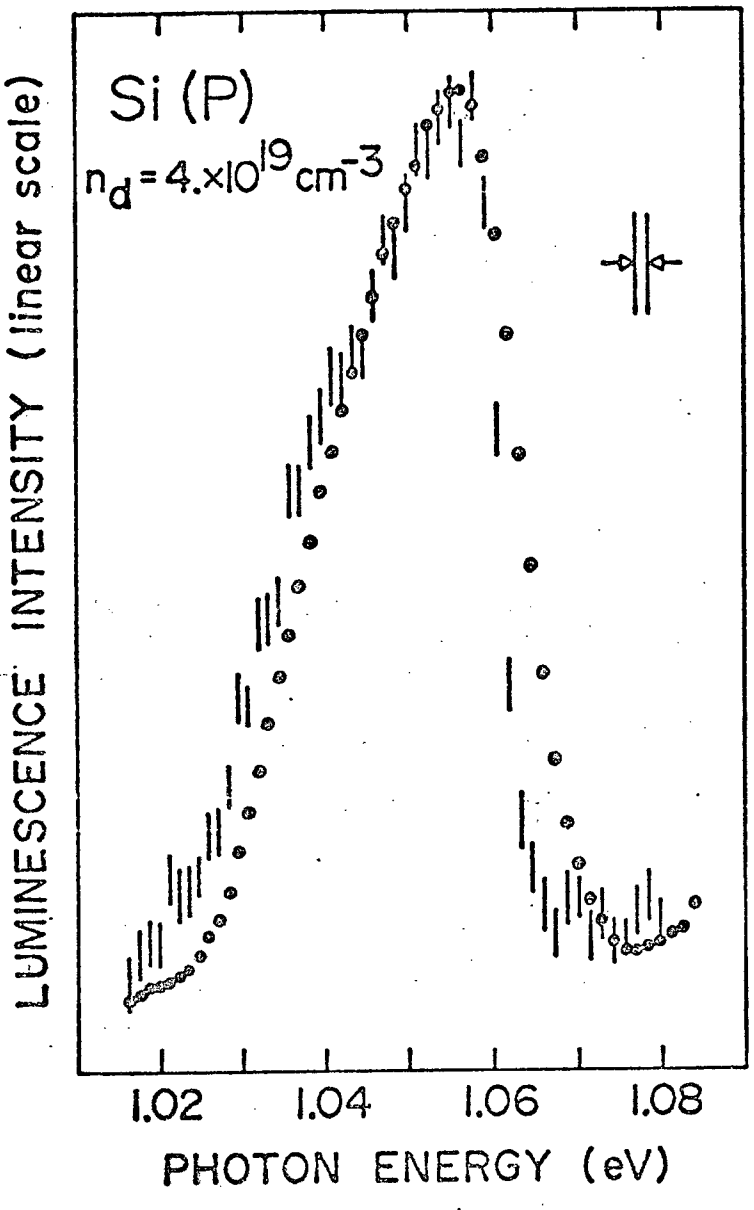

Figure 3.11: Photoluminescence spectra of silicon containing 4×10^{19} phosphorus cm^{-3} at T = 4.2 K are shown at two excitation levels. The solid points show a high excitation level (150 Wcm^{-2}, 10 scans) spectrum. The flags correspond to low level (5 Wcm^{-2}, 110 scans).

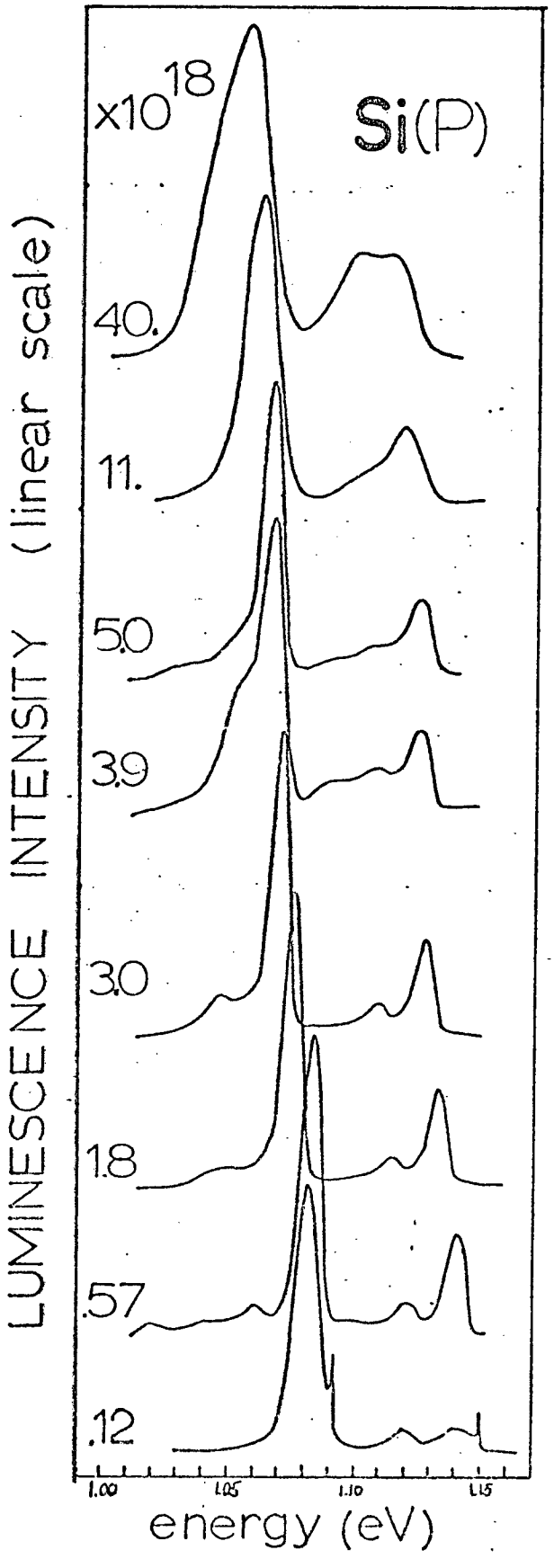

Figure 3.12: Concentration dependence of the photoluminescence of phosphorus-doped silicon at 4.2 K using high excitation intensities.

lower energies with increasing doping concentration follows closely the description of Halliwell and Parsons[11] as can be seen in Figure 3.13. A comparison of the width at half intensity of the EHD peak measured in this investigation with those reported by Halliwell and Parsons[11] is shown in Figure 3.14.

Figure 3.15 shows a plot of the ratio of the relative integrated intensity of the sum of the TA and NP replicas to the relative intensity of the TO phonon replica as a function of impurity concentration. The sum of the TA and NP replicas is used because they cannot be resolved over the whole range of impurity concentration studied here (see Figure 3.12). The fact that the NP plus TA replica grows with increasing n_d, with respect to the TO phonon replica, may be understood because the average inter-donor distance becomes of the order of the average inter-carrier distance in the droplet and consequently the probability of a recombination of an electron-hole in the vicinity of an impurity increases. It is presently not understood why this intensity ratio should level off for $n_d > 10^{18}$ cm^{-3} to a value approximately equal to the NP plus TA to TO ratio for the BE recombination radiation.

The photoluminescence measurements of the IB density of states in heavily phosphorus-doped silicon are summarized in Figure 3.16. The IB line shapes of the samples containing 1.8×10^{18} cm^{-3}, 2.45×10^{18} cm^{-3} and $3. \times 10^{18}$ cm^{-3} are not significantly different from each other. These samples will be referred to as the lower group. The IB peak, within this group, shows a slight shift to higher energy and an increase in band width with increasing concentration. The IB line shapes of the samples containing 3.9×10^{18} cm^{-3}, $5. \times 10^{18}$ cm^{-3} and 1.1×10^{19} cm^{-3} are also not significantly

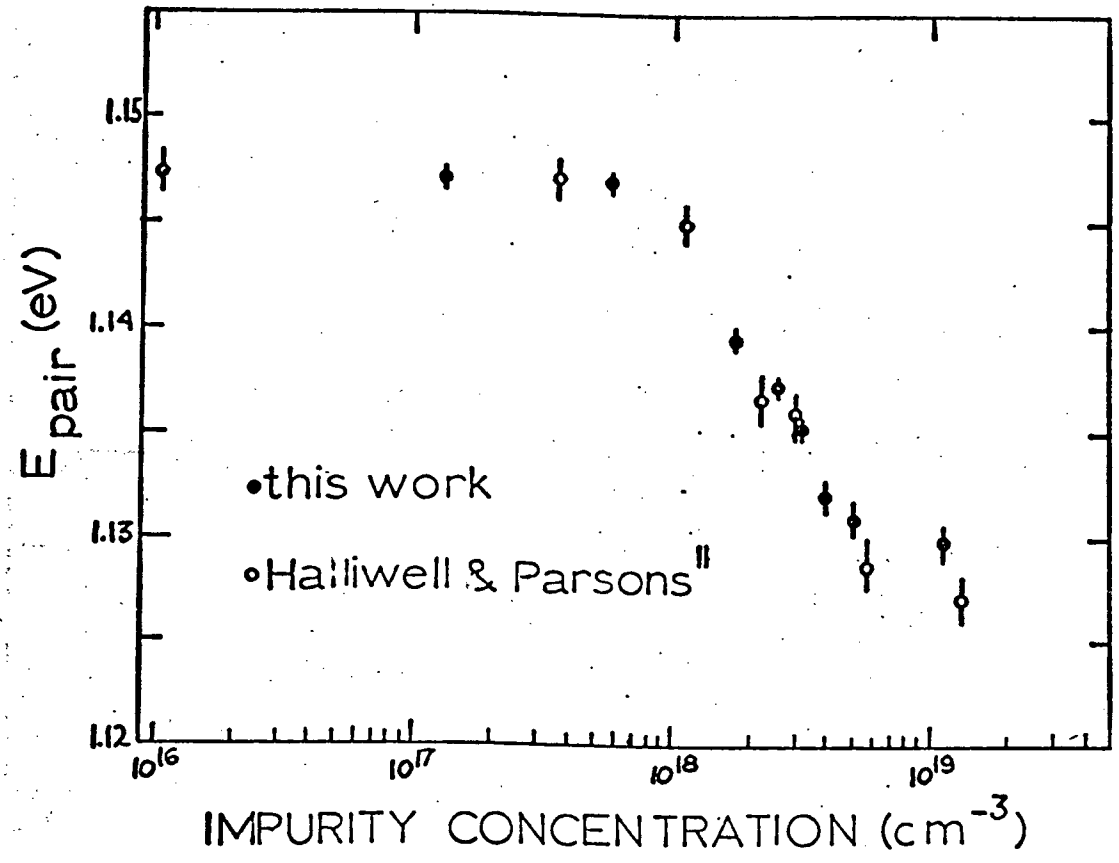

Figure 3.13: Concentration dependence of the threshold energy E_{pair}. Open circles show data points of Halliwell and Parsons[11].

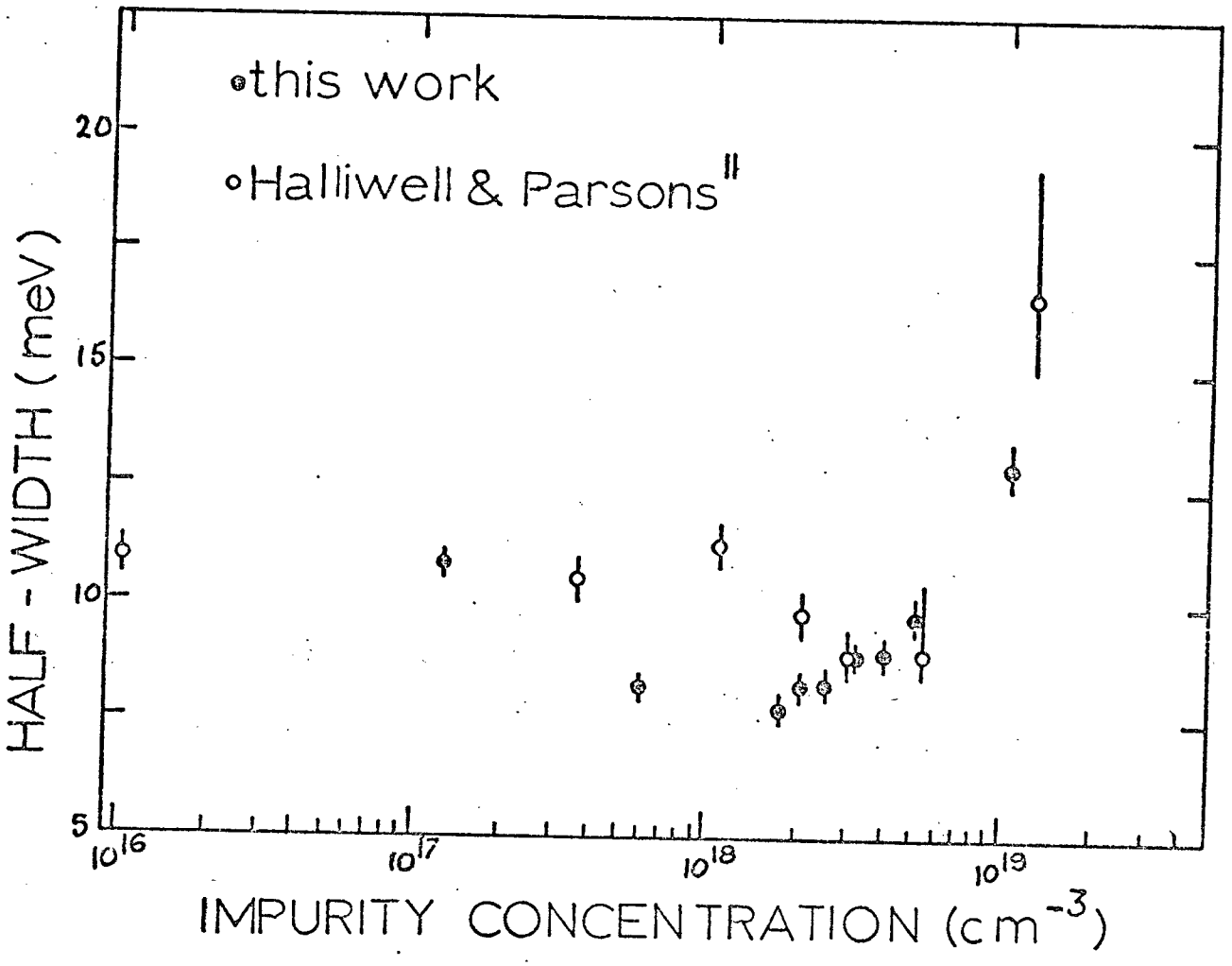

Figure 3.14: Width at half maximum of the TO-assisted peak as a function of phosphorus concentration at 4.2 K. Open circles show data points of Halliwell and Parsons[11] at 2 K.

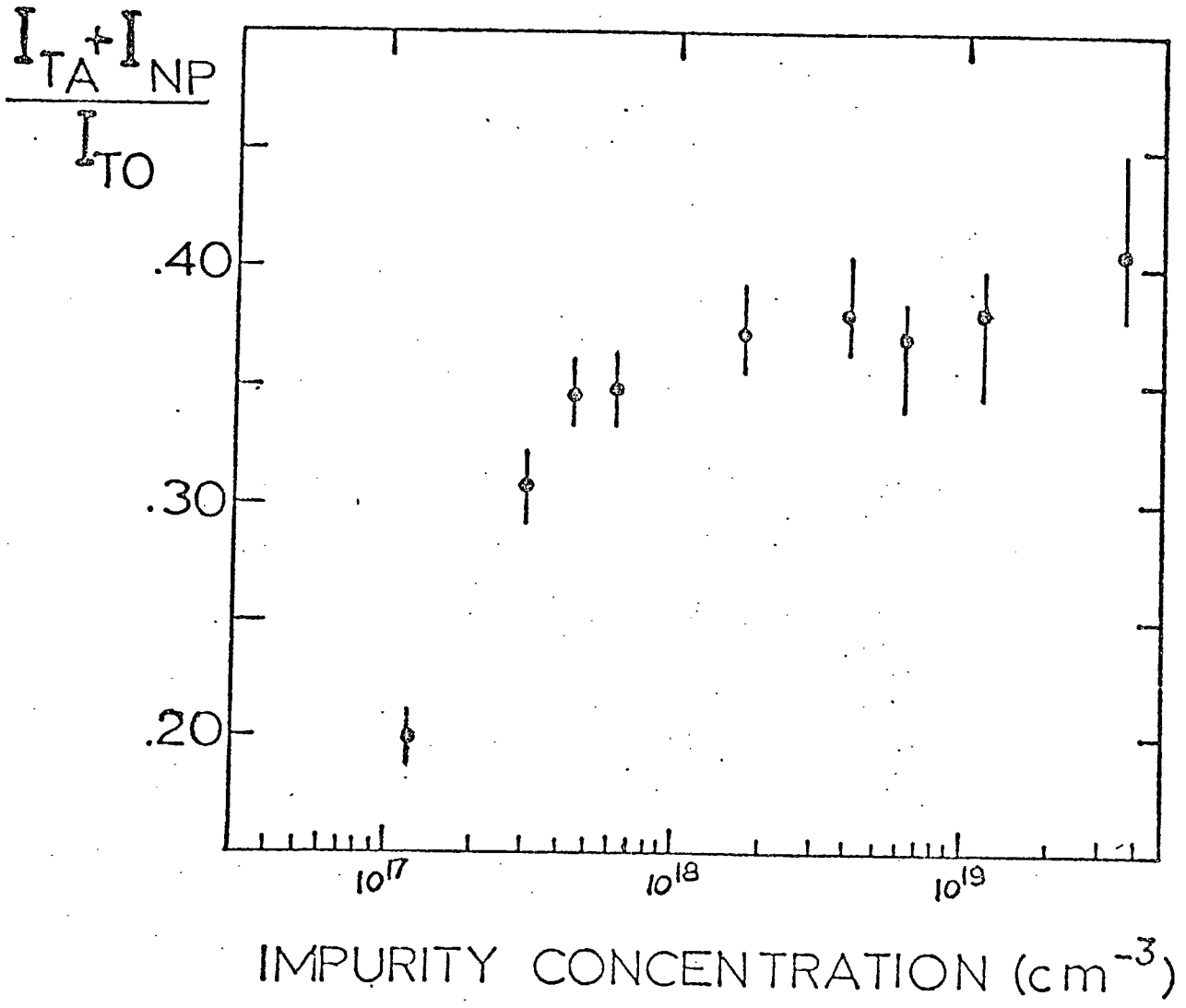

Figure 3.15: Concentration dependence of the ratio of the relative integrated intensity of the sum of the TA and NP replicas to the TO phonon replica.

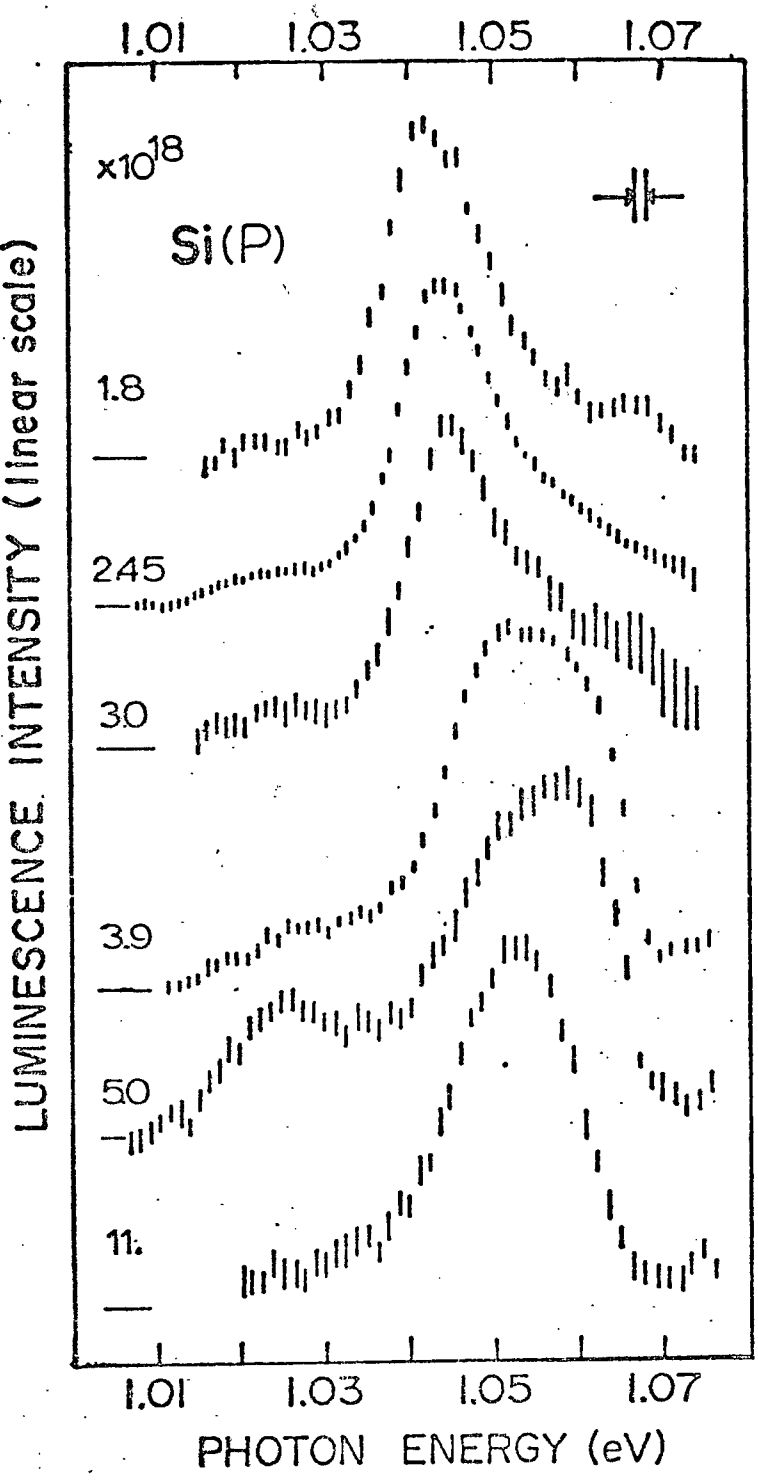

Figure 3.16: Concentration dependence of the experimental IB photoluminescence line shape of phosphorus-doped silicon at 4.2 K.

different from each other. These samples are referred to as the upper group. Within this group, there is only a slight change in the high energy side of the line shape. The change in line shape between the two groups of samples is remarkable. The IB peak of the upper group samples is shifted 8 meV to higher energy with respect to the peak of the lower group samples. The long tail of the line shape at high energies characteristic of the lower group samples is no longer observed in the line shape of the upper group; in fact, an edge is observed. It is clear that a change in the nature of the electronic states has occurred by increasing the impurity concentration from 3×10^{18} cm^{-3} to 3.9×10^{18} cm^{-3} and is attributed to the semiconductor-metal transition.

In Chapter 4 the Hubbard model[17] for the impurity band is presented. The IB line shapes for samples with phosphorus concentration below n_{crit} are successfully described within this model and a plausible explanation for the changes observed at the semiconductor-metal transition is discussed.

CHAPTER 4

IMPURITY BAND

4.1 Introduction

As mentioned in Chapter 3 the photoluminescence spectrum of heavily phosphorus-doped silicon at low excitation intensities is dominated by a peak associated with the recombination of an electron in the impurity band and a free hole. It has also been said that since the experiments are performed at near zero temperature the IB line shape gives directly the density of occupied states in the impurity band. In the present investigation the comparison of the experimental IB line shape with theoretical models of the impurity band is restricted to low impurity concentrations, $n_d < n_{crit} = 3 \times 10^{18}$ phosphorus cm^{-3}.

To calculate the density of states in the impurity band two different approaches are taken in the literature. The first approach is to locate the impurities in a superlattice and then perform a standard band calculation. Such a treatment for phosphorus-doped silicon is presented in the next Section. The second approach is to calculate the energy of a donor electron in all possible impurity configurations. The calculated energies fall in a range of energies referred to as the impurity band and the probability of finding the impurity configuration giving an energy E reflects the density of states of energy E.

Lukes et al[38] have calculated the density of states of the impurity band in the low impurity concentration limit where they reduced all possible impurity configurations by considering only impurity pairs and the distance, R, between the impurities was taken to follow the

Chandrasekhar[39] distribution. They use a simple hydrogen molecular ion (H_2^+) model of interaction between the impurities in a pair and the details of this calculation are given in Appendix B. The resulting impurity band density of states for $n_d = 1.8 \times 10^{18}$ cm^{-3} is compared to the experimental IB line shape in Figure 4.1. The width of the calculated density of states within this model is too broad and is a consequence of ignoring altogether electron-electron interactions. A hydrogen molecule model of interaction, suggested by Macek[40], is used to extend the previous calculation and is solved using the Heitler-London[41] method. The details of this calculation are also given in Appendix B. Figure 4.1 also compares with experiment the calculated IB photoluminescence line shape for the donor concentration $n_d = 1.8 \times 10^{18}$ cm^{-3}. The width obtained in the Heitler-London model is too narrow which is a consequence of the isolated pair approximation.*

The theory of the impurity band when the effect of randomness in the impurity distribution is neglected is reviewed in Section 4.2. From the mathematical point of view the treatment is the same as that of Eswaran and Bergersen which appears in an article published in collaboration with the author and others[19]. In this thesis a much greater emphasis is given to the justification of the assumptions and approximations of the mathematical treatment.

---

*The radius of a sphere of equal volume to a Wigner-Seitz cell obtained by arranging the impurities in a regular close-packed lattice is close to the mean distance of the Chandrasekhar[39] distribution.

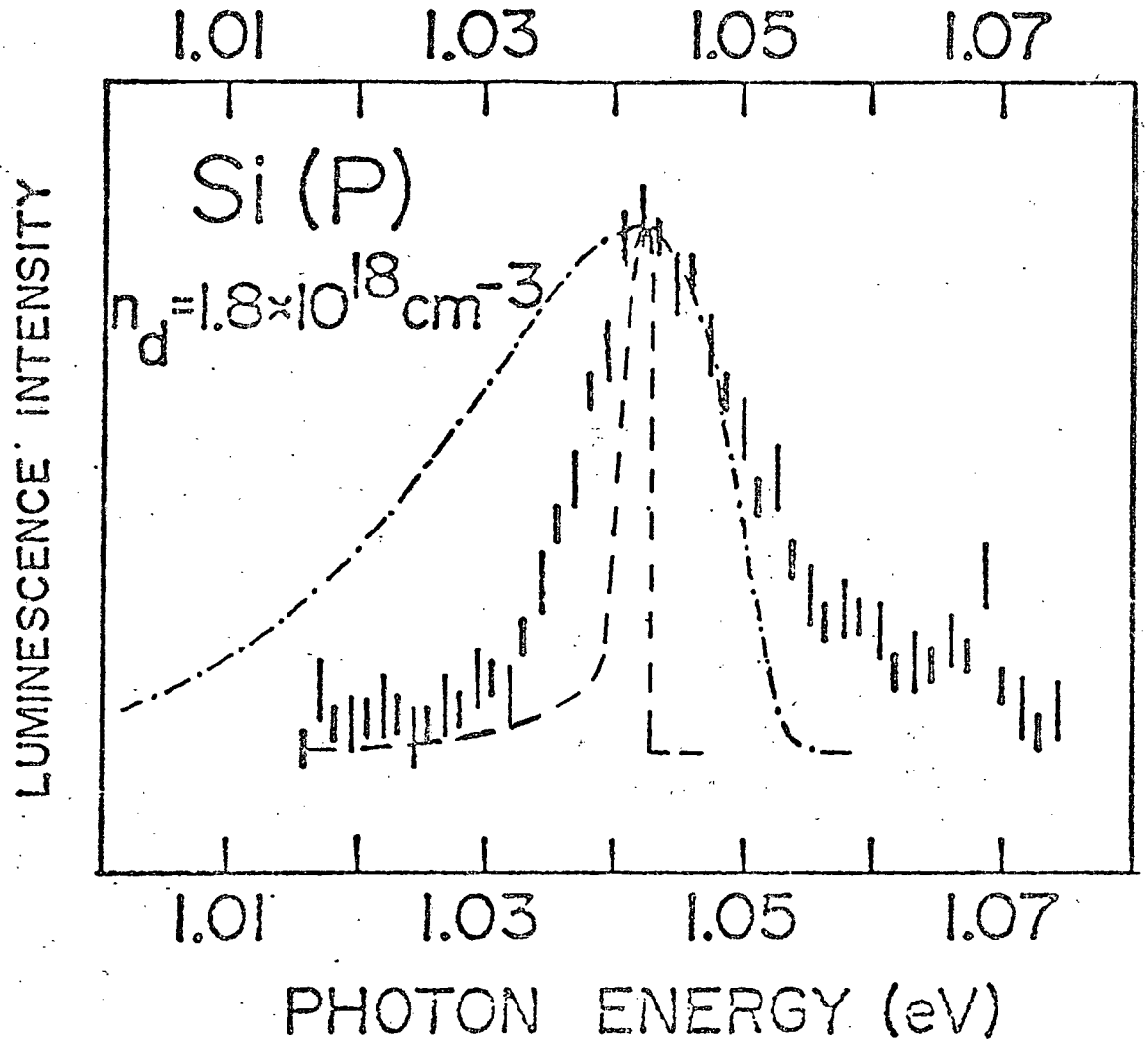

Figure 4.1: The experimental photoluminescence line shape for an electron in the impurity band and a free hole of silicon containing 1.8×10^{18} phosphorus cm^{-3}, represented by flags, is compared to the theoretical IB line shapes calculated in the (- - -) Heitler-London and (·—·—) H_2^+ models. The theoretical bands are shifted in energy and scaled for comparison with experiment.

4.2 The Impurities in a Superlattice

Let us begin by neglecting all electron-electron interactions. If the impurities are placed in a regular lattice the Hamiltonian is:

$$H = \sum_{i \neq j, \sigma} t_{ij} \; a^{+}_{i,\sigma} a_{j,\sigma} + T_o \sum_{i} n_{i,\sigma} \qquad (4.1)$$

where $a^{+}_{i\sigma}(a_{i\sigma})$ creates (destroys) an electron with spin σ in a Wannier state at site i, $n_{i\sigma} = a^{+}_{i,\sigma} a_{i,\sigma}$ the corresponding number operator, t_{ij} is the overlap integral of the lattice Hamiltonian between Wannier functions in the nth energy band from sites distant R_{ij} $(=|\bar{R}_i - \bar{R}_j|)$ apart[42] and is also known as the hopping integral and $T_o = \sum_k \epsilon_k$, ϵ_k being the energies in the nth band.

For impurity concentrations below the metal-semiconductor transition it is reasonable to describe the impurity band in the tight binding approximation. The Hamiltonian describing the impurity electron is given by

$$H = -\frac{\hbar^2}{2m_o} \nabla^2 + V_o(\bar{r}) + \sum_i U(\bar{r} - \bar{R}_i) \qquad (4.2)$$

where $V_o(\bar{r})$ is the periodic potential arising from the host atoms and $U(\bar{r} - \bar{R}_i)$ is the perturbing potential due to the impurity ion (bare potential) at site i:

$$U(\bar{r} - \bar{R}_i) = -\frac{e^2}{\epsilon|\bar{r} - \bar{R}_i|} \qquad (4.3)$$

where ϵ is the dielectric constant of the host. The Hamiltonian in equation 4.2 may be expressed in terms of the isolated donor Hamiltonian

$$H_\ell = -\frac{\hbar^2}{2m_o} \nabla^2 + V_o(\bar{r}) + U(\bar{r} - \bar{R}_\ell) \qquad (4.4)$$

so that

$$H = H_{\ell} + \sum_{m \neq \ell} U(\bar{r} - \bar{R}_m) \quad . \qquad (4.5)$$

So finally[42]

$$t_{ij} = < \phi(\bar{r} - \bar{R}_i) | \sum_{m \neq i} U(\bar{r} - \bar{R}_m) | \phi(\bar{r} - \bar{R}_j) > . \qquad (4.6)$$

where the wavefunction $\phi(\bar{r}-\bar{R}_i)$ has been taken to be the ground state atomic orbital at site i and is the eigenfunction of the isolated donor Hamiltonian H_i (equation 4.4). We restrict ourselves to the case where i and j are neighbouring impurities and the t_{ij} contains one 2-centre integral and five 3-centre integrals. If we know the functions $\phi(\bar{r}-\bar{R}_i)$ the problem is solved and we obtain a typical tight binding band centered at E_o with width[42]

$$\Delta = 2z\,|t_{ij}| \qquad (4.7)$$

where the coordination number z will be assumed hereafter to be 6 applicable to a simple cubic lattice.

As for all one-electron approximations one runs into the traditional problem of describing an insulator when one has only one s-electron per unit cell. One obtains, due to spin degeneracy, a half filled band for any inter-donor distance[42]. It has been known for a long time that in a many-electron system this difficulty is remedied by the electron-electron interactions[43]. A model that takes into account electron correlations to some degree has been presented by Hubbard[17]. He adds to the Hamiltonian given by equation 4.1 a term

$$H^1 = \tfrac{1}{2} U \sum_{i\sigma} n_{i,\sigma}\, n_{i,-\sigma} \, . \qquad (4.8)$$

The significance of this term is that the Coulomb repulsion, U, between electrons is taken into account only if the electrons are on the same site.

If U is larger than the unperturbed (tight binding) band width one has an insulator since now it is necessary to ionize at least one donor and to put the electron back on a distant occupied site for current to flow. The work necessary for this is the ionization energy less the electron affinity[44], thus approximately U.

In the large U limit, the Hubbard model implies that one electron is localized to each impurity site and double occupancy is forbidden. This clearly describes an insulator but when attempting to calculate the band, a question arises on the meaning of the hopping integral. To resolve this problem let us look upon the IB photoluminescence in terms of a transition from an initial state given by a hole in the top of the valence band to a final state of a hole in the impurity band, thus we are interested in the hole density of states in the impurity band. In the large U limit, one has an electron in each impurity site except one and in this picture the hopping integral has again a natural meaning: a hole in site i hops to site j; equivalent to the electron in site j hopping to site i. The hopping integral becomes equal to the leading term of the one electron tight binding one since now the bare potentials at nearest neighbour sites $m \neq i, j$ are screened by the electrons which are localized in those sites and to a good approximation can be neglected. Hence

$$t_{ij} = \langle \phi\,(\bar{r} - \bar{R}_i) | U(\bar{r} - \bar{R}_j) | \phi\,(\bar{r} - \bar{R}_j) \rangle. \qquad (4.9)$$

which is the same as that obtained in the mathematical treatment[19] referred above. In the treatment of Berggren[45] t_{ij} is different - the unperturbed bandwidth defined by him in terms of his integral T is inconsistent with

traditional tight binding[42, 46] and in error. The integral L of Berggren[45] corresponds and is equal to Equation 4.9. Thus, from the discussion above, it is clear that the density of states in the impurity band in the large U limit is going to resemble a tight binding band - scaled to ½ and full - which for narrow bands is parabolic to first approximation[17].

The wave function $\phi(\bar{r})$ for the ground state of an isolated impurity is obtained in the effective-mass approximation. Following Kohn[47] $\phi(F)$ is written as a wave packet consisting of Bloch functions $\psi_{\bar{k}_\ell}(\bar{r})$, at the six conduction band minima ($\bar{k}_\ell$, $\ell = 1, \ldots 6$) of the silicon host:

$$\phi(\bar{r}) = \sum_{\ell=1}^{6} \alpha_\ell F_\ell(\bar{r}) \psi_{\bar{k}_\ell}(\bar{r}) \quad , \tag{4.10}$$

where the coefficients α_ℓ for the ground state are $(6)^{-\frac{1}{2}}$ for all ℓ[47]. The $F_\ell(\bar{r})$ are hydrogen - like envelope functions which are approximately given by[48]

$$F_\ell(\bar{r}) = (\pi a^2 b)^{-\frac{1}{2}} \exp\{ - \{(x^2 + y^2)/a^2 + z^2/b^2\}^{\frac{1}{2}}\} \tag{4.11}$$

with the z-axis oriented along the longitudinal axis of the ℓth valley. The constants a and b are the transverse and longitudinal Bohr-like radii of the orbit and we choose their values, not in a variational procedure of the effective-mass equations[47] but by requiring that the eigenvalue be E_o, the observed ionization energy of an isolated donor[48]:

$$a = (2m_t E_o)^{-\frac{1}{2}} \; ; \quad b = a(m_t/m_\ell)^{\frac{1}{2}} \tag{4.12}$$

with the transverse and longitudinal masses given in Table 3.2. This choice of a and b gives the correct asymptotic behavior of the envelope functions which is of importance in the solution of the two centre integral t_{ij}. This integral has been solved by Miller and Abrahams[48] and the

analytic solution, considering only intra-valley terms, is:

$$t_{ij} = \frac{e^2}{6\epsilon a} \sum_{\ell=1}^{6} e^{-i\bar{k}_\ell \cdot \bar{R}_{ij}} (1 + R_\ell/a)\, e^{-(R_\ell/a)} \quad , \tag{4.13}$$

where

$$R_\ell = a\ (x_{ij}^2 + y_{ij}^2)/a^2 + z_{ij}^2/b^2\ )^{\frac{1}{2}},\ x_{ij} = x_i - x_j. \tag{4.14}$$

Upon squaring, keeping only intra-valley terms and finally spherically averaging over the orientations $\bar{R}_{ij}$, one obtains:

$$|t_{ij}|^2 = \left(\frac{e^2}{6\epsilon a}\right) (A_o + A_1 + A_2) \ , \tag{4.15}$$

where

$$A_n = \left(\frac{R}{a}\right)^n \int_0^1 dx\ (1 + \alpha x^2)^{n/2} \exp\ \{-2(R/a)(1+\alpha x^2)^{\frac{1}{2}}\} \tag{4.16}$$

with $\alpha = (a/b)^2 - 1$ and $R = |\bar{R}_{ij}|$, the inter-donor distance. (The corresponding expressions of Berggren[45] contain algebraic errors.)

Figure 4.2 compares the experimental IB line shapes for $n_d = 1.8 \times 10^{18}$ cm^{-3}, 2.45×10^{18} cm^{-3} and 3.9×10^{18} cm^{-3} with theoretical ones calculated by Bergersen et al[19] following the treatment of Hubbard[17] for finite U. The calculated density of states is not significantly different from a parabolic form:

$$n(E) \propto (\Delta/2)^{-1} \left\{1 - [(E - E_o)/(\Delta/2)]^2\right\}^{\frac{1}{2}} \text{ if } |E-E_o| < \Delta/2$$
$$= 0 \quad \text{otherwise.} \tag{4.17}$$

The theoretical line shapes have been energy shifted and scaled for comparison. As can be seen there is good agreement between the calculated and observed density of states and the theory predicts successfully the observed broadening of the band with impurity concentration. The observed tails of the IB photoluminescence are due to the randomness of the impurity distribution[45, 49-51].

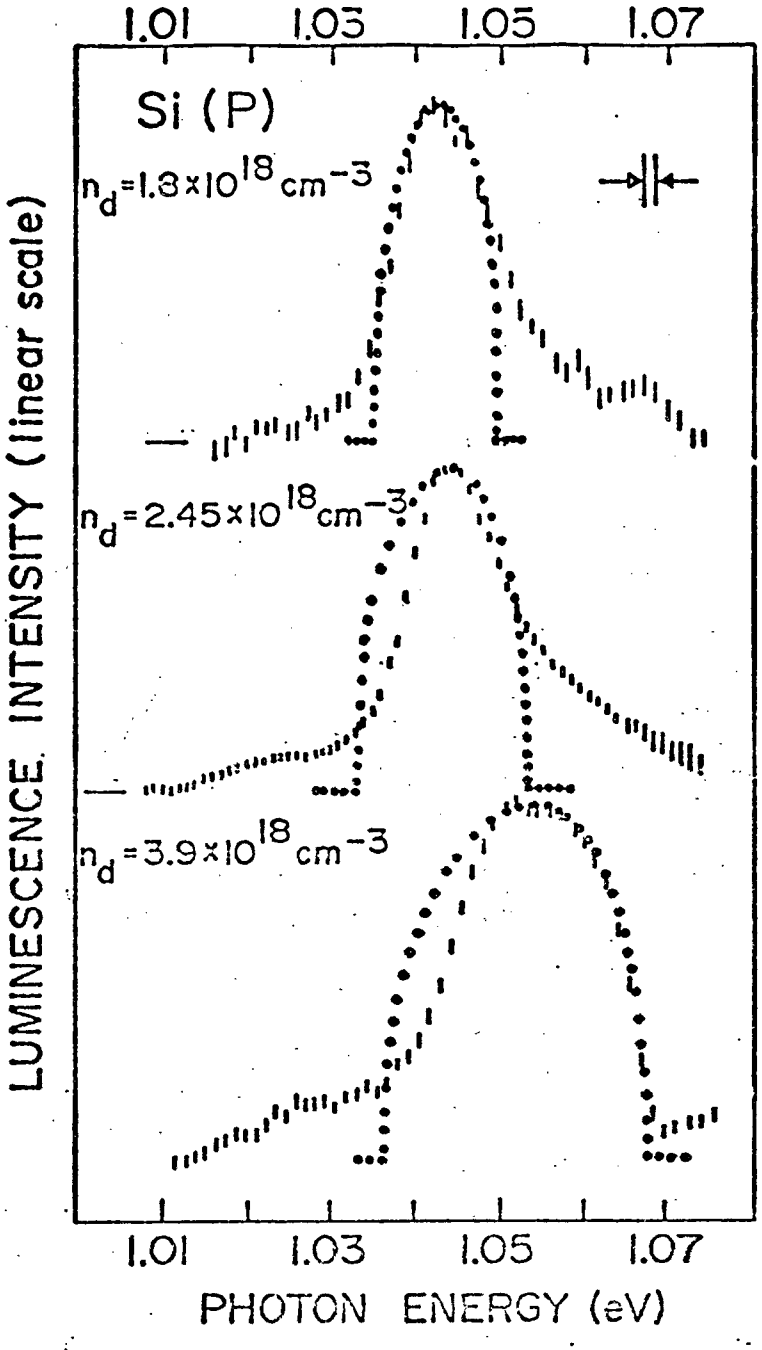

Figure 4.2 The experimental photoluminescence line shapes for the impurity band in Si(P) at donor concentrations 1.8 x 10^{18} cm^{-3}, 2.45 x 10^{18} cm^{-3} and 3.9 x 10^{18} cm^{-3} are represented by flags. The solid-dotted curves represent the theoretical impurity band density of states obtained in the Hubbard model.

To explain the lack of a high energy tail of the IB line shape of the sample containing 3.9×10^{18} phosphorus cm^{-3} it is necessary to look at Hubbard's model[17] in a less restrictive way. Hubbard[17] has shown that if $\Delta/U<1.15$ one obtains two distinct sub-bands separated by an energy gap. The lower sub-band closely resembles the band, calculated above, for the large U limit. Thus in this model the semiconductor - metal transition occurs at a donor concentration at which the two Hubbard sub-bands begin to overlap[17, 45, 51]. In reality, the transition is more complicated than that. The experimental results show that the occupied lower band has tails and it is reasonable to assume that the upper sub-band has developed tails as well. The tails are made up of localized states in the Anderson sense[49-51]. In reality, the tails of the lower and upper sub-bands will overlap at a lower concentration than in the case of a regular superlattice* and the semiconductor-metal transition is now believed to occur not when the bands start to overlap, but when the Fermi level lies in a region of delocalized states[51, 52]. In this picture - the Mott-Hubbard-Anderson model[52] - it is clear that in the metallic region the density of occupied states will not show a high energy tail but rather a Fermi edge. Furthermore, the shift to higher energy of the IB peak when n_d goes from slightly below n_{crit} to slightly above is an indication that every free electron helps loosen the remainder[42].

It was described in Chapter 3 that the relative intensity of the IB and EHD peaks is excitation intensity dependent. This experimental

---

*Using Hubbard's criterion $\Delta/U = 1.15$[17] to define the semiconductor metal transition with Δ as calculated here and U as given by Berggren[45] one obtains a critical density of 6×10^{18} cm^{-3}.

result is an indication that droplets coexist with the lower density phase. In thermodynamic equilibrium the chemical potentials of a pair in each phase are equal. E_{pair} is the chemical potential of a pair in the drop. The minimum energy to create a pair outside the drop assuming the Hubbard model is, intuitively, an energy close to the mobility edge[51] in the upper sub-band. Thus the high energy edge of the EHD shows approximately where the mobility edge is with respect to the lower sub-band so that for impurity concentrations below the semiconductor-metal transition one expects the IB peak to be at a lower energy than the EHD peak and as the impurity concentration increases one expects the two peaks to overlap - this is indeed observed. The conclusion to the above argument is an important one - E_{pair} is equal to the optical gap.

To end this Chapter an outline of the calculation of Eswaran et al[21] of the density of states in the infinite U limit of the Hubbard model when the impurities are randomly distributed is given. The density of states for a single hole is again of interest. The formalism follows Cyrot-Lackmann and Gaspard[53] who have calculated the density of states for the uncorrelated case (U = 0). The Green's function averaged over all configurations is expanded in terms of average moments: the moment μ_k of the density of states being the sum of the hopping contribution of all walks of k steps[54, 55] which return the hole to its home site. The hopping paths when averaged can be decoupled into irreducible paths or diagrams[53] and the sum of all irreducible diagrams of n steps defines the cumulant of nth order[53]. The importance of the cumulant approach is that it allows to judge the approximations to be made in different impurity density regimes by neglecting certain diagrams and that those which are kept contribute to

the moments of the density of states to all orders. In the high density regime the important contributions to the cumulant come from self-avoiding diagrams[21, 53, 54]; in the low density regime from those which the hole hops to and from between two impurity sites[21].

Figure 4.3 compares the calculated[21] density of states in the impurity band in the high and low density regimes with the IB experimental line shape for two different impurity concentrations. The widths at half maximum of the theoretical bands are in very good agreement with experiment. However, those calculations do not explain the sign of the slight skewness of the experimental line shape. The reason for this discrepancy is not understood.

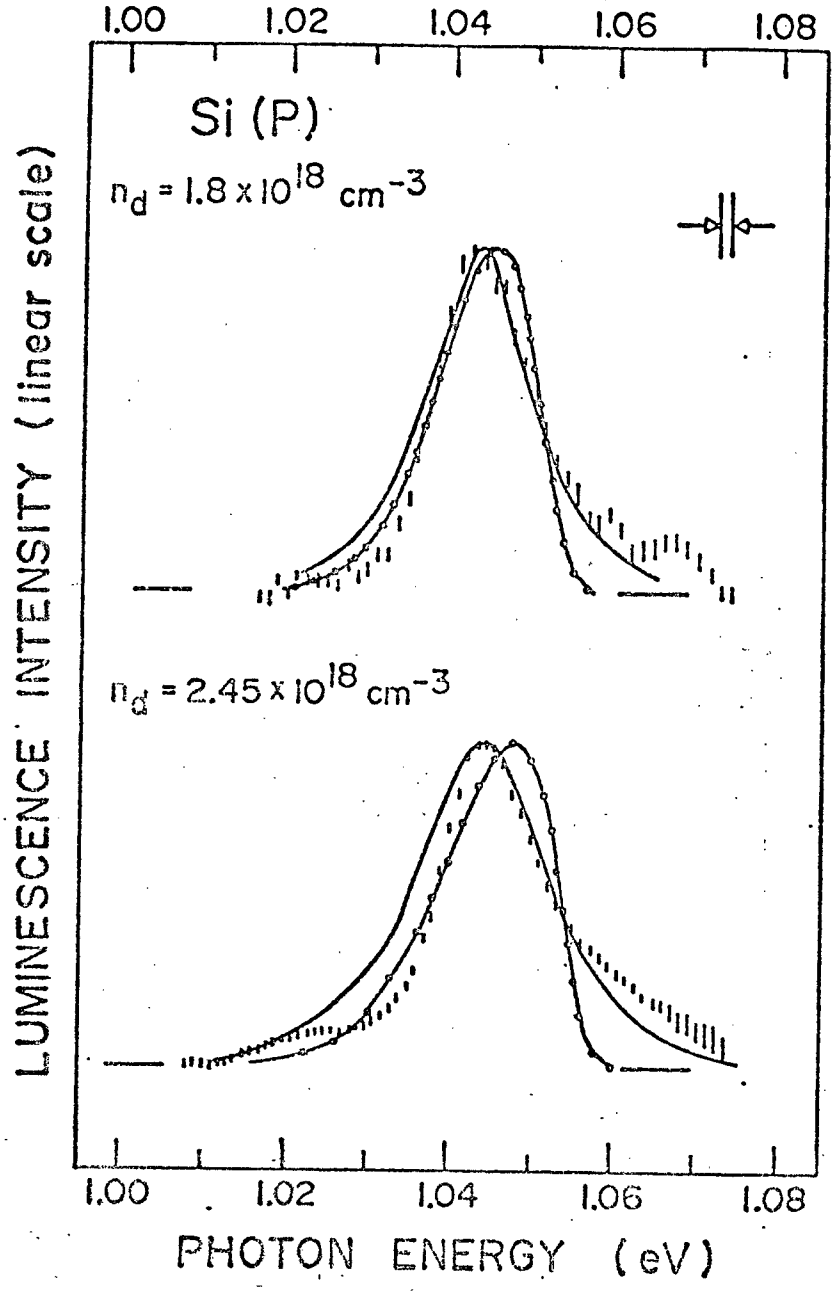

Figure 4.3: The experimental photoluminescence line shape for the impurity band in Si(P) at donor concentrations 1.8 x 10^{18} cm^{-3} are represented by flags. The solid and chained curves represent the theoretical impurity band density of states obtained using the low and high density cumulants, respectively.

CHAPTER 5

THE EHD IN HEAVILY DOPED SILICON

5.1 Introduction

This Chapter is concerned with the theory of the ground state of the EHD in heavily doped silicon and begins by showing that the previously published theoretical treatment by Bergersen et al[18, 19] is in error. The previous prediction of the existence of the EHD is established to be a consequence of subtle computer programming errors. It should be stressed that for donor concentrations above the semiconductor-metal transition the system under consideration by Mahler and Birman [56-58] is exactly the same as the one considered by Bergersen et al[18, 19]. Droplet stability predicted by Mahler and Birman[56-58] is believed to be a consequence of unphysical assumptions.

In Section 5.3, the theory of Bergersen et al [18, 19] is presented with a modification based on the experimental result that the EHD coexists with a lower density electron-hole plasma. This modified model is equally unsuccessful in predicting droplet stability. Speculative arguments for droplet formation in metallic silicon assuming that not all donors are ionized are presented in Section 5.4.

5.2 The Original Model

The silicon crystal is considered to be at absolute zero temperature and has a volume Ω. Let us assume that there exists a droplet of

volume V_d and in addition, that all photo-created carriers are within the droplet; thus $N(= n_h V_d)$ with, N, the total number of pairs kept constant by optical pumping. The total energy per unit volume $e(n_c, n_h)$ is the sum of the kinetic, exchange, correlation and impurity energies per unit volume associated with the indicated densities.

$$e(n_c, n_h) = e_{kin}(n_c, n_h) + e_{exc}(n_c, n_h) + e_{corr}(n_c, n_h) + e_{imp}(n_c, n_h). \quad (5.1)$$

Bergersen et al[18] have worked out these contributions in the Random Phase Approximation (RPA). Their treatment of the first three terms follows that of Combescot and Nozières[7] and is generalized to the case when the electron density differs from the hole density. The last term is added to take into account the interaction of the impurity ions with charge carriers[18]. In their second paper[19] they extend the treatment to include central cell corrections - the simplified analytic form of the dielectric function of the host suggested by Nara and Morita[59] is used in place of the static dielectric constant, which screens the Coulomb interaction between charges.

The details of each of the different energy contributions are treated extensively by Bergersen et al[18, 19] and are not repeated here. The resulting analytic expressions for each energy contribution are listed in Appendix D for computational purposes. Here, the discussion of this model is restricted to the energetics of EHD formation.

Following Bergersen et al[18, 19], the total energy in the crystal is:

$$E_{crystal} = (\Omega - V_d)\, e(n_d, 0) + V_d\, e(n_d + n_h, n_h) \quad , (5.2)$$

where we have assumed, as in Chapter 3, that the drop is neutral ($n_c = n_d + n_h$) and, as we shall assume throughout this chapter, n_d fixed. Using $N = V_d\, n_h$ Equation 5.2 is:

$$E_{crystal} = \Omega\, e(n_d, 0) + N\{\frac{1}{n_h}\,[e(n_d + n_h, n_h) - e(n_d, 0)]\}. \tag{5.3}$$

The free parameter, n_h, is determined by the requirement that $E_{crystal}$ is minimum which leads to the condition:

$$\bar{E}(n_d+n_h,n_h) \equiv \frac{1}{n_h}\,[e(n_d+n_h,n_h) - e(n_d, 0)] = \text{minimum}. \tag{5.4}$$

It is instructive to derive Equation 5.4 from a different starting point, namely, by the requirement of mechanical equilibrium: the pressure inside and outside the droplet is equal. Hence

$$(\frac{\partial}{\partial V_d}\, V_d\, e(n_d+n_h,n_h))_N = (\frac{\partial}{\partial V_{out}}\, V_{out}\, e(n_d,0))_{N=o} = e(n_d,0) \tag{5.5}$$

and changing variables ($N=V_d\, n_h$) Equation 5.5 leads to:

$$\frac{\partial}{\partial n_h}\, e(n_d+n_h,n_h)\Big|_{n_h^*} = \frac{1}{n_h^*}\,[e(n_d+n_h^*,n_h^*) - e(n_d,0)]\ . \tag{5.6}$$

By using the identity[18]

$$\frac{\partial}{\partial n_h}\, e(n_d+n_h,n_h) = \frac{1}{n_h}\,[e(n_d+n_h,n_h) - e(n_d,0)]$$

$$+ n_h\, \frac{\partial}{\partial n_h}\{\frac{1}{n_h}\,[e(n_d+n_h,n_h) - e(n_d,0)]\}\ , \tag{5.7}$$

it follows that n_h^* is also determined by Equation 5.4. (If n_h, when

$n_h \to 0$ is not a solution to Equation 5.4 then droplet formation is energetically favorable.)

In addition, it can be easily shown that the chemical potential of an electron-hole pair in a plasma, at zero temperature, is:

$$\mu(T=0,\ n_c,\ n_h) = \frac{\partial}{\partial n_h} e(n_c,\ n_h) \quad , \tag{5.8}$$

hence at quasi-equilibrium

$$E_{pair} \equiv \mu(T=0,\ n_c,\ n_h^*) = \bar{E}(n_c,\ n_h^*) \quad , \tag{5.9}$$

which, as pointed out in Chapter 3, is experimentally measurable.

Mahler and Birman[56-58] have chosen to formulate the energetics of droplet formation in terms of average energies per carrier. This choice complicates the problem unnecessarily. To solve for the quasi-equilibrium pair density (equal to n_h) they calculate the pressure inside the droplet in terms of partial pressures: one due to the photo-created pairs, the other due to donor electrons. Since from the onset they assumed all donors within the drop to be ionized, that is, photo-created and donor electrons are indistinguishable, hence their partial pressure procedure leads to the violation of the Pauli Exclusion Principle. The treatment of Bergersen et al[18, 19] leading to the condition of quasi-equilibrium (Equation 5.4) does not have the difficulties described above. Furthermore, it is rigorous and therefore will be followed.

Before starting with the actual calculation one should determine in which density regime the RPA is valid. Past experience with this high

density approximation shows that, in the present context, it is reasonable to assume that it works well for such densities where the inter-carrier distance is less than the Bohr radius of an isolated impurity, namely for $n_c > 3 \times 10^{19}$ cm^{-3}. It is then necessary to justify the use of RPA for carrier concentrations which are an order of magnitude less. For the EHD in intrinsic material, where such carrier densities are also encountered, Bhattacharyya et al[60] argue that one can expect corrections to the correlation energy that go beyond RPA to be about 20 percent. On the other hand, following Bergersen et al[19], consider the two terms $e(n_c, n_h)$ and $e(n_d, 0)$ when calculating $\bar{E}(n_c, n_h)$: for impurity densities of the order of magnitude of the quasi equilibrium hole density ($n_h^* \sim 1\text{-}3 \times 10^{18}$ cm^{-3} obtained in Chapter 3), $e(n_c, n_h)$ and $e(n_d, 0)$ are of the same order and their absolute errors could well be about the same and therefore cancel to a considerable degree. The same is true - more so - for the chemical potential. For lower impurity densities the calculation of $e(n_d, 0)$ is totally unreliable and was replaced, from physical arguments, by

$$e(n_d, 0) = n_d E_o \qquad (5.10)$$

with E_o the ionization energy of an isolated donor. For these impurity concentrations the cancelling of errors described for higher densities may not take place and theoretical results for $n_d < 3 \times 10^{18}$ cm^{-3} should be viewed with caution.

The arguments given here for the correlation energy carry over to the impurity energy contribution so that it is believed that the RPA should work reasonably well for metallic silicon.

Figure 5.1 shows the result of calculating $\bar{E}(n_c, n_h)$ as a function of n_h for the donor concentrations 3.1×10^{18} cm^{-3}, 6.2×10^{18} cm^{-3} and 1.24×10^{19} cm^{-3}. For all three impurity concentrations it is quite clear that the condition of quasi equilibrium is found when $n_h \to 0$, therefore, droplet formation is not predicted for metallic silicon within the model of Bergersen et al[18, 19].

To show that the results of Mahler and Birman[56-58] are not a consequence of ignoring the impurity energy contribution in Equation 5.1, Figure 5.2 shows the corresponding results. Again it is quite clear that $\bar{E}(n_c, n_h)$ has a minimum when $n_h \to 0$. By comparing Figures 5.1 and 5.2 one observes that the effect of including the impurity energy contribution is to lower the energy by an amount which is almost independent of n_h.

The experimental results in this thesis point to the most serious problem in this calculation: the rigid band approximation. For high hole densities this assumption is justifiable by the excellent fit of the EHD line shape but in the gas phase the experiment shows that the parabolic band assumption is nonsense. Therefore, the calculation of $e(n_d, 0)$ is suspected. In fact, for example for $n_d = 6.2 \times 10^{18}$ cm^{-3}, if one increases $e(n_d, 0)$ by 2 percent one obtains a minimum in $\bar{E}$ vs. n_h with n_h^* approximately equal to $1. \times 10^{18}$ cm^{-3} - but E_{pair} turns out to be larger than $\mu(n_h \to 0)$ so that droplet formation is energetically unfavorable.

Figure 5.3 shows the results of calculating $\bar{E}(n_c, n_h)$ as a function of n_h for the impurity concentrations of 2×10^{17} cm^{-3} and

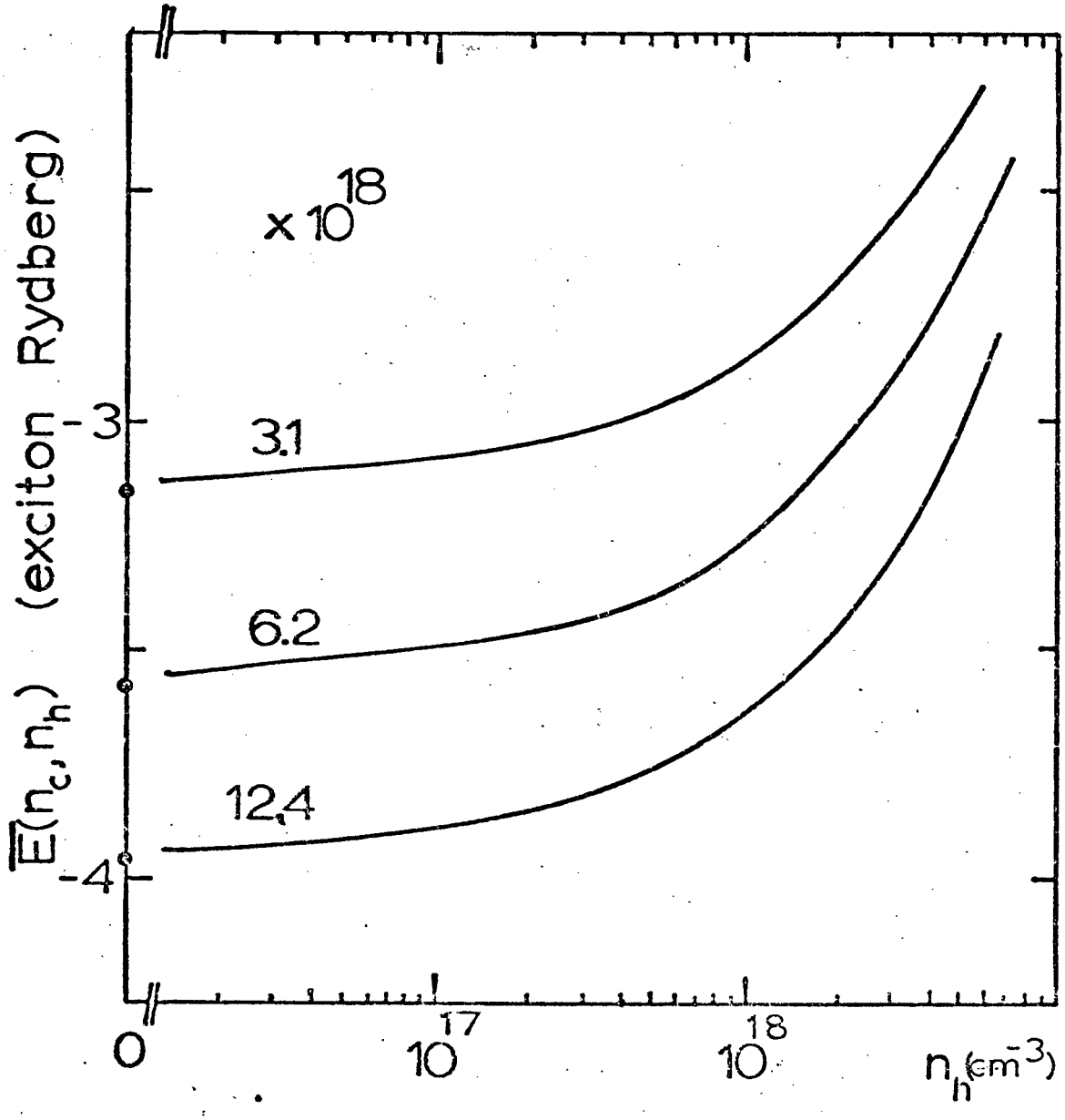

Figure 5.1: The calculated average energy per pair as a function of hole density for the indicated phosphorus impurity concentrations. The points on the ordinate-axis are the calculated values of the chemical potential of a pair in the limit of zero pair density.

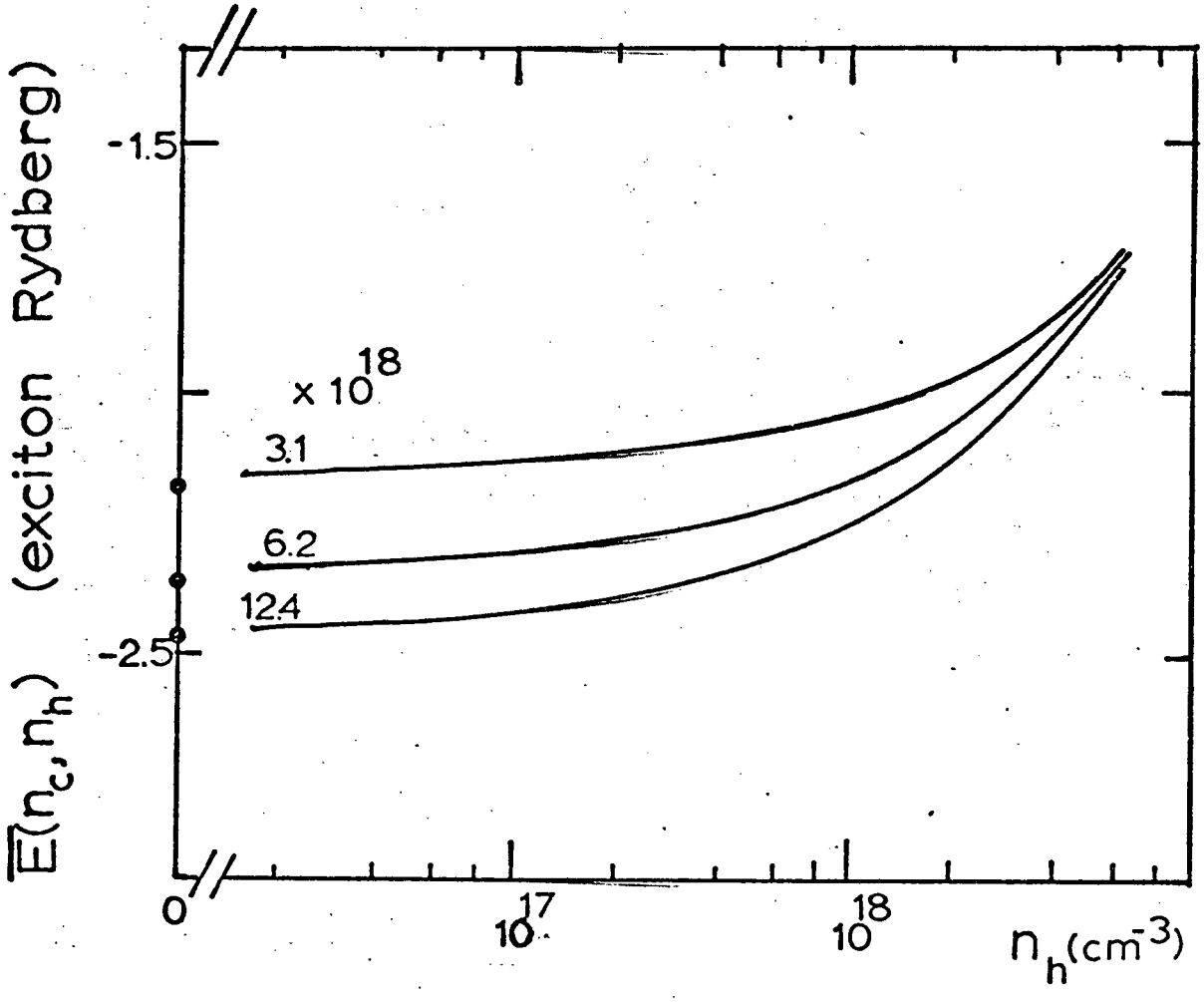

Figure 5.2: The calculated average energy per pair as a function of hole density for the indicated phosphorus impurity concentrations. The impurity energy contribution (Equation 5.1) is neglected. The points on the ordinate-axis are the calculated values of the chemical potential of a pair in the limit of zero pair density.

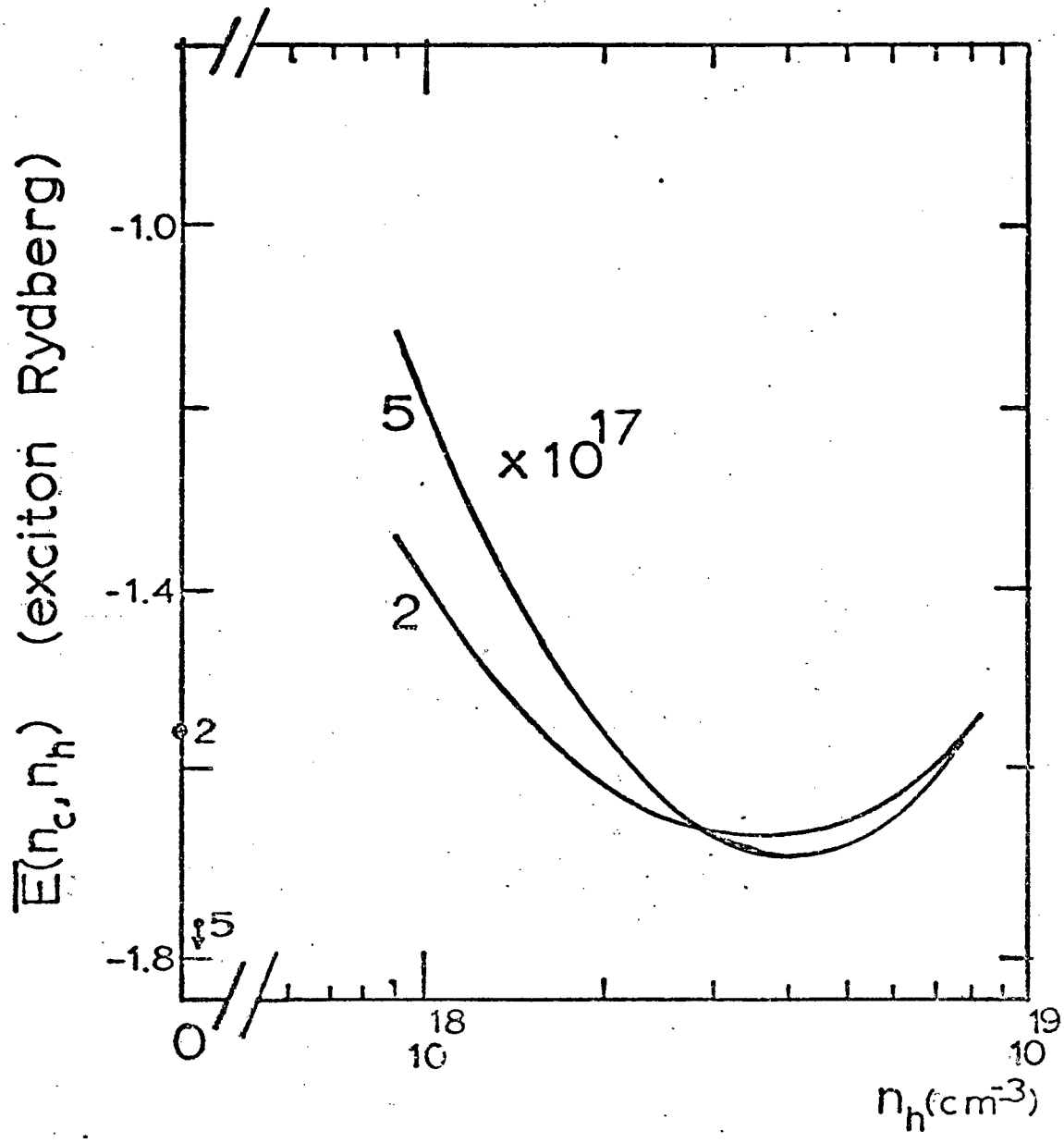

Figure 5.3: The calculated average energy per pair as a function of hole density for the indicated phosphorus impurity concentrations. The ionization energy of an isolated phosphorus donor is used as the energy per electron outside the droplet. The point on the ordinate-axis is the calculated value of the chemical potential of a pair in the limit zero pair density for $n_d = 2 \times 10^{17}$ cm^{-3}: the calculated value for $n_h = 5 \times 10^{17}$ cm^{-3} is off scale.

5×10^{17} cm^{-3} using Equation 5.10 to calculate $e(n_d, 0)$. In these cases $\bar{E}(n_c, n_h)$ has a clear minimum. E_{pair} is within three percent of the experimental value and is not excessively dependent on variations to $e(n_d, 0)$. On the other hand, variations to $e(n_d, 0)$ produce very large changes in the quasi-equilibrium hole density. The condition, $\mu(n_h \to 0) > E_{pair}$, for droplet to be energetically favorable is only met for $n_d < 3 \times 10^{17}$ cm^{-3}. Special significance should not be given to this result since $\mu(n_h \to 0)$ could be very wrong for this low impurity densities.

5.3 The Modified Model

As pointed out in previous Chapters there is reason to believe that at 4.2K the EHD and the gas phase coexist. Furthermore, since N, the number of photo-created pairs, is kept constant by optical pumping, it will be assumed that the two phases are in quasi- thermodynamic equilibrium. Hence

$$T_{gas} = T_{liq} \quad , \tag{5.11}$$

$$P_{gas} = P_{liq} \quad , \tag{5.12}$$

and

$$\mu_{gas} = \mu_{liq} \quad . \tag{5.13}$$

In the present situation it is more convenient to show the chemical potential vs n_h isotherms than the usual pV diagrams for liquid-gas phases. A typical μ vs n_h which describes two phases in equilibrium[61] is shown in Figure 5.4.a. The region with $d\mu/dn_h < 0$ cannot sustain a stable phase. The Maxwell construction produces the two phases. When we decrease the

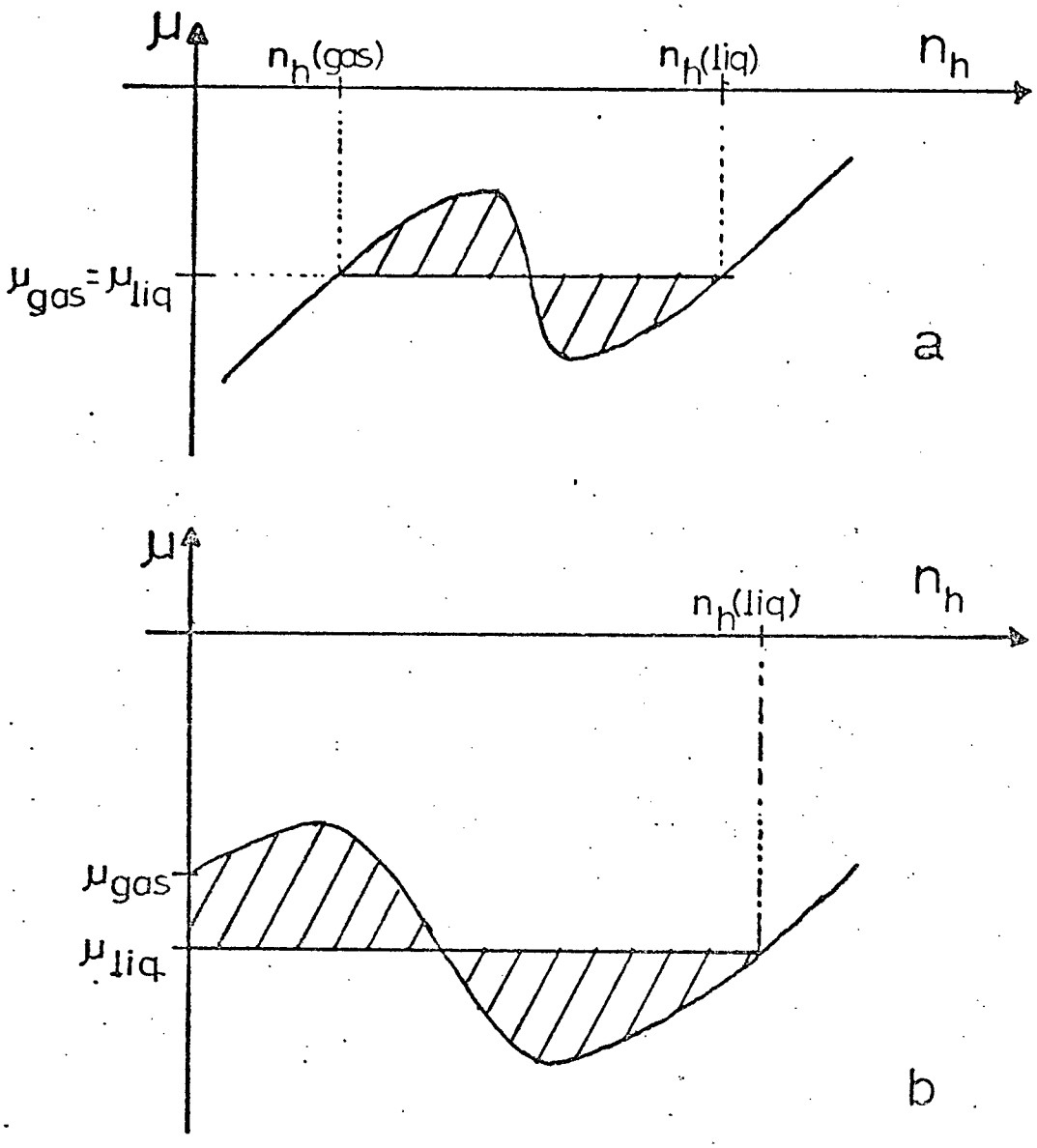

Figure 5.4: Chemical potential of a pair as a function of hole density in the following cases:

a) Droplets are in thermodynamic equilibirum with a gas phase.

b) The gas phase contains no holes in contact with droplets which are energetically favored. There is mechanical equilibrium.

temperature to zero two things may happen: the hole density in the gas phase may remain larger than zero or may become zero. In the former case the μ vs n_h isotherm will be as in Figure 5.4.a. If the stable gas phase has no holes in contact with the liquid the ordinary Maxwell construction does not work but is easily generalized* and as shown in Figure 5.4.b.

$$\mu_{gas} > \mu_{liq} \quad , \tag{5.14}$$

and there is no thermodynamic equilibrium but formation of droplets is energetically favorable. This quasi-equilibrium situation is the model of Bergersen et al[18, 19] and Mahler and Birman[56-58] discussed in the previous Section.

In both cases, if droplets exist, the μ vs n_h at T = 0 diagram shows a local maximum and a local minimum, hence it is unnecessary to determine a priori what the density of holes should be in the gas phase. The drawback of this model is that one encounters again the problem that the density of states is far from being parabolic even in metallic silicon at low hole densities so that we have no hope of calculating realistically μ vs n_h for all n_h. A brute force calculation, assuming the rigid band approximation to be valid for all n_h in metallic silicon, was performed hoping that a local minimum would show up at a high hole density where the calculation could be believable - the minimum was not found. For completeness the results of this calculation for impurity concentrations of 3.1×10^{18} cm^{-3}, 6.2×10^{18} cm^{-3} and 1.24×10^{19} cm^{-3} are shown in Figure 5.5.

---

*I thank Dr. G. Kirczenow for pointing this out.

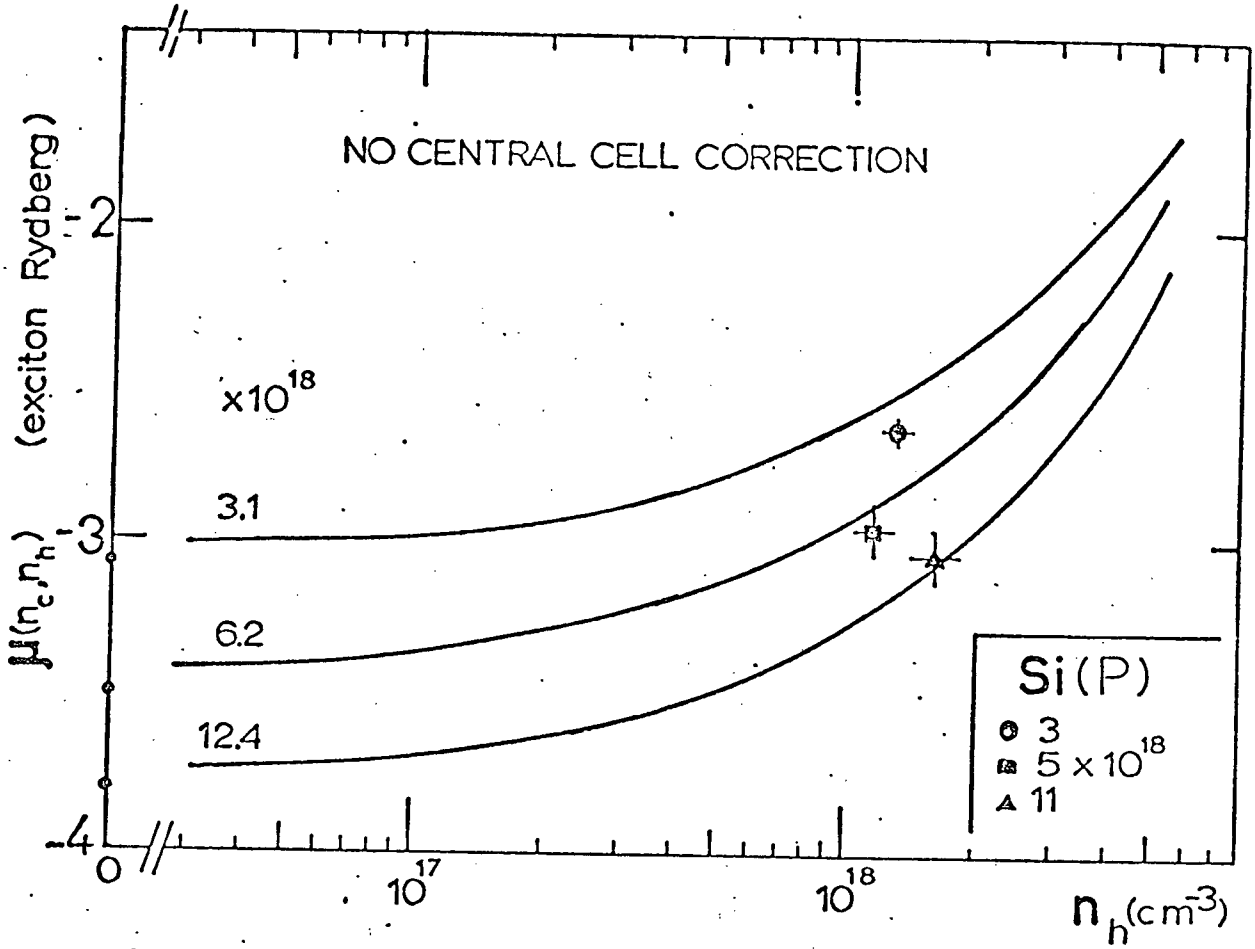

Figure 5.5: The calculated chemical potential of a pair as a function of hole density for the indicated phosphorus impurity concentrations. The points on the ordinate-axis are the calculated values in the limit of zero pair density. The experimental points (see Chapter 3) are shown for comparison.

5.4 Droplets?

In Section 5.2 droplet formation was dismissed even though the equilibrium condition given by Equations 5.4 and 5.9 were met by changing $e(6.2 \times 10^{18}, 0)$ by two percent because $\mu(n_h \to 0) < E_{pair}$. In Section 5.3 droplet formation is again dismissed because μ vs n_h does not show a "kink" which would have had to appear at low hole densities. The question arises: should one conclude that there are no droplets based on the calculation of the chemical potential of a pair for low hole densities for which the rigid band approximation is shown experimentally to be nonsense? Clearly, the theoretical calculations are inconclusive one way or the other. The need of more theoretical work is evident.

A promising route for further theoretical development is to consider localized states. Quirt and Marko[62, 63] have extensively studied the ratio of delocalized to localized electrons in Si(P) for the same impurity concentrations used here. They have used spin susceptibility studies to determine that at impurity concentrations two times above n_{crit} 10 to 20 percent of the electrons are localized, in fact even for $n_d \sim 2 \times 10^{19}$ cm^{-3} they claim two percent localized electrons. If this is in fact the situation when no photo-created carriers are present then it is reasonable to assume, to first approximation, that the density of localized electrons is equal to the density of neutral donors. Furthermore, let us assume that the density of ionized donors, n_{di}, and the density of neutral donors, n_{dn}, are functions of the hole density n_h. The simplest approach is to calculate the total energy per unit volume in the plasma by summing two terms: to calculate the first term we ignore all the neutral donors, thus this term is calculated exactly as in previous sections

except that the impurity density is assumed to be n_{di}; the second term calculates energy contribution of the neutral donors assuming that average energy of the electrons is E_n below the conduction band minimum. The total energy per unit volume is now

$$e(n_c, n_h) = e(n_{di}(n_h) + n_h, n_h) + E_n\, n_{dn}(n_h) \quad , \qquad (5.15)$$

with

$$n_d = n_{di}(n_h) + n_{dn}(n_h) \quad , \qquad (5.16)$$

for all n_h and the chemical potential at zero temperature is now:

$$\mu(n_c, n_h') = \left(\frac{\partial}{\partial n_h} e(n_{di}(n_h) + n_h, n_h)\right)_{n_{di}(n_h)} + \left[\left(\frac{\partial}{\partial n_{di}} e(n_{di}(n_h) + n_h, n_h)\right)_{n_h} - E_n\right] \times \frac{\partial}{\partial n_h} n_{di}(n_h)\Big|_{n_h'} \qquad (5.17)$$

which will depend on how the density of ionized impurities changes with the photo-created pair density. The problem could be solved by using the mechanical equilibrium condition to obtain an equation that would then be solved self-consistently with Equations 5.16 and 5.17 for n_h(gas) and n_h(liq) with only one parameter, either $n_{di}(0)$ or E_n. This calculation is beyond the scope of this thesis and I will restrict myself to speculating on the chemical potential as given in Equation 5.17.

Let us imagine that $n_{di}(n_h)$ varies linearly over a very large range of n_h so that the second term in Equation 5.17 is neglected. We calculate the first term for the two extremes of $n_{di}(n_h)$, namely for n_d and $n_{di}(0)$. The solid curve in Figure 5.6 shows the chemical potential as a function of n_h for $n_{di}(n_h) = n_d$: the dashed curve for $n_{di}(n_h) = n_{di}(0) < n_d$. We can envisage now that if $n_{di}(n_h)$ is varing slowly that the first term in

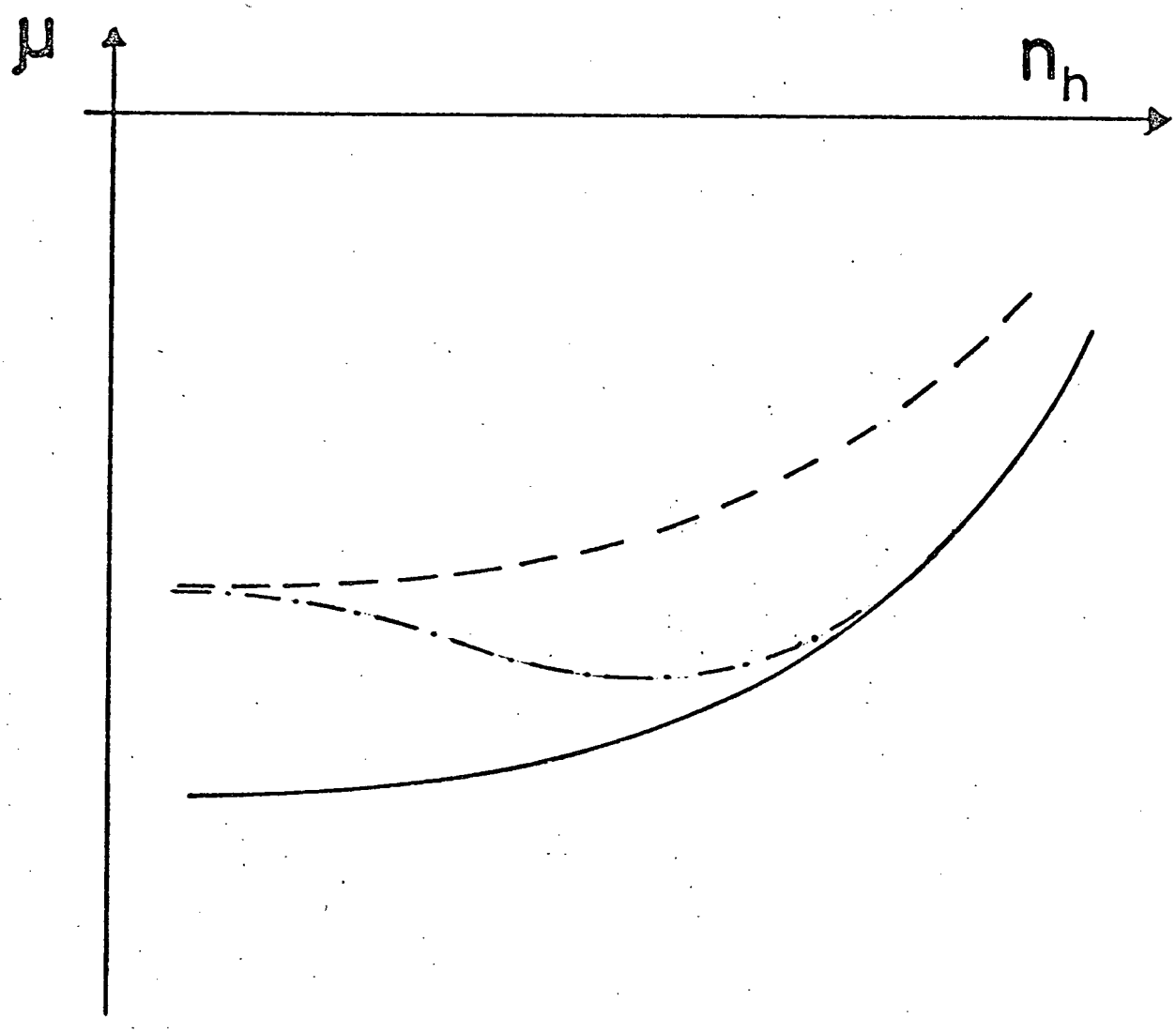

Figure 5.6: The chemical potential of a pair as a function of hole density. The solid curve is for the density of ionized donors (n_{di}) equal to n_d; the dashed curve is for $n_{di} = n_{di}(0) < n_d$; the chained curve represents a free hand interpolation for $n_{di}(0) < n_{di}(n_h) < n_d$ when $n_{di}(n_h)$ varies slowly.

Equation 5.17 will result in values which fall on a line which results in interpolating the two curves referred to above and is represented by a chained curve in Figure 5.6. If $n_{di}(n_h)$ varies in this manner then droplets are formed and the stable gas phase contains no holes.

Let us examine now the second term in the chemical potential (Equation 5.17). Test calculations of

$$\left(\frac{\partial}{\partial n_{di}} e(n_d + n_h, n_h)\right)_{n_h} \tag{5.18}$$

show this term to be always larger (less negative) than any reasonable value of E_n obtained from the IB photoluminescence. Therefore one may assume that the second term in the chemical potential is always positive and if $n_{di}(n_h)$ varies mainly over a narrow range of n_h then μ vs n_h will show a positive spike in that range of n_h.

CHAPTER 6

SUMMARY AND CONCLUSIONS

The work reported in this thesis has involved the measurement of the photoluminescence in heavily-doped Si(P) at liquid helium temperatures. The spectra were studied as a function of excitation intensity and found to contain two components due to two distinct recombination phenomena. Careful line shape analysis of the spectral component which dominates at high excitation intensity confirms the hypothesis of Halliwell and Parsons[11] on the existence of EHD's in metallic silicon. The present study is inconclusive about the existence of droplets in silicon containing $n_d > n_{cb} \sim 2 \times 10^{19}$ phosphorus cm^{-3}, the density when the Fermi level is in the conduction band.[12] The second component of the spectra is observed for the first time. This component dominates the spectra at low excitation intensities and is attributed to the recombination of an electron in the impurity band and a free hole. The line shape of the IB peak is found to be well described by the density of states of the impurity band within the Hubbard model[17] for $n_d < n_{crit}$. The effects of the semiconductor-metal transition on the experimental IB line shape are well understood in terms of the so-called[52] Mott-Hubbard-Anderson transition model.

The change in the relative intensity of the EHD and IB peaks is indicative of the coexistence of two phases. This hypothesis is further strenghtened because it predicts the observed relative positions of the EHD and IB peaks with donor concentration.

The theory of the EHD ground state in the model of Bergersen et al[18, 19] and Mahler and Birman[56-58] was reviewed and found in error. New numerical results based on this model were presented which show that the droplet is energetically unfavorable in metallic silicon. On the basis of the experimental results obtained in this work it is found that the use of the rigid band approximation for low photo-created carrier densities is at fault. It is shown in this work, by hand-waving arguments, that droplets may be energetically favorable if for low photo-created densities not all donors are ionized in metallic silicon as the work of Quirt and Marko[62, 63] strongly suggests.

The speculative discussion in Chapter 5 suggests that the co-existence curve for the EHD and IB phases in heavily doped silicon may be very complicated. In fact, depending how we visualize the density of ionized donors as a function of photo-created carriers to change with temperature, several critical temperatures are possible: there could be a range of temperature, in between them, where droplets are energetically unfavorable and possibly a temperature region close to zero temperature where droplets are formed but are not in thermodynamic equilibrium with the gas. Clearly the photoluminescence study of these samples as a function of temperature could yield surprising results. The work of Parsons and Thewalt[64], restricted only to $n_d = 2 \times 10^{18}$ phosphorus cm^{-3}, shows a critical temperature of approximately 51K which is three times higher than the critical temperature for intrinsic silicon[65]. Of additional interest is that the results of Parsons and Thewalt[64] seem to indicate that between 13 and 20K the chemical potential as well as the equilibrium hole density in the drop show a minimum[66].

The near-infrared absorption (or reflection) experiments on these samples at low temperatures are also of great interest to determine whether the coexistence hypothesis is valid since the optical gap measures the chemical potential of a pair in the gas phase. The absorption experiments at approximately 35K reported by Balkanski et al[27] indicate an optical gap larger than E_{pair} measured in this work. Nevertheless, these results are inconclusive since as pointed out above, at least for a sample containing 2×10^{18} phosphorus cm^{-3}, the chemical potential of a pair seems to increase above 20K with temperature.

APPENDIX A

HEAT TREATMENT EFFECTS IN Si(P)

A.1 Experimental Results

Figure A.1 shows the effects on the photoluminescence spectra of the heat treatment described in Chapter 2. The photoluminescence measurements were done at 4.2 K and the excitation intensity is low, about 10 watts/cm^2. In Figure A.1 the dashed line gives the spectrum before treatment; the solid line, after treatment. No effects of the heat treatment are observed for impurity concentrations below $\simeq 3.0 \times 10^{18}$ cm^{-3}. The luminescence peak observed in the range 1.045 eV - 1.055 eV for the 1.8×10^{18} cm^{-3} - 1.1×10^{19} cm^{-3} spectra in Figure A.1 is the IB peak and the peak observed at about 1.07 eV is associated with the electron-hole droplet. Both peaks have been fully studied in the main body of this thesis. As depicted by the 3.0×10^{18} cm^{-3} spectra, it is more difficult to form the droplet after heat treatment, i.e. higher excitation levels are required to obtain the droplet peaks after heat-treatment. As shown by the 3.9×10^{18} cm^{-3} and 5.0×10^{18} cm^{-3} spectra a peak is observed at $\simeq$ 1.088 eV in the 5.0×10^{18} cm^{-3} spectra. At other concentrations this peak was weak and difficult to separate from the background luminescence. No effect of the heat treatment was observed in a sample containing 4.3×10^{19} cm^{-3}.

If a heat-treated sample is left at room temperature for a few days, the photoluminescence peaks at 1.028 and 1.088 eV are reduced in intensity relative to the IB^{TO} peak. After about one week at this tempe-

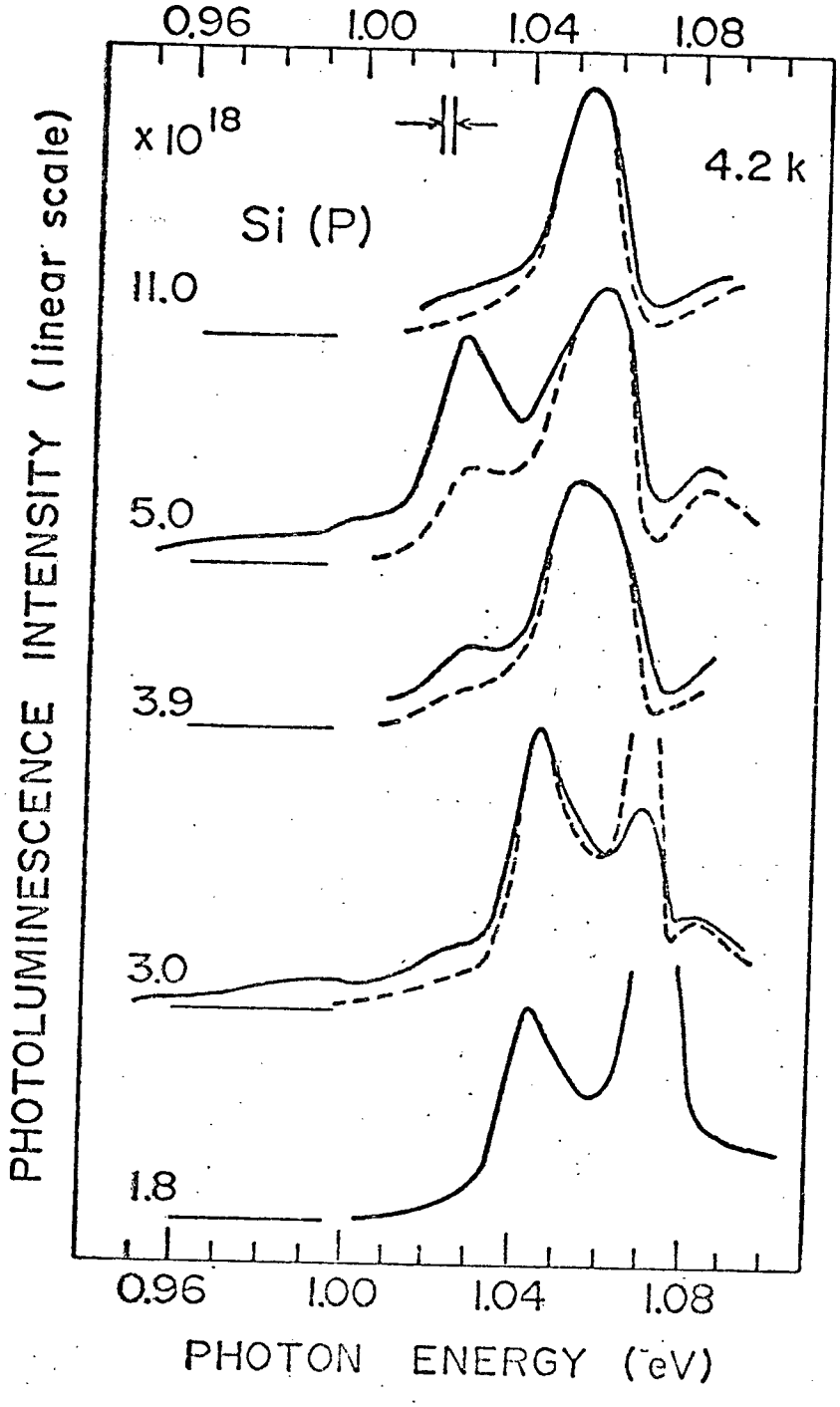

Figure A.1: The effects of heat treatment on the photoluminescence spectra of Si(P) containing impurity concentrations in the range 1.8×10^{18} cm^{-3} to 1.1×10^{19} cm^{-3}. The dashed lines give the spectra before treatment; the solid lines, after treatment. The spectra have been arbitrarily scaled to make comparison of line shapes easier.

rature the photoluminescence spectrum completely reverts to its form before treatment, but the 1.028 eV peak (and probably the 1.088 eV peak) does not disappear upon further room temperature annealing.

Halliwell[23] has studied the electron paramagnetic resonance (EPR) of similar samples under the same heat treatment. Halliwell[23] uses a standard x-band homodyne EPR spectrometer[67]. The spectrometer was fitted with a double-sample modulation-switched cavity designed by Quirt[63] (see also Quirt and Marko[62]) which allows direct comparison of untreated and heat-treated samples.

As in the photoluminescence case, the effects of the heat-treatment on the EPR spectrum are observed only for phosphorus concentrations greater than a certain value. No changes at all were observed for $n_D < 2.0 \times 10^{18}$ cm^{-3}. As shown in Figure A.2, taken from Reference (23), for sample temperature 1.1 K marked changes were observed with the treatment for higher concentrations $n_D \lesssim 2.0 \times 10^{18}$ cm^{-3}. At 4.3×10^{19} cm^{-3} a very small effect was observed as a 10% broadening of the phosphorus line. In accord with the photoluminescence results the EPR spectra show significant annealing effects. After several days at room temperature the spectra completely revert to their form before treatment.

The EPR comparison technique[62, 63] mentioned above was used by Halliwell[23] to determine the number n of electrons responsible for the EPR. Although this method is claimed to be accurate to about 3 percent if the line shapes are known and there is no change in spin susceptibility[62, 63], the uncertainties in the correct line shape for these studies

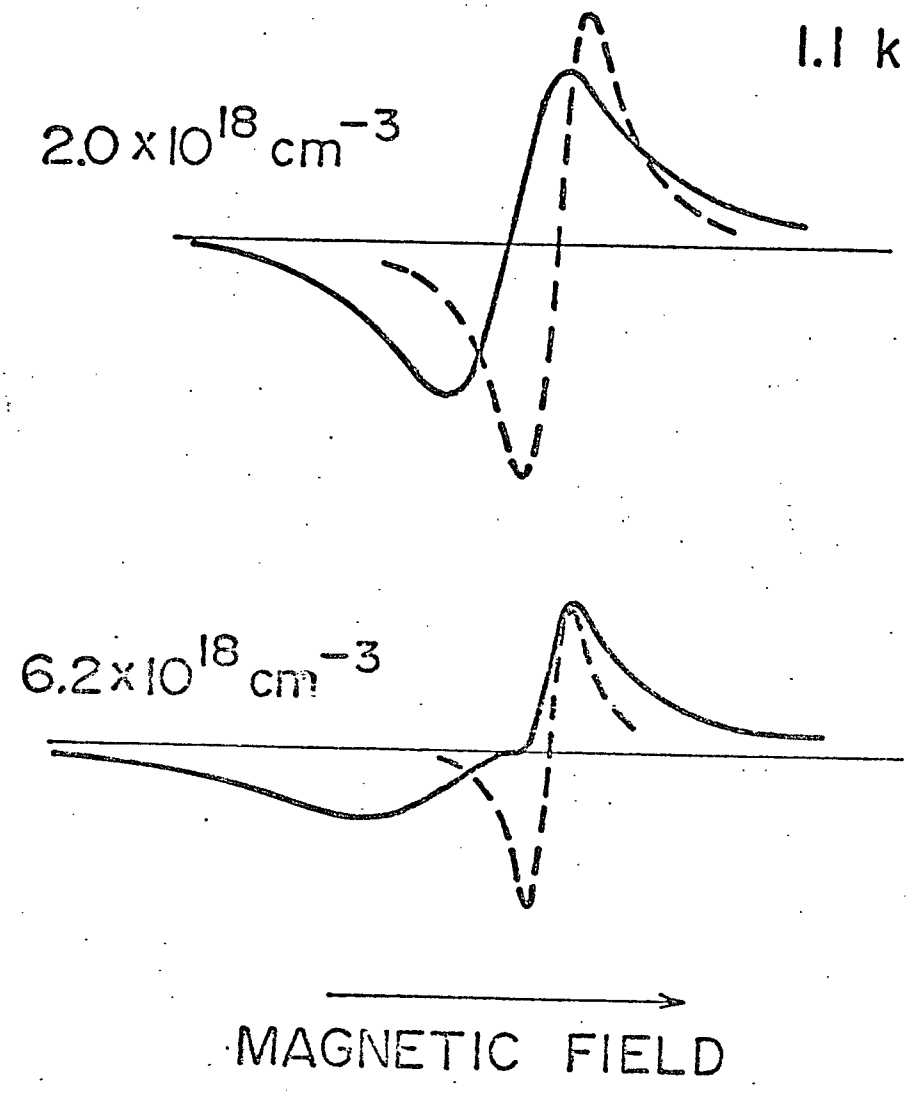

Figure A.2: The effects of heat treatment on the EPR of Si(P) containing impurity concentrations: 2.0 x 10^{18} cm^{-3} and 6.2 x 10^{18} cm^{-3}. Magnetic field modulation was used and the output signal is proportional to the derivative $d\chi''/dH$ where χ'' is the imaginary part of the susceptibility. The dashed lines give the spectra before treatment; the solid lines, after treatment. The spectra have been arbitrarily scaled to make comparison of line shapes easier. The spectra are taken from Reference(23).

made it impossible to determine n to better than 15 percent[23]. To this accuracy there was no change in the total number of electrons responsible for the observed EPR spectra before and after heat reatment.

If the sample was ground to a powder before heat treatment, no heat-induced effects could be observed in the EPR spectra[23]. Photoluminescence spectra could not be obtained on the powdered samples because the surface recombination drastically reduced the quantum yield beyond the limits of our detectivity. In the optical experiments the sample dimensions were typically 2 x 5 x 10 mm^3. The grain size of the powdered samples was about 5 microns diameter.

A.2 Discussion of Results

The changes produced by the heat treatment are nearly confined to the same concentration range in the case of both the EPR and the photoluminescence range in the case of both the EPR and the photoluminescence properties of Si(P). In addition the annealing behaviour observed for the two sets of measurements is similar. It is reasonable to assume, therefore, that these changes are related to a common crystal defect. The concentration threshold 2-3 x 10^{18} cm^{-3} for the induced effects is very nearly equal to the critical concentration $n_{crit} \simeq 3.0 \times 10^{18}$ phosphorus cm^{-3} for the semiconductor-metal transition[12]. This fact combined with the constant electron-spin density result in the comparison measurement suggest that the induced defect becomes paramagnetic with the capture of a delocalized donor electron and that the induced luminescence is due to recombination of this captured electron with a hole, which we assume to be free. In this argument the defect trap could satisfy the following

conditions when the P concentration is less than n_{crit}: (1) its electron-capture cross-section must be less than that of an ionized P impurity, and (2) the probability of transfer of electrons from the P states to the trap states must be negligible at liquid helium temperatures. We have not been able to show that it is possible to have a trap with these properties. Therefore, our present discussion of the results in speculative. We do not have an alternate explanation.

The energy separation of the 1.028 and 1.088 eV peaks in the 5.0×10^{18} cm^{-3} spectrum in Figure A.1 suggests that the peaks are associated with the emission of a TO-phonon (0.058 eV) and a no-phonon process respectively. Comparing the energy positions of the former peak with the 1.06 eV of the IB^{TO} peak in the above spectrum, we conclude that the electron states of the induced trap form a distribution centered at about 0.032 eV below the center of the donor impurity band. At 4.2 K, therefore, an electron in a defect state would have little probability for re-excitation to the impurity band.

Consistent with the interpretation of the photoluminescence data, the EPR results on the heat-treated samples could be interpreted in terms of two unresolved line shapes: one due to electrons loosely bound to phosphorus sites; the other due to electrons trapped by the induced defects. The EPR spectrum is located at magnetic field corresponding to $g \simeq 2.0$ and can be separated into two components. One of these components has the same width and g-value as the single line due to donor electrons observed in samples that have not been heat treated (dashed lines in Figure A.2). After subtraction of this component there remains a broad asymmetric line with a higher g-value. Although lack of knowledge as to the shape of this

line makes proper resolution of the two lines impossible, one can say that the g-value is relatively insensitive to impurity concentration, whereas the linewidth increases rapidly with concentration. The fact that the EPR spectra are unchanged when the samples were crushed before heat-treatment shows that the results are not associated with a surface effect. Presumably, the heat-induced defects in the powdered samples are able to quickly diffuse to the surface where they are removed during the etching procedure.

In order to observe the large changes shown in Figure A.2 for the ~6 x 10^{18} cm^{-3} EPR spectra the concentration of the heat-induced defects must be comparable to that of the phosphorus impurities $\gtrsim 10^{18}$ defects cm^{-3}. This concentration is at least 10 times greater than the typical concentrations of residual impurities, e.g. oxygen, carbon, metals in vacuum float-zoned samples of the type used here[68]. Consequently, we do not think that the heat-induced defect is due to a chemical impurity. The fact that we do not observe heat-induced effects for $n_d < 2\text{-}3 \times 10^{18}$ cm^{-3} and that we do not measure a change in the total spin density suggests that the heat-induced defect is not associated with the phosphorus dopant. The origin of the heat-induced trap, therefore, seems to be due to intrinsic lattice point defects: i.e. vacancies or interstitial Si atoms. On the other hand indirect evidence coming from diffusion studies and high voltage transmission electron microscopy[69] as well as theoretical calculations[70] seem to indicate that dominant high temperature defects are self-interstitials and not vacancies, in contrast to metals, thus only this defect will be considered.

A self-interstitial in silicon is highly mobile at room temperature[69, 70] and, therefore, could not explain the heat-treatment effects observed here which persist, in the case of the luminescence studies, after prolonged room temperature annealing. However, interstitials are known to form aggregates[69] which are stable at room temperature. It is possible that these aggregates possess a distribution of electron traps and could explain our data. The effect of the heat treatment could be understood if large aggregates break up into small clusters of interstitials on high temperature treatment and thereby increase the density of trap centers.

The concentration of self-interstitials depends crucially on the growth rate of the crystal[69] and therefore is difficult to estimate theoretically. Using the diffusion study results of Seeger and Chik[71], Fölls et al.[72] has deduced $\sim 10^{18}$ self-interstitials cm^{-3} at the melting point 1420°C in silicon. This is in agreement with the concentration deduced here.

The fact that heat treatment produces very little effect on the photoluminescence and EPR spectra for very high phosphorus impurity concentrations $n_d > 1 \times 10^{19}$ cm^{-3} can be qualitatively understood. At sufficiently high donor concentrations all states, including those of the traps, will be screened by the free carriers.

APPENDIX B

IMPURITY BAND DENSITY OF STATES

IMPURITY PAIR MODELS

As mentioned in Chapter 4 Lukes et al[38] have used a simple H_2^+ ion model of interaction between impurities in a doped semiconductor to calculate the density of states in the impurity band. The donors are taken to be randomly distributed and the distance, R, between nearest neighbours forming the H_2^+-like ion is assumed to follow the Chandrasekhar distribution[39]. Using the Green's function formalism they show that the density of states may be written as follows:

$$n(E) = -\pi^{-1} \iint 4\pi R^2 n_d \exp\left[-4\pi R^3 n_d/3\right] * \left[\frac{\Psi_+(\bar{r})}{E-E_+ + ie} + \frac{\Psi_-(\bar{r})}{E-E_- + ie}\right] d\bar{r}\, dR \quad , \quad (B.1)$$

where the antibonding band given by the second term will be ignored. The wave function for the ground state is the same as for an isolated impurity as calculated in the effective-mass approximation and is the same as used in Chapter 4, Equation 4.10. Here, we will follow Kohn[47] by taking the envelope function to be spherical symmetric with the effective-mass equation[47]. Since the wave function is normalized Equation B.1 reduces to a trivial one-dimensional integral and one obtains

$$n\left[E_+(R')\right] = -\pi^{-1}\, 4\pi (R')^2 n_d \exp\{-4\pi (R')^3 n_d/3\} \,/\, \left|\frac{dE_+}{dR}\right|_{R'} \quad (B.2)$$

hence to obtain the density of states we need only to calculate the ground state energy and if inter-valley terms are ignored one obtains the analytic

expression for the energy which is identical to the well known solution[41] of the bonding state energy of the hydrogen molecule ion, H_2^+, with the appropriate Bohr radius. The calculated density of states was compared with the experimental IB line shape with the result already described in Chapter 4.

A natural extension of the H_2^+ ion model of interaction between impurities is the H_2 molecule model so that electron-electron interactions are taken into account. Equation B.1 also expresses the density of states in this model. The Heitler-London method[41] is used to set up the molecular wave functions in terms of the "atomic orbitals", that is, the isolated impurity wave functions used in the H_2^+ ion model. Since the Heitler-London wave functions are not normalized the integral over $\bar{r}$ in Equation B.1 is

$$\int \Psi_+ (\bar{r})\, d\,\bar{r} = 1 + S\,(R)^2 \qquad (B.3)$$

where S is the atomic orbital overlap integral which will depend on the inter-impurity distance. In this case one writes

$$n[E_+^{HL}(R')] = - \frac{\pi^{-1}\, 4\pi(R')^2 n_d \exp\,[-4\pi(R')^3\, n_d/3]\,[1+S(R')^2] \,/\, \left|\frac{dE_+^{HL}}{dR}\right|_{R'}}{\int_0^\infty dx\; 4\pi x^2\, n_d \exp\,[-4\pi x^3\, n_d/3][1+S(x)^2]} \qquad (B.4)$$

and again the problem reduces to calculating the ground state energy and if inter-valley terms are again ignored one obtains the analytic expression for the energy which in this case is identical to that given by the Heitler-London model for the H_2 molecule with the appropriate Bohr radius;

the analytic solution of the two center integrals listed by Slater[41] was used.

In the Heitler-London model, the photoluminescence line shape does not correspond to the calculated density of states because it is unreasonable to assume that both electrons associated with the impurity pair will recombine simultaneously. To calculate the photoluminescence line shape it has been assumed that the recombination of a donor electron with a free hole is a Franck-Condon process that leaves an H_2^+ ion-like behind in its ground state and gives

$$I\left[E_+^{HL}(R') - E_+(R')\right] \propto \eta\left[E_+^{HL}(R')\right] \qquad (B.5)$$

where $E_+(R')$ is the ground state energy of the H_2^+ ion. When evaluating the line shape care should be exercised since the argument of the L.H.S. of (B.5) is not a single value function of R'. The calculated line shape was compared to the experimental one with the result already described in Chapter 4.

APPENDIX C

DATA ANALYSIS PROGRAMME

This section describes a computer programme which has been extensively used to analyze the photoluminescence spectra obtained for this work. The programme is written in the BASIC language which is fully described in "An Introduction to BASIC".[73] An extension to the manufacturers compiler, programmed by TRIUMF at U.B.C. is used. This compiler allows to call Machine Language Subroutines (MLS) with the instruction CALL. The MLS called by this programme are explained and listed in M.L.W. Thewalt's thesis.[28]

For the purpose of this programme a spectrum is a set of four dimensional prints: one dimension for the energy of the measured photon; a second for the intensity; a third for the standard deviation due to signal averaging; and a fourth which was reserved for digitally smoothed data which is no longer used. This implies that if a spectrum of "n" points is to be stored in memory, given the starting location in the memory Buffer, the programme will use "4n" consecutive memory locations the first being the starting location given. Care must be then taken so that the data will not overlap with other information stored in the memory Buffer.

The Buffer consists of 2000 memory locations. The programme listed below requires that the memory locations 1850 to 2000 be reserved for the EHD theoretical line shape calculations. Locations 1600 to 1800 are reserved for the IB theoretical line shape calculations.

As pointed out in Chapter 3, the difference between two experimental spectra are taken to disentangle the IB and EHD contributions and to do so the following convention is followed: the second spectra read into memory

is subtracted from the first; scaling and base line changes are only done on the second; the resulting difference will be stored in the first "4n" locations of the Buffer, where "n" is the number of points of the second spectrum.

Most spectra analyzed in this work consisted of less than 125 points, for such spectra it is convenient to choose memory location 500 as starting location for the first experimental spectrum read into the Buffer and location 1000 for the second spectrum.

The following programme has been written in modular form. The subroutines will be listed first and two main programmes for slightly different purposes which use these subroutines are listed at the end.

A.1 The Subroutines

```
9100  REM          ****************************************
9101  REM                        LOAD
9102  REM          ****************************************
9103  PRINT "LOAD TAPE, INPUT STARTING POINT,0 OF #'S AND"
9104  PRINT "  '1' FOR STANDARD DEVIATIONS"
9105  INPUT A1,A2,C8
      REM  This subroutine will load the contents of a paper tape into buffer
           starting at location A1.  The spectrum is represented by A2 points.
           The "1" for standard deviations, is a control number and should be
           set to one if the paper tape also contains the standard deviations
           of the data points.
9106  CALL 16,A1,A2
9107  IF C8<>1 GOTO  9110
9108  CALL 16,A1+3*A2,A2
      REM  The MLS #16 transfers data on paper tape to memory Buffer.
9109  GOTO  9116
9110  PRINT "INPUT ST.DEV.TO SIG.RATIO,'0' IF UNKNOWN"
9111  INPUT C9
9112  LET C9=C9*1960
```

```
      REM  The multiplicative factor 1900 is required for scaling our data for
           output due to the requirement of the D/A converters used in this
           system as it will appear many times throughout the programme.

9113  FOR I= 0 TO A2-1
9114    CALL 7,A1+3*A2+I,C9
9115  NEXT I

      REM  The MLS #7 stores in memory location given by the first expression
           the number given by the second.

9116  FOR I= 0 TO A2-1
9118    CALL 8,A1+I,F[I]
9120  NEXT I


      REM  The MLS #8 recalls the contents of memory location given through
           the first expression and identifies it with the variable listed
           next.

9122  REM          SCALES DATA
9124  LET M1=-20000
9126  LET M2=20000

      REM  The maximum and minimum possible values are ±20000 and are a
           characteristic of the A/D converters used in this system.  This
           values will appear several times in the programme.

9128  FOR I=1 TO A2-1
9130    IF M1>F[I] GOTO  9134
9132    LET M1=F[I]
9134    IF M2<F[I] GOTO  9138
9136    LET M2=F[I]
9138  NEXT I
9186  FOR I= 0 TO A2-1
9188    LET F[I]=(F[I]-M2)*1900/(M1-M2)
9190    CALL 7,A1+I,F[I]
9191    IF C8<>1 GOTO  9195
9192    CALL 8,A1+3*A2+I,C
9193    LET C=C*1900/(M1-M2)
9194    CALL 7,A1+3*A2+I,C
9195  NEXT I
9196  RETURN


      REM  For the spectrometer described in Chapter 2 it was necessary to
           recalibrate periodically the wavedrive.  The following subroutine
           calculates the energy axis of a given spectrum.  It requires that
           the calibration parameters used when the spectrum was taken be
           given.
```

```
9400  REM   ****************************************
9401  REM                    CALCULATE ENERGY AXIS
9402  REM   ****************************************
9403  PRINT "NEW CAL.TYPE 1,0 OTHER.SR=1 FOR DISP,THEN 0 TO CONTI"
9404  INPUT Z5
9405  IF Z5<>1 GOTO  9410
9406  PRINT "INPUT CALIB.PAR."
9407  PRINT
9408  INPUT Z0,Z1,Z2,Z3,Z4
9409  DEF  FNW(X)=Z0+Z1*X+Z2*X*X+Z3*X*X*X+Z4*X*X*X*X
9410  PRINT "ST.WD,STEP SIZE"
9411  PRINT
9412  INPUT W0,W1
9413  FOR I= 0 TO A2-1
9414    LET W2= FNW(W0)
9415    LET W2=2.47971/W2
9416    LET W2=(W2-1.085)*21000
9417    CALL 7,A1+A2+I,W2
9418    LET W0=W0+W1
9419  NEXT I
9426  CALL 9,-1,C
```

REM The MLS #9 reads selected bits of the Switch Register (SR) by performing a logical AND with the MASK given by the first parameter and the result is identified with the variable listed next. This subroutine is heavily used to interact with the computer and in the present case if SR=1 it will display on the scope the last spectrum read into the Buffer. The display will continue until the SR is set to cero.

```
9427  IF C<>1 GOTO  9432
9428  CALL 25,A1+A2,A1,A2
9429  CALL 26
```

REM The MLS #25 points to the location in the Buffer where the energy values are stored, by the first parameter. The second parameter points to the location in Buffer where the intensities corresponding to the previous energy values are located and the third parameter gives the number of points to be displayed on the scope. The MLS #26 actually performs the display on the scope.

```
9430  CALL 9,-1,C
9431  IF C=1 GOTO  9428
9432  RETURN
9500  REM          ****************************************
9501  REM             DIFFERENCE FOR TWO EXPERIMENTAL
9502  REM          ****************************************
9510  PRINT "SCOPE POSITION,INPUT A #"
9511  INPUT C
9512  CALL 9,-1,C
```

REM The contents of the Sr are read and depending on the number (octal) read the programme will do the following:

- SR=1 Returns to main.
- SR=2 Will shift the energy axis of the second spectrum.
- SR=4 Will scale the intensity of the second spectrum.
- SR=10 Will change the base line and slope.
- SR=20 Displays the difference of the two spectra on the scope.
- SR=100 Displays the second spectrum on the scope.
- SR=140 Displays both the first and second spectra simultaneously on the scope.
- SR=200 Punches the data of the difference for future use.

If none of the octal numbers listed above is set on the switches the programme will loop for another try.

```
9513  IF C=1 GOTO  9546
9514  IF C<>2 GOTO  9516
9515  GOSUB  9530
9516  IF C<>4 GOTO  9518
9517  GOSUB  9548
9518  IF C<>8 GOTO  9520
9519  GOSUB  9564
9520  IF C<>16 GOTO  9522
9521  GOSUB  9580
9522  IF C<>32 GOTO  9524
9523  GOSUB  9586
9524  IF C<>64 GOTO  9526
9525  GOSUB  9594
9526  IF C<>96 GOTO  9528
9527  GOSUB  9592
9528  IF C=128 GOTO  9597
9529  GOTO  9512
9530  PRINT "ENERGY SHIFT"
9532  INPUT C
9534  LET E1=C*23.5
9536  FOR I= 0 TO C4-1
9538    CALL 8,C3+C4+I,E0
9540    CALL 7,C3+C4+I,E0+E1
9542  NEXT I
9544  GOSUB  9600
9546  RETURN
9548  PRINT "INTENSITY FACTOR"
9550  INPUT C
9552  FOR I= 0 TO C4-1
9554    CALL 8,C3+I,E0
9556    CALL 7,C3+I,E0*C
9557    CALL 8,C3+3*C4+I,E0
9558    CALL 7,C3+C4*3+I,E0*C
9559  NEXT I
```

```
9560  GOSUB  9600
9562  RETURN
9564  PRINT "BASELINE & SLOPE"
9566  INPUT C,C5
9568  FOR I= 0 TO C4-1
9570    CALL 8,C3+I,E0
9572    CALL 7,C3+I,E0+C+I*C5
9574  NEXT I
9576  GOSUB  9600
9578  RETURN
9580  CALL 25,C3+C4, 0,C4
9582  CALL 26
9584  RETURN
9586  CALL 25,C1+C2,C1,C2
9588  CALL 26
9590  RETURN
9592  CALL 25,C1+C2,C1,C2
9593  CALL 26
9594  CALL 25,C3+C4,C3,C4
9595  CALL 26
9596  RETURN
9597  CALL 17, 0,C4
9598  CALL 17,C3+C4,C4
9599  GOTO  9450
```

REM The MLS #17 will punch as many numbers as given by the second parameter starting in Buffer location given by the first parameter.

```
9450  REM          THIS IS PART OF SUB 9500
9452  CALL 17,3*C4,C4
9464  GOTO  9512
```

REM Since in general the energy axis of the two experimental spectra do not coincide exactly, the first spectrum is linearly interpolated to obtain the luminescence intensities that correspond to the energies of the second. For this purpose the following subroutine is called.

```
9600  REM     ***************************************
9601  REM        INTERPOLATE FIRST SUBTRACT SECOND
9602  REM     ***************************************
9603  LET I1= 0
9604  FOR I= 0 TO C4-1
9605    CALL 7,3*C4+I, 0
9606  NEXT I
9607  FOR J= 0 TO C4-1
9608    CALL 8,C3+C4+J,J1
9610    LET I2=I1
9612    FOR I=I2 TO C2-1
9614      CALL 8,C1+C2+I,J2
9616      IF J2<J1 GOTO  9622
```

```
9618      LET I1=I
9620    NEXT I
9622    CALL 8,C1+C2+I1,J3
9624    CALL 8,C1+C2+1+I1,J2
9626    CALL 8,C1+1+I1,J4
9628    CALL 8,C1+I1,J5
9630    LET J6=J5+(J1-J3)*(J4-J5)/(J2-J3)
9632    CALL 8,C3+J,J7
9634    CALL 7,J,J6-J7
9636    CALL 8,C3+3*C4+J,X0
9638    CALL 8,C1+3*C2+I1,X1
9640    CALL 7,3*C4+J,X0+X1
9642  NEXT J
9644  FOR I= 0 TO C4-1
9646    CALL 8,C3+C4+I,X0
9648    CALL 7,C4+I,X0
9649  NEXT I
9650  RETURN
8200  REM       ************************************************
8201  REM            NEWTON-COTES INTEGRATION
8202  REM       ************************************************
```

REM A Newton-Cotes formula of fourth degree with error calculation is used. On input

X7 = X minimum,
X8 = X maximum,
N = number of points

It also requires that the integrand be evaluated in the subroutine 8250 and its value returned as FI and error as E4. On output the value of the integral is given in the variable S and the error in E1.

```
8204  LET S= 0
8205  LET E1= 0
8206  LET D4=(X8-X7)/N
8207  LET D1=D4/4
8208  LET X9=X7
8209  LET D9= 0
8210  GOSUB  8250
8211  LET F[5]=FI
8212  LET E2=E3
8213  FOR I=I TO N
8214    LET F[I]=F[5]
8215    FOR J=2 TO 5
8216      LET X9=X9+D1
8217      GOSUB  8250
8218      LET E2=E2+E3
8219      LET F[J]=FI
8220    NEXT J
8221    LET V9=F[I]+4*F[2]+2*F[3]+4*F[4]+F[5]
```

```
8222    LET U9=(F[1]+4*F[3]+F[5])*2
8223    LET D2=(U9-V9)/15
8224    LET S=S+V9-D2
8225    LET D3= ABS (D2)
8226    LET E1=E1+D3+2*E2
8227    IF D3<D9 GOTO  8229
8228    LET D9=D3
8229  NEXT I
8230  LET S=S*D1/3
8231  LET E1=E1*D1/3
8232  RETURN
8250  REM     ************************************************
8252  REM                      FUNCTION
8254  REM     ************************************************
8256  LET F1= FNF(X9)
8258  LET E4= 0
8260  RETURN
8400  REM     ************************************************
8401  REM       INITIALIZE  EHD  THEOR. DATA
8402  REM     ************************************************
```

REM When calculating Equation 3.2 in Chapter 3 this should be the first subroutine to be called. There are four parameters this subroutine will ask to be given.

- E(1) = EHD energy gap - phonon energy.
- E(2) = Density of electrons.
- E(3) = Density of holes.
- E(4) = Temperature.

Note that E(2) = E(1) + impurity density.

```
8408  REM
8409  DIM E[5]
8410  PRINT "SELECT PARAMETERS YOU WANT CHANGED ON SR"
8411  PRINT "TYPE 1 WHEN YOU ARE READY"
8412  INPUT C
```

REM On first call of this subroutine the SR should read 17 (octal). On subsequent calls the programme will do the following depending on the number (octal) read in the SR:

- SR = 0 Will ask for a new selection of parameters.
- SR = 15 Will change the EHD energy gap.
- SR = 14 Will change the electron density.
- SR = 13 Will change the hole density.
- SR = 12 Will change the temperature.

```
8413  CALL 9,15,C
8414  IF C= 0 GOTO  8410
8415  CALL 9,1,C
8416  IF C<>1 GOTO  8420
8417  PRINT "TRIAL EHD GAP - PHONON ENERGY"
```

```
8418  PRINT
8419  INPUT E[1]
8420  CALL 9,2,C
8421  IF C<>2 GOTO  8425
8422  PRINT "TRIAL ELECTRON DENSITY"
8423  PRINT
8424  INPUT E[2]
8425  CALL 9,4,C
8426  IF C<>4 GOTO  8430
8427  PRINT "TRIAL HOLE DENSITY"
8428  PRINT
8429  INPUT E[3]
8430  CALL 9,8,C
8431  IF C<>8 GOTO  8435
8432  PRINT "TRIAL TEMPERATURE"
8433  PRINT
8434  INPUT E[4]
```

REM Calculation and print of the Fermi energies and chemical potentials for the electrons and holes.

```
8435  LET U1= 0
8436  LET U2= 0
8437  LET U1=1.14/10↑14*(E[2]/6)↑(2/3)
8438  LET U3=(3.14159*E[4]*8.61746/10↑5)↑2/12
8439  PRINT "EL.FERMI EN.IS=",U1
8440  LET U1=U1-U3/U1
8441  PRINT "EL.CHEM.POT. IS=",U1
8442  LET U2=.6324/10↑14*E[3]↑(2/3)
8443  PRINT "HOLE FERMI EN. IS=",U2
8444  LET U2=U2-U3/U2
8445  PRINT "HOLE CHEM.POT. IS=",U2
8446  PRINT "INPUT # OF POINTS TO INTEGRATE,#TO DISPLAY"
```

REM Each calculated point is 1 meV apart. As a general rule the number of points to be integrated is chosen to exceed by about 20% the integer value of the sum of the two Fermi energies. If the number of points to be displayed exceeds the number to be integrated the programme will produce a base line. The maximum number of points to be integrated and/or displayed in 49.

```
8447  INPUT K0,K1
8448  RETURN
```

```
8100  REM     ************************************
8101  REM          CALCULATE LUM.  EHD
8102  REM     ************************************
8103  DIM L[49]
8104  LET X7= 0
8105  FOR K=1 TO K0
8106    LET X8=K/1000
8107    LET N=K
8108    DEF  FNE(X)=10↑(-17)*( EXP ((X8-X-U1)/8.61746*10↑5/E[4])+1)
8109    DEF  FNH(X)=10↑(-17)*( EXP ((X-U2)/8.61746*10↑5/E[4])+1)
8110    DEF  FNF(X)=10↑(-34)* SQR (X)* SQR (X8-X)/ FNE(X)/ FNH(X)
8111    GOSUB  8200
8112    LET L[K]=S
8113  NEXT K
```

REM FNF is the integrand.
The factors 10^{-17} and 10^{-34} are included to avoid floating point overflow in this small machine.

```
8114  LET L[ 0]= 0
8115  FOR K=K0 TO K1
8116    LET L[K]= 0
8117  NEXT K
8118  GOSUB  8300
8119  RETURN
8297  REM   ************************************************
8298  REM      SCALES & STORES THEORETICAL LUM.
8299  REM   ************************************************
8300  PRINT "INPUT BASELINE"
8301  INPUT L6
8302  LET L0= 0
8303  FOR J= 0 TO K0
8304    LET L[J]=L6+L[J]
8305    IF L[J]<L0 GOTO  8307
8306    LET L0=L[J]
8307  NEXT J
8308  FOR J= 0 TO K0
8309    LET L[J]=L[J]*1900/L0
8310  NEXT J
8311  REM     X,Y THEORETICAL DATA FROM 1900 TO TOP BUFFER
8312  FOR J= 0 TO K1
8313    LET J1=(E[1]-1.085+J/1000)*21000
8314    CALL 7,1900+J,J1
8315    CALL 7,1950+J,L[J]
8316  NEXT J
8317  RETURN
8650  REM     ************************************************
8651  REM        DISPLAY FITTING
8652  REM     ************************************************
```

```
      REM  This subroutine expects to find the experiemental EHD line shape
           starting in Buffer location A1 consisting of A2 points with the
           energy values of each point starting at buffer location A1 + A2.

8653  PRINT "SET PARAMETERS IN SR,TYPE 1 WHEN READY"
8654  PRINT "WANT OUT?SET SR=0 FOR ANOTHER TRY,1 RETURNS TO MAIN"
8655  PRINT
8656  INPUT C
8657  CALL 9,16,C
8658  IF C= 0 GOTO  8679

      REM  To perform a trial and error fit of the EHD line shape the pro-
           gramme allows two distinct levels of operator interactions which
           are chosen by the fifth bit of the SR, that is, by switch #11.
           If switch #11 is down a new EHD line shape will be calculated.
           If switch #11 is up only changes that do not alter the line
           shape are performed.  The programme will test the status of
           switches #12 to #14 and will do the following depending on the
           octal number given by this 3 bits.

           - SR(12, 13, 14) = ϕ  Will go to display mode.
           - SR(12, 13, 14) = 2  Will scale the intensity of the theoretical
             line shape, a new difference of the experimental and theore-
             tical line shape is performed and finally the programme is
             diverted to display mode.
           - SR(12, 13, 14) = 4  Will shift the theoretical peak, new
             difference is performed and control given to display mode.
           - SR(12, 13, 14) = 6  Will shift the theoretical peak as well as
             scale it.  New difference is performed and control given to
             display mode.
           - SR(12, 13, 14) = 10  Will change the base line of the theoreti-
             cal peak, new difference is performed and control given to
             display mode.

8659  CALL 9,14,C
8660  IF C<> 0 GOTO  8711
8661  CALL 25,A1+A2,A1,A2
8662  CALL 26
8663  CALL 9,-1,C

      REM  On display mode the contents of the SR are read and depending on
           the number (octal) read the programme will do the following:

           - SR =  0  Will restart the subroutine for another fit.
           - SR =  1  Will return to main.
           - SR = 32  Will display the experimental spectrum as well as the
                      difference between this spectrum and the theoretical
                      line shape.

           On any other SR reading the programme will display the experimen-
           tal and theoretical spectra.
```

```
8664  IF C= 0 GOTO  8655
8665  IF C=1 GOTO  8683
8666  IF C=32 GOTO  8645
8667  GOTO  8640
8669  IF C<>6 GOTO  8673
8670  GOSUB  8685
8671  GOSUB  8700
8672  GOTO  8661
8673  CALL 9,2,C
8674  IF C<>2 GOTO  8677
8675  GOSUB  8700
8676  GOTO  8661
8677  GOSUB  8685
8678  GOTO  8661
8679  GOSUB  8420
8680  GOSUB  8100
8682  GOTO  8661
8683  RETURN

      REM  This subroutine continues
8640  CALL 25,1900,1950,K1+1
8641  CALL 26
8642  GOTO  8661
8645  CALL 25,1900,1850,K1+1
8646  CALL 26
8647  GOTO  8661

      REM  The following four subroutines are called from the previous
           subroutines.
8685  REM           ************************************
8686  REM                    SHIFT ENERGY
8687  REM           ************************************
8688  PRINT "ENERGY SHIFT IN MEV"
8689  INPUT C
8690  LET E[1]=E[1]+C/1000
8691  LET E1=C*21
8692  FOR I= 0 TO 49
8693    CALL 8,1900+I,E0
8694    CALL 7,1900+I,E0+E1
8695  NEXT I
8696  GOSUB  8800
8697  RETURN

8700  REM           ************************************
8701  REM                  INTENSITY CHANGE
8702  REM           ************************************
8703  PRINT "INTENSITY FACTOR"
8704  INPUT C
8705  FOR I= 0 TO 49
8706    CALL 8,1950+I,E0
8707    CALL 7,1950+I,E0*C
8708  NEXT I
```

```
8709  GOSUB  8800
8710  RETURN
8711  REM                    BASELINE CHANGE
8712  REM          ****************************************
8713  IF C<>8 GOTO  8669
8714  GOSUB  8300
8715  GOSUB  8800
8716  GOTO  8661
8800  REM     ********************************************
8801  REM        INTERPOLATE EXPERIMENTAL SUBTRACT TH.
8802  REM     ********************************************
8803  LET I1= 0
8804  FOR J= 0 TO K0
8805    CALL 8,1900+J,J1
8806    LET I2=I1
8807    FOR I=I2 TO A2-1
8808      CALL 8,A1+2*A2-I-1,J2
8809      IF J2>J1 GOTO  8812
8810      LET I1=I
8811    NEXT I
8812    CALL 8,A1+2*A2-1-I1,J3
8813    CALL 8,A1+2*A2-2-I1,J2
8814    CALL 8,A1+A2-2-I1,J4
8815    CALL 8,A1+A2-1-I1,J5
8816    LET J6=J5+(J1-J3)*(J4-J5)/(J2-J3)
8817    CALL 8,1950+J,J7
8818    CALL 7,1850+J,J6-J7+L6*1900/L0
8819  NEXT J
8820  RETURN
5000  REM          ************************************
5001  REM                NEW PLOTS
5002  REM          ************************************
5003  INPUT C
5004  CALL 9,-1,C
```

REM The input is just a pause to get the x-y plotter ready. The SR is read and depending on the number (octal) read the programme will do the following:

- SR = ϕ Reads SR again.
- SR = 1 Will return to main.
- SR = 2 Will plot the first experimental spectrum read into buffer.
- SR = 4 Will plot the second experimental spectrum.
- SR =10 Will plot the difference of the two experimental spectra.
- SR =20 Will plot fixed energy axis from .99 to 1.18 eV (21000 x .095 = 1995<2000 which is maximum of our D/A converter).
- SR =40 Will plot IB theoretical line shape.
- SR=100 Will plot EHD theoretical line shape.
- SR=200 Will plot the difference between the experimental and theoretical EHD line shape.

```
5005  IF C= 0 GOTO  5004
5006  IF C=1 GOTO  5099
5008  IF C<>2 GOTO  5016
5010  LET C5=C1
5012  LET C6=C2
5014  GOTO  5070
5016  IF C<>4 GOTO  5024
5018  LET C5=C3
5020  LET C6=C4
5022  GOTO  5070
5024  IF C<>8 GOTO  5032
5026  LET C5= 0
5027  LET C6=C4
5030  GOTO  5070
5032  IF C<>16 GOTO  5100
5033  CALL 11, 0
5034  CALL 12,21000*(-.095),-50
5036  CALL 11,1
5038  FOR I= 0 TO 19
5040    LET X0=21000*(-.095+I/100)
5042    CALL 12,X0,-50
5044    CALL 12,X0,-25
5046    CALL 12,X0,-50
5048  NEXT I
5050  FOR I= 0 TO 19
5052    LET X0=21000*(.095-I/100)
5054    CALL 12,X0,1950
5056    CALL 12,X0,1925
5058    CALL 12,X0,1950
5060  NEXT I
5062  CALL 12,X0,-50
5064  CALL 11, 0
5066  GOTO  5004
5070  CALL 11, 0
5071  CALL 9,-1,C
5072  IF C<> 0 GOTO  5071
5073  FOR I= 0 TO C6-1
5074    CALL 8,C5+C6+I,X0
5076    CALL 8,C5+I,Y0
5078    CALL 8,C5+3*C6+I,Y1
5080    CALL 12,X0,Y0+Y1
5082    CALL 11,1
5084    CALL 12,X0,Y0-Y1
5086    CALL 11, 0
5088    CALL 9,-1,C
5090    IF C=1 GOTO  5073
5092    IF C=2 GOTO  5003
```

```
5094  NEXT I
5096  GOTO  5004
5099  RETURN
5100  IF C<>32 GOTO  5130
5102  CALL 11, 0
5104  CALL 9,-1,C
5106  IF C<> 0 GOTO  5104
5108  FOR I= 0 TO 49
5110    CALL 8,1600+C7*100+I,X0
5112    CALL 8,1650+C7*100+I,Y0
5114    CALL 12,X0,Y0
5116    CALL 11,1
5118    CALL 11, 0
5120    CALL 9,-1,C
5122    IF C=1 GOTO  5108
5124    IF C=2 GOTO  5003
5126  NEXT I
5128  GOTO  5004
5130  IF C<>64 GOTO  5160
5131  LET R[49]=1
5132  CALL 11, 0
5134  CALL 9,-1,C
5136  IF C<> 0 GOTO  5134
5138  FOR I= 0 TO K0
5140    CALL 8,1900+I,X0
5142    CALL 8,1850+R[49]*100+I,Y0
5144    CALL 12,X0,Y0
5146    CALL 11,1
5148    CALL 11, 0
5150    CALL 9,-1,C
5152    IF C=1 GOTO  5140
5154    IF C=2 GOTO  5003
5156  NEXT I
5158  GOTO  5004
5160  IF C<>128 GOTO  5004
5162  LET R[49]= 0
5164  GOTO 5132
```

```
      REM  The following subroutines deal with the calculation of the IB
           line shape.  In these subroutines we are forced to use an array
           for variable names because at this stage of the programme we have
           exceeded the storage allocated by the compiler to variables names
           which has a disastrous effect on the legibility of these subroutines.

5200  REM          ********************************
5201  REM                IMPURITY INHCIALIZE
5202  REM          ********************************
5204  LET R[ 0]=3.14159
5206  LET R[1]=11.33
5208  LET R[2]=.0906
5209  LET R[3]=.57722
5210  PRINT "INPUT IMPURITY CONC."
5211  LET R[43]=1
5212  INPUT R[4]
5214  LET R[5]=(3/4/R[ 0]/R[4])↑(1/3)*1E+8
5215  LET R[5]=R[5]/R[1]
5216  LET R[6]=2.266
5218  RETURN
5250  REM          ************************************
5252  REM               IMPURITY BAND
5254  REM            HYDROGEN MOLECULE ION
5256  REM          ************************************
5258  GOSUB  5200


      REM  The following dictionary is helpful
           R(8) = V1(R)
           R(9) = V2(R)
           R(10)= Δ
           where V1(R), V2(R) and Δ are defined by Lukes et al.[38]

5260  FOR I= 0 TO 49
5262    LET S=R[6]/R[1]
5264    LET R[8]=1/S- EXP (-2*S)*(1+1/S)
5266    LET R[9]=(1+S)* EXP (-S)
5268    LET R[10]=(1+S+S*S/3)* EXP (-S)
5270    LET R[11]=-2*R[2]*(R[8]+R[9])/(1+R[10])
5271    LET R[11]=-.0453+R[11]/2
5272    LET R[12]=-1/S/S+2* EXP (-2*S)*(1+1/S/S/2+1/S)
5273    LET Q[I]=R[11]
5274    LET R[13]=-S*S* EXP (-S)
5276    LET R[14]=-S*S/3*(S+1)* EXP (-S)
5278    LET R[15]=-(R[12]+R[13])/(1+R[10])
5279    LET R[15]=R[15]+(R[8]+R[9])/(1+R[10])↑2*R[14]
5280    LET R[15]=R[15]*R[2]
5284    LET R[11]=(R[7]-1.985+R[11])*21000
5286    LET R[16]=S*S/R[5]↑3* EXP (-(S/R[5])↑3)
5287    LET L[I]=3*R[16]/R[15]
5288    LET R[6]=R[6]+2.266
5290    CALL 7.1600+1.R[11]
5292  NEXT I
```

```
5294  GOSUB  5420
5295  GOSUB  5470
5298  RETURN
5300  REM    ************************************
5302  REM                IMPURITY BAND
5304  REM          HEITLER-LONDON MODEL
5306  REM    ************************************
5307  GOSUB  5200
5308  GOSUB  5800
      REM  The following dictionary is helpful
           R(23)        =  S
           R(24)        =  S'
           R(25)        =  J
           R(26)        =  K
           R(27)        =  J'
           R(28)+R(29)  =  K'
           R(30)        =  ∂S/∂R
           R(31)        =  ∂S'/∂R
           R(32)        =  ∂J/∂R
           R(33)        =  ∂K/∂R
           R(34)        =  ∂J'/∂R
           R(35)+R(36)  =  ∂K'/∂R
           R(44)        =  |∂E+/∂R|R'
           where S, S', J, K, J', K' are defined by Slater.[41]
5309  DEF  FNT(X)=1+4* INT (X/2)-2*X
5310  FOR I= 0 TO 49
5312    LET S=R[6]/R[1]
5314    LET R[17]= 0
5316    LET R[18]= 0
5318    LET R[19]= 0
5320    LET R[20]= 0
5322    IF S>2 GOTO  5354
5324    LET R[17]=R[3]+ LOG (2*S)
5326    LET R[18]=R[3]+ LOG (4*S)
5328    LET R[19]=1/S
5330    LET R[20]=1/S
5332    FOR J=1 TO 32
5334      LET R[21]=1
5336      FOR K=1 TO J
5338        LET R[21]=R[21]*K
5340      NEXT K
5342      LET R[22]=R[21]*J
5344      LET R[17]=R[17]+ FNT(J)*(2*S)↑J/R[22]
5346      LET R[18]=R[18]+ FNT(J)*(4*S)↑J/R[22]
5348      LET R[19]=R[19]- FNT(J-1)*(2*S)↑(J-1)/R[21]*2
5350      LET R[20]=R[20]- FNT(J-1)*(4*S)↑(J-1)/R[21]*4
5352    NEXT J
5354    LET R[23]= EXP (-S)*(1+S+S*S/3)
```

```
5356    LET R[24]= EXP (S)*(1-S+S*S/3)
5358    LET R[25]=-1/S+ EXP (-2*S)*(1+1/S)
5360    LET R[26]=- EXP (-S)*(1+S)
5362    LET R[27]=1/S- EXP (-2*S)*(1/S+11/8+.75*S+S*S/6)
5364    LET R[28]=-1/5* EXP (-2*S)*(-25/8+23*S/4+3*S*S+S↑3/3)
5365    LET S0=R[23]*R[23]*(R[3]+ LOG (S))+R[24]*R[24]*R[18]
5366    LET R[29]=6/5/S*(S0-2*R[23]*R[24]*R[17])
5367    LET S0=-R[43]+2*R[26]*R[23]-R[23]*R[23]+2*R[25]+R[27]+R[28]
5368    LET R[40]=(S0+R[29])/(1+R[23]*R[23])*R[2]
5370    LET R[30]=-R[23]+ EXP (-S)*(1+2*S/3)
5372    LET R[31]=R[24]+ EXP (S)*(2*S/3-1)
5374    LET R[32]=1/S/S-2* EXP (-2*S)*(1+1/S+1/S/S/2)
5376    LET R[33]=-R[26]- EXP (-S)
5378    LET R[34]=-1/S/S+ EXP (-2*S)*(2/S+2+7/6*S+S*S/3+1/S/S)
5380    LET R[35]=-2*R[28]- EXP (-2*S)*(23/4+6*S+S*S)/5
5382    LET S0=R[23]*R[23]/S+2*R[24]*R[31]*R[18]+R[24]*R[24]*R[20]
5383    LET S0=S0+2*R[23]*R[30]*(R[3]+ LOG (S))
5384    LET R[36]=-R[29]/S+6/5/S*S0
5385    LET S0=-2*(R[24]*R[30]*R[17]+R[23]*R[31]*R[17])
5386    LET R[37]=6/5/S*(S0-2*R[23]*R[24]*R[19])
5388    LET S0=-R[43]+2*R[23]*R[26]-R[23]*R[23]+2*R[25]+R[27]+R[28]
5389    LET S0=(S0+R[29])*R[23]*R[30]/(1+R[23]*R[23])↑2
5390    LET R[38]=-2*S0
5392    LET S0=2*(R[23]*R[33]+R[26]*R[30])-2*R[23]*R[30]
5393    LET S0=S0+2*R[32]+R[34]+R[35]+R[36]+R[37]
5394    LET R[39]=S0/(1+R[23]*R[23])
5396    LET R[41]=(R[38]+R[39])*R[2]
5397    LET R[41]= ABS (R[41])
5399    LET R[42]=S*S/R[5]↑3* EXP (-(S/R[5])↑3)
5400    LET L[I]=6*R[42]/R[41]/R[44]*(1+R[23]*R[23])
5401    GOSUB  5650
5402    CALL 7,1700+I,R[40]
5404    LET R[6]=R[6]+2.266
5406  NEXT I
5408  GOSUB  5420
5409  GOSUB  5450
5410  RETURN
5412  NEXT I
5414  RETURN
5420  REM          ***********************************************
5422  REM               SCALE THEOR. IMPURITY BAND
5424  REM          ***********************************************
5426  PRINT "BASELINE IB"
5428  INPUT L6
5430  LET L0= 0
5432  FOR J= 0 TO 49
5434    LET L[J]=L[J]+L6
5436    IF L[J]<L0 GOTO  5440
5438    LET L0=L[J]
5440  NEXT J
5442  RETURN
```

```
5450  REM          ************************************
5452  REM              STORE HEITLER LONDON
5454  REM          ************************************
5456  FOR J= 0 TO 49
5458    LET J1=L[J]*1900/L0
5460    CALL 7,1750+J,J1
5462  NEXT J
5464  RETURN
5470  REM          ************************************
5472  REM                   STORE MOLECULAR ION
5474  REM          ************************************
5476  FOR J= 0 TO 49
5478    LET J1=L[J]*1900/L0
5480    CALL 7,1650+J,J1
5482  NEXT J
5484  RETURN
5650  REM    ************************************
5652  REM      STORE HEITLER-LONDON AXIS
5654  REM    ************************************
5659  LET R[40]=R[40]-Q[1]
```

REM The array Q is where the energies of the molecular ion model were stored (instruction #5273). We are subtracting it now because we want to equate (see Appendix B)

$$I\,(E_+^{HL}(R^1)-E_+(R^1)) = n(E_+^{HL}(R^1))$$

```
5660  LET R[40]=(R[7]-1.085+R[40])*21000
5662  RETURN
5800  REM    ************************************
5802  REM        CALCULATE NORMALIZING INTEGRAL
5804  REM    ************************************
5806  DEF  FNH(X)=6*X*X/R[5]↑3* EXP (-(X/R[5])↑3)
5808  DEF  FNF(X)= FNH(X)*(1+(1+X+X*X/3)↑2* EXP (-2*X))
5810  LET X7= 0
5812  LET X8=20
5814  LET N=100
5816  GOSUB  6200
5818  PRINT S
5820  LET R[44]=S
5622  RETURN
```

```
5500  REM        ********************************
5502  REM         DISPLAY FIT IMPURITY BAND
5504  REM        ********************************
5506  PRINT "INPUT 0 FNR MOLEC.ION.1 HEITLER LONDON"
5508  INPUT C7
5510  PRINT
5512  PRINT "SET PARAM. IN SR.0 ANOTHER TRY THEN 1 FOR OUT"
5514  PRINT
5516  CALL 9,-1,C
```

REM The SR is read and depending on the number (octal) read the programme will do the following:
- SR = 0 Will read the SR again.
- SR = 1 Will return to main.
- SR = 2 Will display the experimental and theoretical IB line shapes.
- SR = 4 Will shift the IB line shape and display the result.
- SR = 10 Will scale the IB line shape and display the result.
- SR = 20 Will change the baseline of the IB line shape.

```
5518  IF C=0 GOTO  5516
5520  IF C=1 GOTO  5618
5522  IF C<>2 GOTO  5544
5524  CALL 25,1600+C7*100,1650+C7*100,50
5526  CALL 26
5528  CALL 25,C4, 0,C4
5530  CALL 26
5531  CALL 9,-1,C
5532  IF C<> 0 GOTO  5524
5534  GOTO  5516
5544  IF C<>4 GOTO  5550
5546  GOSUB  5580
5548  GOTO  5524
5550  IF C<>8 GOTO  5556
5552  GOSUB  5600
5554  GOTO  5524
5556  IF C<>16 GOTO  5524
5558  PRINT "BASELINE"
5560  INPUT L6
5562  FOR I= 0 TO 49
5563    CALL 8,1650+C7*100+I,E0
5564    CALL 7,1650+C7*100+I,E0+L6
5566  NEXT I
5568  GOTO  5524
5580  REM        ********************************
5582  REM         EN.SHIFT IMPURTY BAND
5584  REM        ********************************
5586  PRINT "EN.SHIFT"
5588  INPUT C
5590  LET E1=C*21
```

```
5592  FOR I= 0 TO 49
5594    CALL 8,1600+C7*100+I,E0
5596    CALL 7,1600+C7*100+I,E0+E1
5598  NEXT I
5599  RETURN
5600  REM        ***********************************
5602  REM          INTENSITY FACTOR IMP.BAND
5604  REM        ***********************************
5606  PRINT "INTEN.FACTOR"
5608  INPUT C
5610  FOR I= 0 TO 49
5612    CALL 8,1650+C7*100+I,E0
5614    CALL 7,1650+C7*100+I,E0*C
5616  NEXT I
5618  RETURN
```

A.2 Examples of Main Programmes

A.2.1 Main #1

Let us suppose that we have two experimental spectra. In the first one both the EHD and IB peaks are present while in the second spectrum the IB peak dominates. We can then use the line shape of the IB peak of the second spectrum to subtract the IB peak from the first. The resulting spectrum will show the EHD line shape. We will proceed then as follows:

```
2   CALL 1
4   DIM f(255), L(49), R(49), Q(49), E(5)
6   GOSUB 9100
    REM  Will load first spectrum
8   GOSUB 9400
    REM  Will generate its energy axis.  The LOAD subroutine defines A1, the
         starting memory location in buffer for the loaded data, as well as
         A2, the number of data points.  We assign the values to another
         variable name before they are lost by loading the second spectrum.
10  LET C1=A1
12  LET C2=A2
    REM  The variable names chosen will permit the use of other subroutines
         without problems.  Now we can proceed to load a second spectrum.
14  GOSUB 9100
16  GOSUB 9400
    REM  Generates its energy axis.
18  LET C3=A1
20  LET C4=A2
    REM  The variable names chosen will again permit the use of other sub-
         routines without problems.  We now turn control to the subroutine
         that will take the difference.
22  GOSUB 9500
    REM  At this point of the main programme we will have the experimental
         EHD line shape stored in the buffer starting in location cero and
         having C4 points.  If we eventually will like to fit to this expe-
         rimental line shape a theoretically calculated one we will turn
         control to the subroutines that will do the calculation of the
         theoretical EHD line shape.
24  GOSUB 8400
26  GOSUB 8100
    REM  The fitting routine which will be called next expects to find the
         experimental EHD line shape stored in buffer starting at location A1
         and having A2 points so we have to redefine A1 and A2 so that the
         fitting is done to the appropriate data.
28  LET A1=ϕ
30  LET A2=C4
32  GOSUB 8650
    REM  If the fit was successful we would like a plot.
```

```
34  GOSUB 5000
36  STOP
```

A.2.2 Main #2

A variation of the previous example may occur if in the second spectrum the EHD peak dominates. We would follow the previous main programme to instruction 22 inclusive. At that stage of the programme we would have the experimental IB line shape stored in the buffer. At this point we will turn control to the subroutine that will calculate the theoretical IB line shape

```
26  GOSUB 5250
    REM  If the Heitler-London model is to be calculated use the next instruc-
         tion, if not skip it.
28  GOSUB 5300
    REM  We will now do the fit.
30  GOSUB 5500
    REM  And finally we would like a plot.
32  GOSUB 5000
34  STOP
```

APPENDIX D

THE EHD COMPUTER PROGRAMMES

D.1 Correlation and Impurity Energies

The correlation energy per unit volume is related to the pair correlation function $S(q, \omega)$ through[19]

$$e_{corr}(n_c, n_h) = \frac{1}{2}\int \frac{d^3q}{(2\pi)^3}\int_{-i\infty}^{i\infty} \frac{d\omega}{2\pi i}\left\{ \frac{4\pi e^2}{\epsilon(\bar{q})q^2} S(\bar{q},\omega) + \right.$$

$$\left. + \ln\left[1 - \frac{4\pi e^2}{\epsilon(\bar{q})q^2} S(\bar{q},\omega)\right]\right\} \qquad (D.1)$$

where following Nara and Morita[59]

$$\frac{1}{\epsilon(q)} = A\,\frac{q^2}{q^2+\alpha^2} + \frac{(1-A)q^2}{q^2+\beta^2} + \frac{\epsilon^{-1}(0)\,\gamma^2}{q^2+\gamma^2} \quad , \qquad (D.2)$$

with $A \simeq 1.175$, $\alpha = 0.7572$ a.u., $\beta = 0.3123$ a.u., $\gamma = 2.044$ a.u. and $\epsilon(0)=11.4$.

To claculate D.1 Bergersen et al[18] found it convenient to distort the ω - contour along the imaginary axis $\omega = iz$.

Similarly the energy per unit volume associated with the impurity interaction is approximately given by[19]

$$e_{imp} = \frac{2\pi Z e^2 n_d}{(2\pi)^3}\int \frac{d^3q}{\epsilon(\bar{q})q^2}\,\frac{4\pi e^2\epsilon^{-1}(\bar{q})\; S\;(\bar{q},0)}{[q^2-4\pi e^2\epsilon^{-1}(\bar{q})\; S\;(\bar{q},0)]} \quad . \qquad (D.3)$$

In the RPA the total pair correlation function $S(q, iz)$ may be written as a sum of contributions from the conduction valley electrons, S^c and light and heavy holes, S^h.

D.1a. Valence Band Contribution

For further computations it is useful to define the following:

$$\gamma_c = m_t/m_\ell \quad ; \qquad r_h = m_{\ell h}/m_{hh} \quad ,$$

$$\bar{m} = (m_\ell m_t^2)^{1/3}$$

$$m_A^{-1} = \frac{1}{3}(m_\ell^{-1} + 2\, m_t^{-1}) + \frac{1}{2}(m_{\ell h}^{-1} + m_{hh}^{-1})$$

$$k_F^c = (3\pi^2 n_c/\nu)^{1/3} a_o \quad ; \quad k_F^h = \{3\pi^2 n_h/(1+\gamma_h^{3/2})\}^{1/3} a_o$$

$$E_F^c = \frac{\hbar^2 (k_F^c)^2}{2\,\bar{m}} \quad ; \quad E_F^h = \frac{\hbar^2 (k_F^h)^2}{2\, m_{hh}}$$

where ν is the number of conduction band valleys and $a_o = \hbar^2/m_e e^2$ the atomic Bohr madices so that the electron and hole densities are per cm^3. The hole polarization function is written[18]

$$\frac{4\pi e^2}{\epsilon (k_F^h)^2}\, S^h(q, iz E_F^h) =$$

$$- \frac{1}{(2\pi)^3} \int_{p<\gamma_h^{1/2} k_F^{hh}} d^3p \left\{ \frac{\Lambda_{\ell\ell}}{iz E_F^h + \hbar^2(2\bar{p}\cdot\bar{q} + q^2)/2m_{\ell h}} + \right.$$

$$\left. + \frac{\Lambda_{\ell h}}{iz E_F^h + \hbar^2(\bar{p}+\bar{q})^2/2m_{hh} - \hbar^2 p^2/2m_{\ell h}} + \text{c.c.} \right\} \frac{4\pi e^2}{\epsilon (k_F^{hh})^2} -$$

$$- \frac{1}{(2\pi)^3} \int_{p<k_F^{hh}} d^3p \left\{ \frac{\Lambda_{h\ell}}{iz E_F^h + \hbar^2(\bar{p}+\bar{q})^2/2m_{\ell h} - \hbar^2 p^2/2m_{hh}} + \right.$$

$$\left. + \frac{\Lambda_{hh}}{iz E_p^h + \hbar^2(\bar{p}+\bar{q})^2/2m_{hh} - \hbar^2 p^2/2m_{hh}} + \text{c.c.} \right\} \frac{4\pi e^2}{\epsilon (k_F^{hh})^2} \qquad (D.4)$$

where
$$\Lambda_{\ell\ell} = \Lambda_{hh} = \frac{1}{2}\left|4 - \frac{3q^2(1-\mu^2)}{p^2+q^2+2pq\mu}\right| \tag{D.5}$$

and
$$\Lambda_{h\ell} = \Lambda_{h\ell} = \frac{3}{2}\frac{q^2(1-\mu^2)}{p^2+q^2+2pq\mu} \tag{D.6}$$

with
$$\mu \equiv \cos(\hat{p}.\hat{q}) \tag{D.7}$$

Bergersen et al[18] expressed Equation D.4 in momentum and energy hole Fermi units and have performed the angular integration, they found:

$$-\frac{4\pi e^2}{\varepsilon(k_F^{hh})^2} S^h(q,izE_F^h) = \alpha^h Q^h(q,z) \tag{D.8}$$

where
$$\alpha^h = \frac{2m_{hh}}{\varepsilon\pi k_F^h} \tag{D.9}$$

and
$$Q^h(q,z) = \frac{2}{q}\int_0^1 pdp\Big[\Big[\theta(\gamma_h^{\frac{1}{2}} - p)\ x$$

$$x\left\{\frac{\gamma}{2}\ell n\frac{z^2\gamma_h^2 + (2pq+q^2)^2}{z^2\gamma_h^2 + (2pq-q^2)^2} + \ell n\frac{z^2+(2pq+q^2)^2}{z^2+(2pq-q^2)^2} + \right.$$

$$+\frac{1}{16p^2}\ \mathrm{Re}\frac{\gamma_h}{-z\gamma_h+p^2}\Big[(-12p^2q^2 + 3(iz\gamma_h+q^2)^2)\ x$$

$$x\ \ell n\left(\frac{iz\gamma_h + q^2 + 2pq}{iz\gamma_h + q^2 - 2pq}\right)$$

(Continued...)

$$+ (12p^2q^2 - 3(iz - \gamma_h^{-1}p^2 + p^2 + q^2)^2) \times$$

$$\times \ell n \left(\frac{iz - \gamma_h^{-1}p^2 + p^2 + q^2 + 2pq}{iz - \gamma_h^{-1}p^2 + p^2 + q^2 - 2pq}\right)\Bigg] + \frac{1}{16p^2} \mathrm{Re} \frac{1}{-iz + p^2} \times$$

$$\times\Bigg[\Big(- 12p^2q^2 + 3(iz + q^2)^2\Big) \ell n \left(\frac{iz + q^2 + 2pq}{iz + q^2 - 2pq}\right) -$$

$$- \Big(- 12p^2q^2 + 3(iz\gamma_h + p^2 - \gamma_h p^2 + q^2)^2\Big) \times$$

$$\times \ell n\left(\frac{iz\gamma_h + p^2 - \gamma_h p^2 + q^2 + 2pq}{iz\gamma_h + p^2 - \gamma_h p^2 + q^2 - 2pq}\right)\Bigg]\Bigg\} + \theta(p - \gamma_h^{\frac{1}{2}}) \times$$

$$\times\Bigg\{\frac{1}{2} \ell n \left(\frac{z^2 + (2pq + q^2)^2}{z^2 + (2pq - q^2)^2}\right) - \frac{3q}{4p}(\gamma_h - 1) + \frac{1}{16p^2} \mathrm{Re} \frac{1}{-iz + p^2} \times$$

$$\times\Bigg[\Big(- 12p^2q^2 + 3(iz + q^2)^2\Big) \ell n \left(\frac{iz + q^2 + 2pq}{iz + q^2 - 2pq}\right) -$$

$$-\Big(- 12p^2q^2 + 3(iz\gamma_h + p^2 - \gamma_h p^2 + q^2)^2\Big) \times$$

$$\times \ell n \left(\frac{iz\gamma_h + p^2 - \gamma_h p^2 + q^2 + 2pq}{iz\gamma_h + p^2 - \gamma_h p^2 + q^2 - 2pq}\right)\Bigg]\Bigg\}\Bigg] \qquad (D.10)$$

(The typographical errors appearing in the corresponding formulas to Equations D.4 and D.10 in the paper of Bergersen et al[18] are here corrected).

Equation D.10 is calculated numerically with programme one is listed below and is independent of the hole density since q and z are in hole Fermi units and to avoid unnecessary repetitions of this highly time consuming integration, one should define a priori a grid of q and z values (in hole Fermi units) for which the integrands of Equations D.1 and D.3 will be calculated. Care must be exercised when choosing the grid: if the largest values of q and z are too small then for low hole densities the integrations given by Equation D.1 and D.2 will be in error; for high hole densities the values of q and z may become too coarse. It was found that to ensure accuracy in the low hole density region of 10^{16} cm^{-3} it was necessary to extend the grid used by Bergersen et al[18, 19] by at least an order of magnitude. The evaluation of Equation D.10 is prohibitive in computer time for such a large grid but may be considerably simplified by performing the angular integration considering only the dominant terms of Equation D.4 when q and/or z are large. The result in this case is

$$Q^h(q,z) = \frac{4}{3}\left\{\frac{(\gamma_h^{3/2}+1)(q^2/\gamma_h)}{z^2+(q^2/\gamma_h)^2} + \frac{(\gamma_h^{3/2}+1)\,q^2}{z^2+q^4}\right\} \qquad (D.11)$$

which is evaluated in programme two listed below.

D.1b. Conduction Band Contribution

Bergersen et al[18] indicate that to calculate the electronic polarization function it is useful to define

$$\tilde{q}_{\parallel} = \gamma_c^{1/3}\,\bar{q}_{\parallel} \quad ; \quad \tilde{q}_{\perp} = \gamma_c\,\bar{q}_{\perp} \tag{D.12}$$

and $\tilde{q}^2 = \tilde{q}_{\parallel}^2 + \tilde{q}_{\perp}^2$

where $\bar{q}_{\parallel}$ is oriented along the longitudinal axis of a conduction band valley and $\bar{q}_{\perp}$ is the projection of $\bar{q}$ on the plane perpendicular to that axis. Clearly, for each of the six valleys in silicon we have a set of definitions as in Equation D.12, namely

$$\tilde{q}_{1,4}^2 = \bar{q}^2\,(\gamma_c^{2/3}\cos^2\theta + \gamma_c^{-1/3}\,\operatorname{sen}^2\theta)$$

$$\tilde{q}_{2,5}^2 = \bar{q}^2\,(\gamma_c^{2/3}\sin^2\theta\sin^2\phi + \gamma_c^{-1/3}\,(\cos^2\theta + \operatorname{sen}^2\theta\cos^2\phi))$$

$$\tilde{q}_{3.6}^2 = \bar{q}^2\,(\gamma_c^{2/3}\operatorname{sen}^2\theta\cos^2\phi + \gamma_c^{-1/3}\,(\cos^2\theta + \operatorname{sen}^2\theta\operatorname{sen}^2\phi)) \tag{D.13}$$

where the principal axis is along the longitudinal one of the first valley and ϕ is the azimuthal angle.

The polarization function due to the conduction valley i can now be written as:

$$S^C(\tilde{q}_i, izE_F^C) = -\frac{2}{(2\pi)^3}\int_{\tilde{p}\,\tilde{K}_F^C} d^3\tilde{p}\;\left\{\frac{1}{izE_F^C + h^2(2\tilde{p}\cdot q_i + q_i^2)/2\bar{m}}\right.$$

$$\left. + \frac{1}{-izE_F^C + h^2(2\tilde{p}\,q_i + q_i^2)/2\bar{m}}\right\} \tag{D.14}$$

Expressing momentum and energy in electron Fermi units, the above integral can be easily shown to yield:

$$\frac{-4\pi e^2}{\varepsilon (k_F^C)^2} S^C(\tilde{q}, iz\varepsilon_F^C) = \alpha_e \sum_i Q^C(\tilde{q}_i, z) \qquad (D.15)$$

with $$\alpha_e = \frac{2\bar{m}}{\varepsilon \pi k_F^C} \qquad (D.16)$$

and $$Q^C(\tilde{q}_i, z) =$$

$$1 - \frac{1}{2\tilde{q}_i}\{1 - \frac{1}{4}(\tilde{q}_i - \frac{z^2}{\tilde{q}_i^2})\} \ln \frac{z^2 + (\tilde{q}_i^2 - 2\tilde{q}_i)^2}{z^2 + (\tilde{q}_i + 2\tilde{q}_i)^2} -$$

$$- \frac{z}{2\tilde{q}_i}\{\tan^{-1}(\frac{2\tilde{q}_i - \tilde{q}_i^2}{z}) + \tan^{-1}(\frac{2\tilde{q}_i + \tilde{q}_i^2}{z})\} \qquad (D.17)$$

where z and $\tilde{q}_i$ are now dimensionless quantities measuring energy and momentum. Bergersen et al[18, 19] approximate S^C by its spherical average replacing $\tilde{q}_i$ by $\tilde{q}$ for all i. This approximation is adequate when calculating the correlation energy but for the impurity energy contribution z is always zero and the logarithmic singularity in $S^C(2,0)$ produces excessive noise which is bothersome when calculating μ, therefore the exact S^C was used here.

As pointed out in the previous subsection the electronic polarization function (Equation D.15) has to be evaluated for a predetermined grid

of q and z (in hole Fermi units). Much of the complexity of programme three arises from this required change of variables.

D.2 Kinetic and Exchange Energies

This energy contribution in Rydbergs per unit volume can be easily expressed in terms of previously defined quantatives:

$$e_{kin}\,(n_c,\, n_h) = \frac{3}{5}\; m_A^{-1}\, \epsilon^2 \left[(k_F^C)^2\, \frac{n_c}{\bar{m}} + (k_F^h)^2\; \frac{n_h}{m_{hh}} \right] \qquad (D.18)$$

$$e_{exc}\,(n_c,\, n_h) = -\frac{3}{2\pi}\; m_A^{-1}\, \epsilon \left[k_F^C\, n_c\, \Phi\,(\gamma_c) + k_F^h\, n_h\, \psi\,(\gamma_h) \times \right.$$

$$\left. \times\, (1 + \gamma_h^{3/2})^{1/3} \right] \qquad (D.19)$$

where $\Phi(\gamma_c)$ and $\psi(\gamma_c)$ are given explicitly by Combescot and Nozières[7].

D.3 Computer Programmes

The following computer programmes are revised and corrected versions of those used by Bergersen et al[18, 19]. The programmes are written in Fortran IV and the IBM 370 computer model 168 is used.

As mentioned above, programme one calculates the hole polarization function per Equation D.10 for small q and z; programme two calculates the large q and/or z assymtotic expansion of the hole polarization function per Equation D.11; programme three uses the results of the previous two and after calculating the electronic polarization function evaluates all the energy contributions.

D.3a. Programme One

```
MICHIGAN TERMINAL SYSTEM FORTRAN G(41336)          MAIN          01-04-

                C
                C       COMPUTATION OF THE HOLE POLARIZATION FUNCTION FOR
                C       SMALL VALUES OF Q AND Z
                C
                C       BY  BERGERSEN,JENA AND BERLINSKY
                C
 0001                   DIMENSION ZA(99),QA(99),HST(10),NST(10),XST(10)
 0002                   DIMENSION SHST(99)
 0003                   COMMON Q,Z,GH
 0004                   EXTERNAL SH
 0005                   REAL ML,MT,MHH,MLH
                C
                C       TABULATION OF DATA
                C
                C       COURSE MESH
 0006                   DATA HST/.1,.2,.5,2./
 0007                   DATA NST/11,17,21,41/
                C       SILICON DATA
 0008                   DATA ML,MT,MHH,MLH,DE/.91,.19,.48,.16,11.4/
 0009                   NU=6
 0010                   PI=3.14159
 0011                   GH=MLH/MHH
 0012                   T=SQRT(GH)
 0013                   T2=T/2.
 0014                   T3=T+(1.-T)/2.
 0015                   MAX=NST(4)
                C
                C       MESH FOR Z AND Q VARIABLES
                C
 0016                   N=1
 0017                   ZZ=-HST(1)
 0018                   QQ=ZZ
 0019                   DO 10 I=1,4
 0020                   NN=NST(I)
 0021                   H=HST(I)
 0022                   DO 11 J=N,NN
 0023                   ZZ=ZZ+H
 0024                   QQ=QQ+H
 0025                   ZA(J)=ZZ
 0026                11 QA(J)=QQ
 0027                10 N=NN+1
                C
                C       INTEGRATE FUNCTION SH OVER P
                C
 0028                   SHST(1)=0.
 0029                   DO 12 I= 1,MAX
 0030                   Z=ZA(I)
 0031                   WRITE(6,101)Z
 0032                   WRITE(7,104)Z
 0033                   DO 15 J=2,MAX
 0034                   Q=QA(J)
 0035                   QSQ=Q*Q
                C       THE INTEGRATIONS OVER P  ARE DONE USING THE
                C       GAUSS-LEGENDRE INTEGRATION FORMULA BY CALLING THE
                C       U.B.C. COMPUTER CENTRE'S FUNCTION FGAU16(A,B,F).
 0036                   HS=FGAU16(0.,T2,SH)+FGAU16(T2,T,SH)+
                       *FGAU16(T,T3,SH)+FGAU16(T3,1.,SH)
 0037                   HS=HS*QSQ
```

```
MICHIGAN TERMINAL SYSTEM FORTRAN G(41336)              MAIN              01-04-

   0038                SHST(J)=HS
   0039             15 CONTINUE
   0040                WRITE(7,103)(SHST(J),J=1,MAX)
   0041             12 CONTINUE
   0042            101 FORMAT(10X,'Z=',F10.4)
   0043            103 FORMAT(6E13.6)
   0044            104 FORMAT(10X,'Z=',F10.4)
   0045                STOP
   0046                END
    *OPTIONS IN EFFECT*   ID,EBCDIC,SOURCE,NOLIST,NODECK,LOAD,NOMAP
    *OPTIONS IN EFFECT*   NAME = MAIN      , LINECNT =       60
    *STATISTICS*     SOURCE STATEMENTS =       46,PROGRAM SIZE =     2410
    *STATISTICS*   NO DIAGNOSTICS GENERATED
NO ERRORS IN MAIN
```

```
MICHIGAN TERMINAL SYSTEM FORTRAN G(41336)          SH                01-04-

0001                FUNCTION SH(PP)
0002                REAL *8 P,Q,Z,GH,R1,R2,R3,R4,PQ12,PQP,PQM,DREAL,
                   'DSQRT,DLOG
0003                REAL *8 PQPSQ,PQMSQ,ZSQ,PSQ,QSQ,S1,TPQ
0004                COMMON GG,ZZ,G
0005                COMPLEX*16    CDLOG,CIZ,C1,C2,C3,C4,C5,C6,C7,C8,
                   'C9,C10,C11,C12,C13,C14,DCMPLX
0006                PI=3.141593
0007                GH=G
0008                P=PP
0009                Q=QQ
0010                Z=ZZ
0011                CIZ=DCMPLX(0.D0,Z)
0012                QSQ=Q*Q
0013                PSQ=P*P
0014                ZSQ=Z*Z
0015                TPQ=2.D0*P*Q
0016                PQP=QSQ+TPQ
0017                PQM=QSQ-TPQ
0018                PQPSQ=PQP*PQP
0019                PQMSQ=PQM*PQM
0020                R1  =(Z*GH)**2+PQPSQ
0021                R2  =(Z*GH)**2+PQMSQ
0022                R3  =ZSQ+PQPSQ
0023                R4  =ZSQ+PQMSQ
0024                PQ12=1.2D1*PSQ*QSQ
0025                C1  =-CIZ*GH+PSQ
0026                C2  =-CIZ+PSQ
0027                C3  =PQ12-3.D0*(CIZ *GH+QSQ)**2
0028                C4  =PQ12-3.D0*(CIZ -(1.D0/GH-1.D0)*PSQ+QSQ)**2
0029                C5  =PQ12-3.D0*(CIZ +QSQ)**2
0030                C6  =PQ12-3.D0*(CIZ *GH+(1.D0-GH)*PSQ+QSQ)**2
0031                C7  =CIZ *GH+PQP
0032                C8  =CIZ *GH+PQM
0033                C9  =CIZ -(1.D0/GH-1.D0)*PSQ+PQP
0034                C10  =CIZ -(1.D0/GH-1.D0)*PSQ+PQM
0035                C11  =CIZ +PQP
0036                C12  =CIZ +PQM
0037                C13  =CIZ *GH+(1.D0-GH)*PSQ+PQP
0038                C14  =CIZ *GH+(1.D0-GH)*PSQ+PQM
0039                IF (P.GE.DSQRT(GH)) GO TO 1
0040                S1= (GH*DLOG(R1  /R2  )+DLOG(R3  /R4  ))/2.D0
                   ?   -DREAL(GH*(C3  *CDLOG(C7  /C8  )
                   ?    -C4  *CDLOG(C9  /C10  ))/C1  )/(16.D0*PSQ)
                   ?    -DREAL((C5  *CDLOG(C11  /C12  )
                   ?    -C6  *CDLOG(C13/  C14  ))/C2 .)/(16.D0*PSQ)
0041                 GO TO 2
0042               1 S1= (DLOG(R3  /R4  )-1.5D0*Q*(GH-1.D0)/P)/2.D0
                    ?  -DREAL((C5  *CDLOG(C11  /C12  )
                    ?  -C6  *CDLOG(C13  /C14  ))/C2  )/(16.D0*PSQ)
0043               2 SH=2.D0*S1*P /Q**3
0044                RETURN
0045                END
 *OPTIONS IN EFFECT*   ID,EBCDIC,SOURCE,NOLIST,NODECK,LOAD,NOMAP
 *OPTIONS IN EFFECT*   NAME = SH       , LINECNT =       60
 *STATISTICS*     SOURCE STATEMENTS =       45,PROGRAM SIZE =     3366
 *STATISTICS*  NO DIAGNOSTICS GENERATED
NO ERRORS IN SH
```

D.3b. Programme Two

```
MICHIGAN TERMINAL SYSTEM FORTRAN G(41336)          MAIN          01-04-

                C
                C       CALCULATES THE ASSYMPTOTIC VALUE OF THE HOLE
                C       POLARIZATION FUNCTION FOR LARGE VALUES OF
                C       Q AND/OR Z
                C
                C       BY  JUAN ROSTWOROWSKI
                C
   0001                 DIMENSION Z(99),T(99)
                C       SILICON HOLE MASS RATIO
   0002                 G=.48D0/.16000
   0003                 G2=G*G
   0004                 G3=1.D0/G**(3.D0/2.D0)
   0005                 DATA MAX,MAXQ/79,79/
   0006                 READ(5,100)(Z(I),I=1,MAX)
   0007                 DO 20 I=1,MAX
   0008                 ZZ=Z(I)*Z(I)
   0009                 IF (Z(I)-44.) 10,10,12
   0010           10    NN=41
   0011                 DO 11 J=1,40
   0012           11    T(J)=0.
   0013                 GOTO 13
   0014           12    NN=1
   0015           13    DO 30 J=NN,MAXQ
   0016                 QQ=Z(J)*Z(J)
   0017           30    T(J)=1.33333333D0*QQ*(G3+1.D0)*(G/(ZZ+QQ*QQ*G2)
                       *+1.D0/(ZZ+QQ*QQ))
   0018                 T(1)=0.
   0019                 WRITE(7,200) Z(I)
   0020           20    WRITE(7,300) (T(J),J=1,MAXQ)
   0021           100   FORMAT(8F10.0)
   0022           200   FORMAT(10X,'Z=',F7.2)
   0023           300   FORMAT(6E13.6)
   0024                 STOP
   0025                 END
    *OPTIONS IN EFFECT*   ID,EBCDIC,SOURCE,NOLIST,NODECK,LOAD,NOMAP
    *OPTIONS IN EFFECT*   NAME = MAIN      , LINECNT =       60
    *STATISTICS*     SOURCE STATEMENTS =       25,PROGRAM SIZE =      1762
    *STATISTICS*   NO DIAGNOSTICS GENERATED
NO ERRORS IN MAIN
```

D.3c. Programme Three

```
MICHIGAN TERMINAL SYSTEM FORTRAN G(41336)          MAIN          01-05-77          10:

      C
      C     EHD PROGRAM FOR DOPED SEMICONDUCTORS GE AND SI
      C     COMPUTATION OF CORRELATION ENERGY IN HOLE BAND UNITS
      C     VERSION 2  -  BY JUAN ROSTWOROWSKI
      C
0001        IMPLICIT REAL*8(A-E,G,H,K-M,O-Z)
0002        REAL*8 FO(99),FZ(99),FIMPNH(99),FIMP(99),F(99),FNH(99),FZNH(99)
0003        DIMENSION ZA(99),QA(99),FFSH(99,99),FZZ(99)
0004        EXTERNAL FE0,FE1,FE,FE2,FE3,FE4
0005        COMMON Q,Z,GE,PI,KENE,KEND ,KENH,MHH,MBAR,NU
0006        COMMON /TWO/DEQ(99),DE,AE ,AH,AE0 ,J
0007        COMMON /FCUR/FSH(99)
0008        COMMON/FIVE/HST(20),NST(20),NSMP
0009        READ(5,112)TITLE
0010        READ(5,113)ML,MT,MHH,MLH,DE, ZVAL,SHO,NU
0011        READ (5,100) NAX,NAXQ,NSMP
0012        READ (5,101)(HST(J),J=1,NSMP)
0013        READ (5,100)(NST(J),J=1,NSMP)
      C     NST(J) IS THE NUMBER OF Q AND Z POINTS SPACED BY HST(J)
      C     IN HOLE UNITS AND ARE NECESSARY FOR CALCULATING THE
      C     SIMPSON INTEGRATION IN VARIABLES Q AND Z.
0014        READ (5,108) ICOR,IIMP,INARA
      C     ICOR=0 CALCULATES CORRELATION ENERGY WITH AVERAGE  S
      C     IIMP=0 CALCULATES IMPURITY    ENERGY WITH AVERAGE  S
      C     ICOR=1 CALCULATES CORRELATION ENERGY WITH EXACT  S
      C     IIMP=1 CALCULATES IMPURITY    ENERGY WITH EXACT  S
      C     INARA=0  CALCULATES WITHOUT CENTRAL CELL CORRECTION
      C     INARA=1  CALCULATES WITH    CENTRAL CELL CORRECTION
0015        IF (ICOR.EQ.1) IIMP=1
0016        NA=NST(NSMP)
      C     WE READ NEXT THE VALUES OF THE HOLE POLARIZATION FUNCTION
      C     FOR EACH PAIR (Q,Z).
0017        DO 31 I=1,NA
0018        READ (7,104) FZZ(I)
0019        READ (7,103) (FSH(J),J=1,NA)
0020        DO 32 J=1,NA
0021     32 FFSH(I,J)=FSH(J)
0022     31 CONTINUE
0023        FFSH(1,1)=SHO
0024        DO 11 J=1,NAX
0025        ZA(J)=FZZ(J)
0026     11 QA(J)=ZA(J)
      C
      C     TABULATION OF DATA
      C
0027        PI=3.141592654D0
0028        AO=.529177D-8
0029        MBAR=(ML*MT*MT)**(1.D0/3.D0)
0030        MAM1=(2.D0/MT+1.D0/ML)/3.D0+(1.D0/MHH+1.D0/MLH)/2.D0
0031        READ (5,102) CD
0032     90 READ (5,102,END=99)CH
0033        CE=CD+CH
0034        WRITE(6,300)
0035        IF(ICOR.EQ.0) GOTO 5
0036        WRITE(6,111)
0037     5  CONTINUE
0038        IF(IIMP.EQ.0) GOTO 6
0039        WRITE (6,116)
```

```
0040          6   CONTINUE
0041              IF (INARA.EQ.0) GOTO 9
0042              WRITE(6,123)
0043          9   CONTINUE
0044              WRITE(6,114)TITLE,ML,MT,MHH,MLH,DE,NU,SHO
0045              WRITE(6,115)CH,CE,CD
0046              WRITE (6,107) NAX,NAXQ,NSMP
0047              WRITE (6,140)
0048              WRITE (6,135) (HST(J),J=1,NSMP)
0049              WRITE (6,141)
0050              WRITE (6,136) (NST(J),J=1,NSMP)
0051              WRITE (6,130)
0052              GH=MLH/MHH
0053              GG=(1.D0+GH**(3.D0/2.DC))
0054              KFNH=(3.D0*PI*PI*CH/GG)**(1.D0/3.D0)*A0
0055              KFNE=(3.D0*PI*PI*CE/NU)**(1.D0/3.D0)*A0
0056              AE =2.D0*MBAR*NU/DE/PI/KFNE
0057              KFND=(3.D0*PI*PI*CD/NU)**(1.D0/3.D0)*A0
0058              AE0=2.D0*MBAR*NU/DE/PI/KFND
0059              AH=2.D0*MHH/PI/DE/KFNH
0060              EC0=2.D0/A0**3*DE*DE*KFNH**5*MAM1/MHH /(2.D0*PI)**3
0061              IF (ICOR.EQ.1) EC0=EC0/2.D0/PI
0062              EI0=2.D0*DE**2*MAM1*KFNH*CD/PI
0063              IF (IIMP.EQ.1) EI0=EI0/2.D0/PI
0064              GF=MT/ML
0065              WRITE(6,105)KFNH,KFND,KFNE,AE,AE0,AH,EC0,EI0
0066              EK0=3.D0/5.DC*MAM1*DE**2
0067              EX0=-1.5D0/PI*DE*MAM1
                C
                C     CALCULATE DIALECTRIC FUNCTION FOR HOLE GRID
                C
0068              DEQ(1)= DE
0069              IF (INARA.EQ.1) GOTO 7
0070              DO 8 J=2,NAX
0071          8   DEQ(J)=DE
0072              GOTO 10
0073          7   DO 10 J=2,NAX
0074              QNARA=QA(J)*KFNH
0075              DEQ(J)=ENARA(QNARA)
0076         10   CONTINUE
                C
                C     CORRELATION ENERGY
                C
0077              E (1)=-2.D0*AE *(KFNE/KFNH)**2 - FFSH(1,1)*AH
0078              E0(1)=-2.D0*AE0*(KFND/KFNH)**2
0079              ENH(1)=E(1)
0080              E(1)=E(1)-E0(1)
0081              IF (ICOR.EQ.1) GOTO 1
                C
                C     CORRELATION ENERGY WITH AVERAGE S BEGINS
                C
0082              WRITE(6,109)E(1)
0083              DC 12 I=1,NAX
0084              Z=ZA(I)
                C
                C     Q INTEGRAND FOR FIXED Z
                C
0085              N=NAXQ
```

```
0086                IF (I.EQ.1.AND.IIMP.EQ.0) N=NAX
0087                DO 15 J=2,N
0088                FSH(J)=FFSH(I,J)
0089                C=CA(J)
0090                CQ=Q**2
                C
                C       INTEGRATE ELECTRONIC S
                C
                C       THE ANGULAR INTEGRATIONS ARE DONE USING THE GAUSS-LEGENDRE
                C       INTEGRATION FORMULA BY CALLING THE U.B.C. COMPUTER CENTRE'S
                C       FUNCTION FGAUXX(A,B,F), WHERE XX CAN BE AN EVEN NUMBER .LE.16
                C       AND DENOTES THE NUMBER OF POINTS USED. A AND B ARE THE
                C       LIMITS OF INTEGRATION AND F IS AN EXTERNALLY DECLARED
                C       FUNCTION WHICH EVALUATES THE INTEGRAND.
0091                S =FGAU08(0.,1.,FE)*AF*DE/DEQ(J)
0092                SSO=FGAU08(0.,1.,FEO)*AEO*DF/DEQ(J)
0093                SS=S+AH*FSH (J)*DE/DEQ(J)
0094                IF(I .EQ. 1) FIMPNH(J)=SS
0095                IF(I .EQ. 1) FIMP(J)=SSO
0096                F(J)=-SS+DLOG(1.D0+SS/QQ)*QQ
0097                FO(J)=-SSO+DLOG(1.D0+SSO/QQ)*QQ
0098                FNH(J)=F(J)
0099                F(J)=F(J)-FO(J)
0100             15 CONTINUE
                C
                C       INTEGRAL OVER Q VARIABLE
                C
0101                FZ(I)= SMPSN(F,NAXQ)
0102                FZNH(I)= SMPSN (FNH,NAXQ)
0103                F(1)=0.D0
0104                FO(1)=0.D0
0105                FNH(1)=0.D0
0106             12 CONTINUE
0107                WRITE (6,142)
0108                WRITE(6,135)(FZ(J),J=1,NAX)
0109                WRITE (6,143)
0110                WRITE(6,135)(FZNH(J),J=1,NAX)
                C
                C       INTEGRAL OVER Z VARIABLE
                C
0111                ECOR=EC0*SMPSN(FZ ,NAX)
0112                ECORNH=EC0*SMPSN(FZNH,NAX)
                C
                C       CORRELATION ENERGY WITH AVERAGE S ENDS
                C
0113                GOTO 2
0114              1 CONTINUE
                C
                C       CORRELATION ENERGY WITH EXACT S BEGINS
                C
0115                FNH(1)=FNH(1)*2.D0*PI
0116                F(1)=F(1)*2.D0*PI
0117                DO 42 I=1,NAX
0118                Z=ZA(I)
0119                DO 45 J=2,NAXQ
0120                FSH(J)=FFSH(I,J)
0121                C=CA(J)
0122                CQ=Q*Q
```

```
0123                FNH(J)=FGAUO8(0.,1.,FF2)
0124             45 F(J)  =FGAUO8(0.,1.,FF4)
0125                FZ (I)=SMPSN(F ,NAXQ)
0126                FZNH(I)=SMPSN(FNH,NAXQ)
0127                F(1)=0.DO
0128             42 FNH(1)=0.DO
0129                WRITE (6,142)
0130                WRITE(6,135)(FZ(J),J=1,NAXQ)
0131                WRITE (6,143)
0132                WRITE(6,135)(FZNH(J),J=1,NAXQ)
                 C
                 C      INTEGRAL OVER Z
                 C
0133                ECOR=ECO*SMPSN(FZ ,NAX)
0134                ECORNH=ECO*SMPSN(FZNH,NAX)
                 C
                 C      CORRELATION ENERGY WITH EXACT S ENDS
                 C
0135             2  CONTINUE
0136                FIMPNH(1)=1.DO/DE
0137                IF (IIMP.EQ.1) FIMPNH(1)=FIMPNH(1)*2.DO*PI
0138                FIMP(1)=0.DO
0139                Z=0.DO
                 C
                 C      IMPURITY ENERGY
                 C
0140                DO 20 J=2,NAX
0141                FSH(J)=FFSH(1,J)
0142                Q=QA(J)
0143                QQ=Q**2
0144                IF (IIMP.EQ.1) GOTO 3
                 C      NEXT  3  CARDS IF ELECTRONIC POLARIZATION HAS BEEN AVERAGED
0145                FIMPNH(J)=FIMPNH(J)/DEQ(J)/(QQ+FIMPNH(J))
0146                FIMP(J)=FIMP(J)/DEQ(J)/(QQ+FIMP(J))
0147                FIMP(J)=FIMPNH(J)-FIMP(J)
0148                GOTO 20
0149             3  CONTINUE
                 C      NEXT TWO CARDS IF ELECTRONIC POLARIZATION IS EXACT
0150                FIMP (J)=FGAU10(0.,1.,FF3)/DEQ(J)
0151                FIMPNH(J)=FGAU10(0.,1.,FF1)/DEQ(J)
0152             20 CONTINUE
                 C
                 C      INTEGRATION OVER Q
                 C
0153                FIMP=-FIO*SMPSN(FIMP,NAXQ)
0154                FIMPNH=-FIO*SMPSN(FIMPNH,NAXQ)
                 C
                 C      EXCHANEGE ENERGY
                 C
0155                PH=PHI(GF)
0156                FEX=EXO*(CF*KFNF*PH+CH*KFNH*PSI(GH))
0157                FEXO=EXO*CO*KFNO*PH
0158                FEXNH=FEX
0159                EEX=EEX-FEXO
                 C
                 C      KINETIC ENERGY
                 C
0160                EKIN =EKO*(KFNF**2*CF/MBAR + KFNH**2*CH/MHH)
```

```
0161                EKINO=EKO* KEND**2*CD/MBAR
0162                EKINNH=EKIN
0163                EKIN=EKIN-EKINO
0164                EKX=EKIN+EEX
0165                ETOT=EKIN+EEX+ECOR
0166                ETCN =ETOT+EIMP
0167                EKXNH=EKINNH+EEXNH
0168                ETOTNH=EKXNH+ECORNH
0169                ETCNNH=ETOTNH+EIMPNH
0170                EKINNI=EKINNH-EKIN
0171                EEXNI=EEXNH-EEX
0172                ECORNI=ECORNH-ECOR
0173                EIMPNI=EIMPNH-EIMP
0174                ETOTNI=ETOTNH-ETOT
0175                ETCNNI=ETCNNH-ETCN
0176                EKXNI=EKXNH-EKX
0177                WRITE (6,300)
0178                WRITE(6,132)
0179                WRITE(6,106)EKIN,EEX,ECOR,EIMP
0180                WRITE(6,110)ETOT,ETCN ,EKX
0181                WRITE(6,131)
0182                WRITE(6,106)EKINNH,EEXNH,ECORNH,EIMPNH
0183                WRITE(6,110)ETOTNH,ETCNNH,EKXNH
0184                WRITE(6,137)
0185                WRITE(6,106)EKINNI,EEXNI,ECORNI,EIMPNI
0186                WRITE(6,110)ETOTNI,ETCNNI,EKXNI
0187                EKINNH=EKINNH/CH
0188                EKINNI=EKINNI/CH
0189                EKIN  =EKIN  /CH
0190                EEXNH=EEXNH/CH
0191                EEXNI=EEXNI/CH
0192                EEX   =EEX   /CH
0193                ECORNH=ECORNH/CH
0194                ECORNI=ECORNI/CH
0195                ECOR  =ECOR  /CH
0196                EIMPNH=EIMPNH/CH
0197                EIMPNI=EIMPNI/CH
0198                EIMP  =EIMP  /CH
0199                ETOTNH=ETOTNH/CH
0200                ETOTNI=ETOTNI/CH
0201                ETOT  =ETOT  /CH
0202                ETCNNH=ETCNNH/CH
0203                ETCNNI=ETCNNI/CH
0204                ETCN  =ETCN  /CH
0205                EKXNH=EKXNH/CH
0206                EKXNI=EKXNI/CH
0207                EKX   =EKX   /CH
0208                WRITE (6,118)
0209                WRITE(6,122)
0210                WRITE(6,106)EKIN,EEX,ECOR,EIMP
0211                WRITE(6,110)ETOT,ETCN ,EKX
0212                WRITE(6,121)
0213                WRITE(6,106)EKINNH,EEXNH,ECORNH,EIMPNH
0214                WRITE(6,110)ETOTNH,ETCNNH,EKXNH
0215                WRITE(6,117)
0216                WRITE(6,106)EKINNI,EEXNI,ECORNI,EIMPNI
0217                WRITE(6,110)ETOTNI,ETCNNI,EKXNI
0218                GOTO 90
```

```
MICHIGAN TERMINAL SYSTEM FORTRAN G(41336)          MAIN          01-05-77        10:

0219          100 FORMAT (8I10)
0220          101 FORMAT (5D15.2)
0221          102 FORMAT (D10.2)
0222          103 FORMAT(6E13.6)
0223          104 FORMAT(10X,'Z=',F7.2)
0224          105 FORMAT (1X,'KENH=',D13.6,2X,'KEND=',D13.6,2X,'KENE=',D13.6,/,1X,
                 1'AS=',D13.6,2X,'AEC=',D13.6,2X,'AH=',D13.6,/,1X,'ECO=',D13.6,2X,
                 2'EIO=',D13.6/)
0225          106 FORMAT(/1X ,'E(KINETIC)=',D15.9,3X,'E(EXCHANEGE)=',D15.9,3X,
                 1'E(CORRELATION)=',D15.9,3X,'E(IMPURITY)=',D15.9/)
0226          107 FORMAT (1X,'NAX=',I3,10X,'NAXQ=',I3,10X,'NSMP=',I3/)
0227          108 FORMAT (3I2)
0228          109 FORMAT(1X,'E(1), END',D12.5/)
0229          110 FORMAT(1X,'E(TOTAL)=',D15.9,3X,                    'ETCN(IMP)=',
                 1D15.9,3X,'E(KIN+EX)=',D15.9/)
0230          111 FORMAT (/,10X,'YOU HAVE USED EXACT ELECTRONIC POLARIZATION TO CAL
                 1CULATE THE CORRELATION ENERGY'/)
0231          112 FORMAT(A4)
0232          113 FORMAT(7D10.0,I2)
0233          114 FORMAT(/A15,3X,'ML=',D10.3,3X,'MT=',D10.3,3X,'MHH=',D10.3,3X,
                 1'MLH=',D10.3,3X,'DE=',D10.3,3X,'NU=',I1,3X,'SHO=',D10.3/)
0234          115 FORMAT(10X,'CH=',D11.3,10X,'CE=',D11.3,10X,'CD=',D11.3/)
0235          116 FORMAT (/,10X,'YOU HAVE USED EXACT ELECTRONIC POLARIZATION TO CAL
                 1CULATE THE IMPURITY ENERGY'/)
0236          117 FORMAT(/5X,'FOLLOWING ARE THE CONTRIBUTION TO TOTAL ENERGY, E(ND,0
                 1)/NH',/)
0237          118 FORMAT (/1X,'
                 1XXX',/)
0238          121 FORMAT(/5X,'FOLLOWING ARE THE CONTRIBUTION TO TOTAL ENERGY, E(ND+N
                 1H,NH)/NH',/)
0239          122 FORMAT(/5X,'FOLLOWING ARE THE CONTRIBUTION TO DIFFERENCE ENERGIES
                 1,(E(ND+NH,NH)-E(ND,0))/NH',/)
0240          123 FORMAT(/10X,'CONTRIBUTIONS INCLUDING CENTRAL CELL CORRECTIONS'/)
0241          130 FORMAT (/'IF NAX&NAXQ ARE NOT ONE OF THE NST"S AND IF THE NST"S
                 'ARE NOT ODD THEN THIS OUTPUT IS GARBAGE'/)
0242          131 FORMAT(/5X,'FOLLOWING ARE THE CONTRIBUTION TO TOTAL ENERGY, E(ND+N
                 1H,NH)    ',/)
0243          132 FORMAT(/5X,'FOLLOWING ARE THE CONTRIBUTION TO DIFFERENCE ENERGIES
                 1,(E(ND+NH,NH)-E(ND,0))    ',/)
0244          135 FORMAT(10(1X,D12.5))
0245          136 FORMAT (10(1X,I12))
0246          137 FORMAT(/5X,'FOLLOWING ARE THE CONTRIBUTION TO TOTAL ENERGY, E(ND,0
                 1)    ',/)
0247          140 FORMAT (1X,'LIST OF HST"S'/)
0248          141 FORMAT(/1X,'LIST OF NST"S'/)
0249          142 FORMAT(/1X,'LIST OF FZ"S'/)
0250          143 FORMAT(/1X,'LIST OF FZNH"S'/)
0251          300 FORMAT('1')
0252          99  STOP
0253              END
 *OPTIONS IN EFFECT*   ID,EBCDIC,SOURCE,NOLIST,NODECK,LOAD,NOMAP
 *OPTIONS IN EFFECT*   NAME = MAIN      , LINECNT =       60
 *STATISTICS*     SOURCE STATEMENTS =      253,PROGRAM SIZE =     55220
 *STATISTICS*   NO DIAGNOSTICS GENERATED
NO ERRORS IN MAIN
```

```
MICHIGAN TERMINAL SYSTEM FORTRAN G(41336)          FE              01-05-77        10:

0001                FUNCTION FE (X)
                C
                C       THESE FUNCTIONS ARE REQUIRED FOR AVERAGE  S
                C
0002                IMPLICIT REAL *8(A-E,G,H,K-M,O-T,W,Y,Z)
0003                COMMON P,T,GE,PI,KENE,KENO ,KENH,MHH,MBAR,NU
0004                COMMON /TWO/DEQ(99),DE,AE ,AH,AEO ,J
0005                KENC=KENE
0006                GOTO 1
0007                ENTRY FEO (X)
0008                KENC=KENO
0009              1 CONTINUE
0010                G3=GE**(1.DO/3.DO)
0011                Q    =DSQRT((G3*X)**2 + (1.DO-X*X)/G3)*P
0012                Q=Q/KENC*KENH
0013                QQ=Q*Q
0014                Z=T*(KENH/KENC)**2*MBAR/MHH
0015                ZZ=Z*Z
0016                Q2P=2.DO*Q+QQ
0017                Q2M=2.DO*Q-QQ
0018                Q2M2=Q2M*Q2M
0019                IF(Z.LT.1.D-5)GOTO 10
0020                Y=DATAN(Q2M/Z)+DATAN(Q2P/Z)
0021                GOTO 21
0022              10 Y=PI
0023                IF (Q2M2.GT.1.D-10) GOTO 21
0024                FE =1.DO*(KENC/KENH)**2
0025                FEO=1.DO*(KENC/KENH)**2
0026                RETURN
0027              21 W=(1.DO-(QQ-ZZ/QQ)/4.DO)*DLOG((ZZ+Q2M2)/(ZZ+Q2P*Q2P))
0028                S    =1.DO-.5DO*(W+Z*Y)/Q
0029                S    =S    *(KENC/KENH)**2
0030                FE =S
0031                FEO=S
0032                RETURN
0033                END
 *OPTIONS IN EFFECT*   ID,EBCDIC,SOURCE,NOLIST,NODECK,LOAD,NOMAP
 *OPTIONS IN EFFECT*   NAME = FE       , LINECNT =       60
 *STATISTICS*     SOURCE STATEMENTS =       33,PROGRAM SIZE =     1178
 *STATISTICS*   NO DIAGNOSTICS GENERATED
NO ERRORS IN FE
```

```
MICHIGAN TERMINAL SYSTEM FORTRAN G(41336)          FE1          01-05-77        10:

0001                  FUNCTION FE1(X)
                C
                C     THESE FUNCTIONS ARE REQUIRED FOR EXACT  S
                C
                C
                C
                C     CALLED TO CALCULATE TOTAL EIMP
                C
0002                  COMMON /THREE/XO,JJ,JJ1
0003                  EXTERNAL FEOS,FES
0004                  JJ1=0
0005                  JJ=1
0006                  XO=X
0007                  FE1=4.*FGAU14(0.,1.5708,FES)
0008                  RETURN
0009                  ENTRY FE2(X)
                C
                C     CALLED TO CALCULATE TOTAL ECOR
                C
0010                  JJ1=1
0011                  JJ=1
0012                  XO=X
0013                  FE2=4.*FGAU06(0.,1.5708,FEOS)
0014                  RETURN
0015                  ENTRY FE3(X)
                C
                C     CALLED TO CALCULATE  EIMP DIFFERENCE
0016                  JJ1=0
0017                  JJ=2
0018                  XO=X
0019                  FE3=4.*FGAU14(0.,1.5708,FES)
0020                  RETURN
0021                  ENTRY FE4(X)
                C
                C     CALLED TO CALCULATE  ECOR DIFFERENCE
                C
0022                  JJ1=1
0023                  JJ=2
0024                  XO=X
0025                  FE4=4.*FGAU06(0.,1.5708,FEOS)
0026                  RETURN
0027                  END
 *OPTIONS IN EFFECT*   ID,EBCDIC,SOURCE,NOLIST,NODECK,LOAD,NOMAP
 *OPTIONS IN EFFECT*   NAME = FE1      , LINECNT =       60
 *STATISTICS*     SOURCE STATEMENTS =       27,PROGRAM SIZE =      904
 *STATISTICS*   NO DIAGNOSTICS GENERATED
NO ERRORS IN FE1
```

```
MICHIGAN TERMINAL SYSTEM FORTRAN G(41336)          FES          01-05-77        10:

0001                FUNCTION FES(U)
                C
                C     THESE FUNCTIONS CALCULATE THE INTEGRANDS
                C     FOR EXACT  S  CALCULATIONS
                C
0002                IMPLICIT REAL *8(A-F,G,H,K-M,O-T,W,Y,Z)
0003                COMMON P,T,GE,PI,KENF,KENC ,KENH,MHH,MBAR,NU
0004                COMMON /TWO/DEQ(99),DE,AE ,AH,AEO ,J
0005                COMMON /THREE/X,JJ,JJ1
0006                COMMON /FOUR/FSH(99)
0007                DIMENSION QT(3),S(3),SES(2),SEOS(2)
0008                GO TO 1
0009                ENTRY FEOS(U)
0010              1 U=U
0011                V=DCOS(U)
0012                G3=GE**(1.D0/3.D0)
0013                V2=V**2
0014                X2=X**2
0015                SX=1.D0-X2
0016                SV=1.D0-V2
0017                G32=G3**2
0018                PP=P**2
0019                QT(1)=DSQRT(G32*X2+SX/G3)*P
0020                QT(2)=DSQRT(G32*SX*SV+(X2+SX*V2)/G3)*P
0021                QT(3)=DSQRT(G32*SX*V2+(X2+SX*SV)/G3)*P
0022                DO 30 J1=1,JJ
0023                DO 15 I=1,3
0024                KENC=KENO
0025                IF(J).EQ.1) KENC=KENE
0026                Q=QT(I)
0027                Q=Q/KENC*KENH
0028                QQ=Q**2
0029                Z=T*(KENH/KENC)**2*MBAR/MHH
0030                ZZ=Z**2
0031                Q2P=2.D0*Q+QQ
0032                Q2M=2.D0*Q-QQ
0033                Q2M2=Q2M**2
0034                IF(Z.LT.1.D-5)GOTO 10
0035                Y=DATAN(Q2M/Z)+DATAN(Q2P/Z)
0036                GOTO 21
0037             10 Y=PI
0038                IF (Q2M2.GT.1.D-10) GOTO 21
0039                S(I)=1.DO
0040                GOTO 22
0041             21 W=(1.D0-(QQ-ZZ/QQ)/4.D0)*DLOG((ZZ+Q2M2)/(ZZ+Q2P*Q2P))
0042                S(I)=1.D0-.5D0*(W+Z*Y)/Q
0043             22 S(I)=S(I)*(KENC/KENH)**2
0044                A=AEO
0045                IF (J1.EQ.1) A=AE
0046                S(I)=S(I)*A  *DE/DEQ(J)/NU
0047             15 CONTINUE
0048                SFES=2.D0*(S(1)+S(2)+S(3))
0049                IF (J1.EQ.1) SFES=SFES+AH*FSH(J)*DE/DEQ(J)
0050                SES(J1)=SFES/(PP+SFES)
0051                IF (JJ1.EQ.1) SES(J1)=-SFES+DLOG(1.D0+SFES/PP)*PP
0052             30 CONTINUE
0053                IF (JJ-1) 2,2,3
0054              2 FES=SES(1)
```

```
MICHIGAN TERMINAL SYSTEM FORTRAN G(41336)          FES          01-05-77        10:

   0055                IF (JJ1.EQ.1) FEOS=FES
   0056                RETURN
   0057           3    FES=SES(1)-SES(2)
   0058                IF (JJ1.EQ.1) FEOS=FES
   0059                RETURN
   0060                END
    *OPTIONS IN EFFECT*   ID,EBCDIC,SOURCE,NOLIST,NODECK,LOAD,NOMAP
    *OPTIONS IN EFFECT*   NAME = FES      , LINECNT =      60
    *STATISTICS*     SOURCE STATEMENTS =       60,PROGRAM SIZE =     2076
    *STATISTICS*   NO DIAGNOSTICS GENERATED
NO ERRORS IN FES
```

```
MICHIGAN TERMINAL SYSTEM FORTRAN G(41336)          PSI          01-05-77        10:

0001                  REAL FUNCTION PSI*8(GH)
                C
                C     EQUIVALENT TO CN EQUATION 26
                C     IF DIVIDED BY (1+GH**(3/2))**(1/3)
                C
0002                  IMPLICIT REAL*8(A-J,L-Z)
0003                  G12=DSQRT(GH)
0004                  G32=G12**3
0005                  G2=GH**2
0006                  SUM=0.D0
0007                  DO 1 K=1,99,2
0008                  EX=K/2.D0
0009                  NUMRT=2.D0*(1.D0-GH**EX)
0010                  S=NUMRT/K**2
0011              1   SUM=SUM+S
0012                  PSI=1.D0/(1.D0+G32)*(-3.D0/16.D0*(1.D0-GH)**2*DLOG((1.D0+G12)/
                     1(1.D0-G12))+(G2+3.D0*G32+3.D0*G12+1.D0)/4.D0+3.D0/16.D0*(1.D0-G2)
                     2*SUM)
0013                  RETURN
0014                  END
 *OPTIONS IN EFFECT*   ID,EBCDIC,SOURCE,NOLIST,NODECK,LOAD,NOMAP
 *OPTIONS IN EFFECT*   NAME = PSI       , LINECNT =       60
 *STATISTICS*     SOURCE STATEMENTS =       14,PROGRAM SIZE =      796
 *STATISTICS*   NO DIAGNOSTICS GENERATED
NO ERRORS IN PSI
```

```
MICHIGAN TERMINAL SYSTEM FORTRAN G(41336)          PHI              01-05-77        10:
   0001                 REAL FUNCTION PHI*8(GE)
                C
                C       EQUIVALENT TO CN EQUATION 24
                C
   0002                 IMPLICIT REAL*8 (A-Z)
   0003                 G6=GE**(1.D0/6.D0)
   0004                 IF (GE.LT.1.D0) GO TO 1
   0005                 IF (GE.EQ.1.D0) GOTO 2
   0006                 PHI=DARSIN(DSQRT(1.D0-1.D0/GE))/DSQRT(GE-1.D0)*G6
   0007                 RETURN
   0008               1 PHI=DARSIN(DSQRT(1.D0-GE))/DSQRT(1.D0-GE)*G6
   0009                 RETURN
   0010               2 PHI=1.D0
   0011                 RETURN
   0012                 END
    *OPTIONS IN EFFECT*   ID,EBCDIC,SOURCE,NOLIST,NODECK,LOAD,NOMAP
    *OPTIONS IN EFFECT*   NAME = PHI      , LINECNT =       60
    *STATISTICS*     SOURCE STATEMENTS =        12,PROGRAM SIZE =      680
    *STATISTICS*   NO DIAGNOSTICS GENERATED
NO ERRORS IN PHI
```

```
MICHIGAN TERMINAL SYSTEM FORTRAN G(41336)          SMPSN          01-05-77        10:

   0001                REAL FUNCTION SMPSN*8(F,MAX)
   0002                IMPLICIT REAL*8 (A-H,K,L,O-Z)
   0003                DIMENSION F(99)
   0004                COMMON/FIVE/HST(20),NST(20),NSMP
   0005                SUM=0.D0
   0006                NM=1
   0007                IMAX=0
   0008                DO 24 J=1,NSMP
   0009           24   IF (NST(J).EQ.MAX) IMAX=J
   0010                DO 26 J=1,IMAX
   0011                NN=NST(J)
   0012                MM=NN-2
   0013                SM=0.D0
   0014                DO 28 JJ=NM,MM,2
   0015           28   SM=SM+F(JJ)+4.D0*F(JJ+1)+F(JJ+2)
   0016                SM=SM*HST(J)/3.D0
   0017                SUM=SUM+SM
   0018           26   NM=NN
   0019                SMPSN=SUM
   0020                RETURN
   0021                END
    *OPTIONS IN EFFECT*   ID,EBCDIC,SOURCE,NOLIST,NODECK,LOAD,NOMAP
    *OPTIONS IN EFFECT*   NAME = SMPSN    , LINECNT =      60
    *STATISTICS*     SOURCE STATEMENTS =       21,PROGRAM SIZE =      722
    *STATISTICS*   NO DIAGNOSTICS GENERATED
NO ERRORS IN SMPSN
```

```
 MICHIGAN TERMINAL SYSTEM FORTRAN G(41336)          ENARA          01-05-77        10:!

   0001                REAL FUNCTION ENARA*8(Q)
   0002                IMPLICIT REAL*8(A-H,C-Z)
                C
                C      DIELECTRIC FUNTION OF NARA
                C
   0003                DATA AAN,ALN,ABN,AGN,DE/1.175D0,.757200,.312300,.2044D+1,11.4D0/
   0004                ENARA=AAN*Q**2/(ALN**2+Q**2)+(1.D0-AAN)*Q**2/(ABN**2+Q**2)
                      1     +1.DC/DE*AGN**2/(AGN**2+Q**2)
   0005                ENARA=1.D0/ENARA
   0006                RETURN
   0007                END
    *OPTIONS IN EFFECT*   IC,EBCDIC,SOURCE,NOLIST,NODECK,LOAD,NOMAP
    *OPTIONS IN EFFECT*   NAME = ENARA    , LINECNT =       60
    *STATISTICS*     SOURCE STATEMENTS =         7,PROGRAM SIZE =      454
    *STATISTICS*   NO DIAGNOSTICS GENERATED
NO ERRORS IN ENARA

NO STATEMENTS FLAGGED IN THE ABOVE COMPILATIONS.


NAME       NUMBER OF ERRORS/WARNINGS   SEVERITY

MAIN                    0                  0
FE1                     0                  0
FFS                     0                  0
FE                      0                  0
PSI                     0                  0
PHI                     0                  0
SYPSN                   0                  0
ENARA                   0                  0
EXECUTION TERMINATED
```

BIBLIOGRAPHY

1. G. Wannier, Phys. Rev. 52, 191 (1937);
G. Dresselhaus, Phys. Chem. Solids 1, 14 (1956);
G.G. MacFarlane, T.P. McLean, J.E. Quarrington and V. Roberts, Phys. Rev. 111, 1245 (1958).

2. J.R. Haynes, M. Lax, W.F. Flood, J. Phys. Chem. Solids 8, 392 (1959); "Proc. International Conf. on Semiconductor Physcis, Prague 1960", p.423, Czechocoslavak Acad. Sci., Prague (1961).

3. L.V. Keldysh, "IX International Conference of the Physics of Semiconductors. Moscow, July 23-29, 1968", p. 1303, Nauka, Leningrad (1968).

4. See e.g. C.D. Jeffreys, Science 189, 955 (1975) for a recent general review.

5. Ya. E. Pokrovskii, Phys. Stat. Sol. (a) 11, 385 (1972).

6. C. Benoît à la Guillaume, M. Voos, and F. Salvan, Phys. Rev. B5, 3079 (1972).

7. M. Combescot and P. Nozières, J. Phys. C5, 2369 (1972).

8. M. Inoue and E. Hanamura, J. Phys. Soc. Japan 34, 652 (1973).

9. W.F. Brinkman and T.M. Rice, Phys. Rev. B7, 1508 (1973).

10. P. Bhattacharyya, V. Massida, K.S. Singwi and P. Vashishta, Phys. Rev. B10, 5127 (1974).

11. R.E. Halliwell and R.R. Parsons, Solid State Commun. 13, 1245 (1974); Can. J. Physcs 52, 1336 (1974).

12. M.N. Alexander and D.F. Holcomb, Rev. Mod. Phys. 40, 815 (1968).

13. N.F. Mott, "Metal-Insulator Transitions", Taylor and Francis (1974).

14. R.W. Martin and R. Sauer, Phys. Stat. Sol. (b) 62, 443 (1974).

15. C. Benoît à la Guillaume and M. Voos, Phys. Rev. B7, 1723 (1973).

16. W. Baltensberger, Phil. Mag. 44, 1355 (1975)

17. J. Hubbard, Proc. Roy. Soc. A276, 238 (1963); ibid. A281, 401 (1964).

18. B. Bergersen, P. Jena and A.J. Berlinsky, J. Phys. C.8, 1377 (1975).

19. B. Bergersen, J.A. Rostworowski, M. Eswaran, R.R. Parsons and P. Jena, Phys. Rev. B14, 1633 (1976); Phys. Rev. B15, 2432 (1977).

20. J.A. Rostworowski, M.L.W. Thewalt and R.R. Parsons, Solid State Commun. 18, 93 (1976).

21. M. Eswaran, B. Bergersen, J.A. Rostworowski, and R.R. Parsons, Solid State Commun. 20, 811 (1976).

22. J.C. Irvin, Bell Syst. Tech. Jour. 41, 387 (1962).

23. R.E. Halliwell, Ph.D. Thesis (unpublished), The University of British Columbia (1973).

24. J.R. Haynes, Phys. Rev. Lett. 4, 361 (1960);
C. Benoît à la Guillaume and M. Voos, Solid State Commun. 12, 1257 (1973).

25. P.J. Dean, J.R. Haynes and W.F. Flood, Phys. Rev. 161, 711 (1967).

26. M.L.W. Thewalt and R.R. Parsons, Solid State Commun. 20, 97 (1976).

27. M. Balkanski, A. Aziza, and E. Amzallag, Phys. Stat. Sol. 31, 323 (1969).

28. M.L.W. Thewalt, M.Sc. Thesis (unpublished), The University of British Columbia (1975).

29. K. Kosai and M. Gershenzon, Phys. Rev. B9, 723 (1974).

30. B.N. Brockhouse, Phys. Rev. Lett. 2, 256 (1959).

31. L.V. Keldysh quoted by M. Combescot and P. Nozières[7].

32. R.B. Hammond, D.L. Smith and T.C. McGill, Phys. Rev. Lett. 35, 1535 (1975).

33. A.S. Kaminskii, Ya. E. Pokrovskii, K.E. Svistunova, "IX International Conference of the Physics of Semiconductors, Moscow, July 23-29, 1968", p.1085, Nanka, Leningrad (1968);
R.C. Enck and A. Honig, Phys. Rev. 177, 1182 (1969).

34. J. Collet, J. Battan and M. Brousseau, Solid State Commun. 16, 775 (1975).

35. R.H. Kuwahara, Ph.D. Thesis (unpublished), The University of British Columbia (1971).

36. I.M. Lifshitz, Adv. Phys. 13, 483 (1964).

37. C. Benoît à la Guillaume and J. Cernogora, Phys. Stat. Sol. 35, 599 (1969).

38. T. Lukes, B. Nix and B. Suprapto, Phil. Mag. 26, 1239 (1972).

39. S. Chandrasekhar, Rev. Mod. Phys. 15, 1 (1943).

40. V. Macek, Ph.D. Thesis (unpublished), The University of British Columbia (1971).

41. See, for example, J.C. Slater, "The Quantum Theory of Matter", 2nd Ed. (McGraw-Hill, New York, 1968).

42. J.M. Ziman, "Principles of the Theory of Solids", (University Press, Cambridge, 1969).

43. The statement is attributed to R.E. Peierls in 1937 by Mott and Davies[50].

44. N.F. Mott, Phil. Mag. 6, 287 (1961).

45. K.-F. Berggren, Phil. Mag. 27, 1027 (1973).

46. N.F. Mott and H. Jones, "The Theory of the Properties of Metals and Alloys", (Dover Publications Inc., New York, 1958).

47. W. Kohn in "Solid State Physics", edited by F. Seitz and D. Turnbull, Vol. 5, p.257, (Academic Press Inc., New York, 1957).

48. A. Miller and E. Abrahams, Phys. Rev. 120, 745 (1960).

49. P.W. Anderson, Phys. Rev. 109, 1492 (1958).

50. N.F. Mott and E.A. Davies, "Electronic Processes in Non-Crystalline Materials", (Clarendon Press, Oxford, 1971).

51. N.F. Mott, "Metal-Insulator Transitions", (Taylor and Francis Ltd., London, 1974).

52. K. Morigaki and F. Yonezawa, Prog. Theor. Phys. Suppl. 57, 146 (1975).

53. F. Cyrot-Lackmann and J.P. Gaspard, J. Phys. C7, 1829 (1974).

54. T. Matsubara and Y. Toyozawa, Prog. Theor. Phys. Suppl. 26, 739 (1961).

55. Y. Nagaoka, Phys. Rev. 147, 392 (1966).

56. G. Mahler and J.L. Birman, Solid State Commun. 17, 1381 (1975).

57. G. Mahler and J.L. Birman, Phys. Rev. B12, 3221 (1975).

58. G. Mahler and J.L. Birman, Phys. Rev. B13, 3661 (1976).

59. H. Nara and A. Morita, J. Phys. Soc. Jpn. 21, 1852 (1966).

60. P. Bhattacharyya, V. Massida, K.S. Singwi and P. Vashishta, Phys. Rev. B10, 5127 (1974).

61. M. Combescot, Phys. Rev. Lett. 32, 15 (1974).

62. J.D. Quirt and J.R. Marko, Phys. Rev. Lett. 26, 318 (1971); Phys. Rev. B5, 1716 (1972).

63. J.D. Quirt, Ph.D. Thesis (unpublished), The University of British Columbia (1972).

64. R.R. Parsons and M.L.W. Thewalt, Solid State Commun. (in press).

65. B.N. Ashkinadze, I.P. Krets, S.M. Ryokin and I.D. Yaroshetskii, Sov. Phys. JETP 31, 271 (1970).

66. R.R. Parsons, private communication.

67. C.P. Poole, Jr., "Electron Spin Resonance" (Wiley, New York, 1967).

68. A.J.R. de Kock, Philips Research Reports (Supps.) 1-5, 1 (1973).

69. A.J.R. de Kock, Feskörperprobleme 16, 179 (1976).

70. A. Seeger, Festkörperprobleme 16, 149 (1976).

71. A. Seeger and K.P. Chik, Phys. Stat. Sol. 29, 455 (1968).

72. H. Föll, B.O. Kolbesen, and W. Frank, Phys. Stat. Sol. A29, K83 (1975).

73. Data General Corporation, "An Introduction to BASIC", Data General Corporation (1973).

PUBLICATIONS

J.A. Rostworowski, M. Horn and C.F. Schwerdtfeger. "EPR of Substitutional FE^{3+} in TiO_2 (Brookite)", Journal of Physics and Chemistry of Solids, Vol. 34, pp. 231-234 (1973).

J.A. Rostworowski, M.L.W. Thewalt and R.R. Parsons. "Photolumenescent Detection of the Impurity Band in Si(P)", Solid State Communications, Vol. 18, pp. 93-95 (1976).

B. Bergersen, J.A. Rostworowski, M. Eswaran, R.R. Parsons and P. Jena. "Electron-Hole Droplets and Impurity Band States in Heavily-Doped Si(P): Photoluminescence Experiments and Theory", Physical Review B, Vol. 14, pp. 1633-1648 (1976).

M. Eswaran, B. Bergersen, J.A. Rostworowski and R.R. Parsons. "Impurity Band States in Si(P)", Solid State Communications, Vol. 20, pp. 811-813 (1976).

B. Bergersen, J.A. Rostworowski, M. Eswaran, R.R. Parsons and P. Jena. Erratum: "Electron-Hole Droplets and Impurity Band States in Heavily-Doped Si(P): Photoluminescence Experiments and Theory", Physical Review B, Vol. 15, p.2432 (1977).

R.R. Parsons, J.A. Rostworowski, R.E. Halliwell and R. Barrie. "Heat-Induced Effects in Metallic Si(P): Photoluminescence and Electron Paramagnetic Resonance" (to be published).